SOLUTION AND SOLID-STATE NMR STUDIES OF AMPHOTERICIN B

BY

THOMAS MICHAEL ANDERSON

DISSERTATION

Submitted in partial fulfillment of the requirements
for the degree of Doctor of Philosophy in Chemistry
in the Graduate College of the
University of Illinois at Urbana-Champaign, 2013

Urbana, Illinois

Doctoral Committee:

Professor Martin D. Burke, Chair
Professor Chad M. Rienstra
Professor Paul J. Hergenrother
Professor John A. Katzenellenbogen

ABSTRACT

Since its discovery in 1955, amphotericin B (AmB) has been a vital clinical agent. It remains the drug of last resort for systemic fungal infections despite its significant toxicity. Despite over 50 years of clinical use, very few cases of AmB resistance have been reported. This lack of resistance has been attributed to its unique mechanism of action. AmB is hypothesized to bind to yeast membranes and self-assemble into membrane-spanning ion channels leading to cell death. AmB thus represents a prototype of a small molecule with capacity to perform protein-like function. However, despite extensive scientific inquiry, this capacity remains poorly understood. An atomistic understanding of this mechanism stands to enable efforts to harness this untapped potential and/or improve the therapeutic index of AmB.

The leading model for AmB antifungal activity is self assembly of the natural product into discrete, membrane-embedded barrel-stave pores which disrupt cellular ion gradients and cause cell death. A ring of salt bridges and/or hydrogen bonds at the channel periphery are proposed to stabilize the channel assembly. These polar interactions are proposed to form between the C41 carboxylate and C3' amine of adjacent AmB molecules within the channel architecture.

This dissertation describes experiments carried out to directly test these two major hypotheses of AmB antifungal activity. We have developed a functional group deletion strategy to directly test the role of the C41 carboxylate and C3' amine. Derivatives were prepared lacking either one or both of these functional groups and solution NMR conformational analysis was employed to determine the ground state conformation of AmB and our derivatives. The functional consequences of these deletions were then assessed in antifungal assays. Our results indicate that in stark contrast to the salt bridge hypothesis, oxidation at C41 is not required for antifungal activity.

To test the long-standing hypothesis that AmB is primarily embedded as discrete ion channels in phospholipid bilayers, we have performed an extensive series of solid-state NMR experiments, including homonuclear (^{13}C-^{13}C) and heteronuclear (^{31}P-^{13}C, ^{1}H-^{13}C) correlation experiments and paramagnetic relaxation measurements. These data sets enabled us to assign the ^{13}C signals of AmB and to assess geometric and topological aspects of the structural models. Strikingly, our results demonstrated that AmB primarily exists in extra-membranous aggregates phase-separated from membrane phospholipids. Moreover, PRE studies of ergosterol

demonstrated that these large aggregates function to extract ergosterol from the lipid bilayer. The work described in this dissertation highlights the power of both solution and solid-state NMR for studying the function of small molecules. Moreover, these NMR experiments led to a new model for the antifungal activity of AmB in which large AmB aggregates bind to fungal cell membranes and extract ergosterol, thus depriving the cell of a functionally vital lipid.

To R.A.A.

ACKNOWLEDGEMENTS

The last seven years have been perhaps the most challenging and rewarding in my life thus far. I gratefully acknowledge my adviser, Prof. Martin D. Burke for his tremendous support and encouragement. Marty's abundant enthusiasm for science is infectious, and this enthusiasm helped me through some really difficult times. Marty has been extremely supportive and flexible in working with me as an MD/PhD student, especially for the last 2 years during which I was a full time medical student while still pursuing my PhD.

Marty taught me to never be afraid to go after that big result, regardless of the difficulty of the experiment required to get there. Our decision to pursue SSNMR studies of membrane-bound AmB epitomizes that fearlessness. In retrospect, the image of two organic chemists sitting in Marty's office and, without batting an eye, making plans to pursue SSNMR is inspiring. Though we certainly did not know the challenges that lay ahead, we knew this was a monumental undertaking. We were very fortunate to engage in collaboration with Prof. Chad Rienstra and his group, and we have never looked back. I gratefully acknowledge everything that Chad has done to ensure that this project succeeded. He spent countless hours acquiring data on my samples, repairing probes or spectrometers so that new data could be acquired on my samples, and assisting with data analysis and various other efforts. Chad taught me virtually everything I know about NMR spectroscopy, and he has always been a patient and willing instructor, despite my frequent thickheadedness. Chad has always been quick with very thorough email responses to my questions. I recall a meeting very early on in this collaboration in which Chad told me about the possibility of using doxyl lipids to probe the position of AmB in lipid bilayers; I often wonder how things would have been different had we first pursued PRE studies rather than chase the elusive POPC-AmB REDOR. I also gratefully acknowledge Chad for his letter on my behalf in support of my NIH NRSA Fellowship application.

I acknowledge. Prof. Paul Hergenrother for his support and encouragement during my time here. Since my first semester at UIUC when I was considering joining his group, Paul has pushed me to strive for excellence in all of my academic endeavors. I recall my time as a first year graduate student in a few classes taught by Paul. From the start, he expected me to think deeply and critically about science, both my own and others'. He has also been someone who encouraged me to keep my focus on pursuing big results despite the day-to-day grind of research. I thank Paul for all his support over the last 7 years, and in particular for his letter on my behalf in support of my NIH NRSA Fellowship application.

I have had the privilege to work across the hall from Prof. John Katzenellenbogen for 7 years. At various points in my graduate school career, Dr. K was gracious enough to allow me to work in his lab's space. I'm especially grateful for the space Dr. K offered me during my 2nd year of medical school which allowed me to complete the final experiments for my dissertation. Dr. K has always greeted me with a smile, and even before becoming a member of my committee was inquisitive regarding my progress and congratulatory of my successes. I have also enjoyed the many spontaneous hallway conversations about sightseeing in southern Utah and various other topics.

I acknowledge Prof. Scott Silverman for his letter on my behalf in support of my NIH NRSA Fellowship application. I thank Prof. Silverman also for encouraging me to present my organic chemistry 535 seminar on NMR analysis of intermolecular interactions. That seminar stimulated my thinking about amphotericin B and contributed greatly to the subsequent evolution of my dissertation research.

Fellow members of the Burke Group and members of the Rienstra group have been a great source of support during my career here. More importantly, they have become friends, and I thank each of you for 7 great years in this department, and for making this a great place to do chemistry. I would like to specifically thank Seiko Fujii and Jenna Klubnick for their friendship at a very difficult time in my graduate school career, and for their continuing friendship, for which I am always grateful. I acknowledge my co-authors and thank them for their efforts in the science we have pursued together. Dan Palacios taught me a great deal about how to be a good scientist; his work ethic and insight have always been inspirational to me. Thanks to Brice Uno, Pulin Wang, Matt Endo, Steve Ballmer, and Erin Davis for being good friends and for all the humor that kept things positive, especially during the hard times. I thank Eric Woerly, Seiko Fujii, and Mary Clay for taking time to read portions of this dissertation and for their insightful feedback. Mary Clay has been a fantastic collaborator, and I have always been grateful for her willingness to dedicate large amounts of time to the AmB project when she has so many other ongoing pursuits for her primary project. I am also grateful for her assistance preparing the figures and Supplemental Information for chapters 3 and 4 of this dissertation.

I am very grateful to Deb Berthold for all her input on biosynthesis and sterile technique, and especially for her willingness to allow me to use her equipment. I thank Gemma Commellas, Andy Nieukoop, Ming Tang, Anna Jean Wirth, Ben Wylie, Trent Franks, and Lindsay Sperling for their contributions that helped transform my project from a mere idea to being publication-worthy. I am grateful to the VOICE NMR Lab staff who have been incredibly helpful with many aspects of NMR data acquisition and analysis, namely, Vera Mainz, Paul Molitor, Trent Franks, Jennifer Rapp, Lingyang Zhu, Dean Olson, and Feng Lin.

I thank Nashrah Maryum for her efforts in the nanodisc investigations, and especially for her contributions to figuring out the AmB biosynthesis. Nashrah is an extremely bright, capable individual who pushed me to excel as a mentor and a researcher. I am grateful for our friendship and all her efforts during her time in the Burke lab.

I thank all those who assisted me in learning various biological/biochemical assays and techniques: Prof. Susan Martinis, Rachel Hellman-Whitaker, Jill Grimme, Nicole Kretzer, Courtney Evans, Lena Grinkova, and many others who so willingly shared their expertise.

I thank Stacy Olson, Becky Duffield, Susan Lighty, and Patti Silver, the Organic Chemistry office staff that I have had the privilege of working with here at UIUC. Their constant willingness to assist me has made my time here much smoother. I am also grateful for their moral support, positive attitude, and the candy they always had on their desks!

I acknowledge the National Institute of Diabetes and Digestive and Kidney Diseases (DK081272), the UIUC Department of Chemistry, and Prof. Martin Burke for funding during my time at UIUC.

I am very grateful to all the incredible individuals who make up the Medical Scholars Program, both students and administration. Prof. James Slauch, Deans Jim Hall, Jenny Bloom, Nora Few, and Amanda Cuevas are a big part of what has made being in the MSP so enjoyable, and each of them has taken time to advise me at important times in my MSP career. Jenny and Amanda have since moved on to other positions, but their kindness and support will always be remembered, especially Amanda's infectious enthusiasm and dedication to MSP students' success. My fellow MSP students have been outstanding colleagues and friends. It has been one of the great opportunities of my life to interact with such a diverse group of aspiring physician scientists. In particular, I thank Alex Parent, Lindsey Burnett, and Jenn Baldwin for their

tremendous friendship, encouragement, many helpful scientific discussions, hours spent allowing me to vent, and countless other gestures of genuine friendship.

I had the unique challenge of finishing my PhD during full time M1, M2, and M3 coursework. I am grateful to my med school classmates and study groups who made it possible for me to keep up with med school studies while still making progress toward my dissertation. Their hard work and studying often helped me when I hadn't studied as much as I would have liked. Namely, Alex Parent, Lindsey Burnett, Jenn Baldwin, Freddy Nguyen, Evelyn Huang, and Xavier Stacey were all fantastic classmates during these years.

Most importantly, I thank my amazing family for their immeasurable love and support. I absolutely would not be where I am in life without them. To my parents, Dick and Jane Anderson: I am deeply grateful for all you have done for me, for never giving up on me, and for teaching me by example to work hard, be persistent, and be a good person. Your support and encouragement helped me through the difficult times over the last 7 years. To my grandparents Richard and Louise Anderson and Murray and Marie Nichols: I will never forget how supportive and proud you always were of my academic endeavors. I will always be a little saddened that you did not live to see my career come to fruition, but my memories of each of you and the life lessons I learned from each of you will forever be an inspiration to me. Finally, I thank my wonderful wife, Becca, for her unfailing love and support, especially during all the nights and weekends that you were home alone while I worked late in the lab or studied for medical school exams. Your support has sustained me through the difficult times, and it has been a joy to celebrate the successes with you.

Ac	Acyl
ACME	Amplitude-constrained multiplet evaluation
AmB	Amphotericin B
AmdeB	Amphoteronolide B
AmE	Amphotericin B methyl ester
aq	Aqueous
ax	Axial
COSY	Correlation spectroscopy
COSYPS	Phase-sensitive correlation spectroscopy
CPK	Corey-Pauling-Koltun
CSA	(±)-10-Camphorsulfonic acid
CYP3A4	Cytochrome P450 3A4
DARR	Dipolar-assisted rotational resonance
DDQ	2,3-dichloro-5,6-dicyano-1,4-benzoquinone
DIPEA	Diisopropyl ethyl amine
DLPC	1,2-dilauroyl-*sn*-glycero-3-phosphocholine
DMF	Dimethyl formamide
DMPC	1,2-dimyristoyl-*sn*-glycero-3-phosphocholine

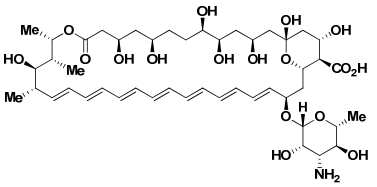

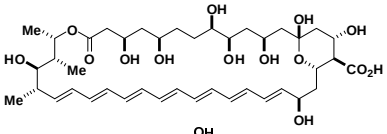

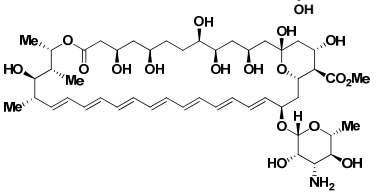

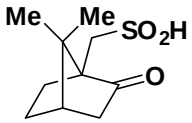

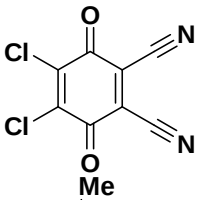

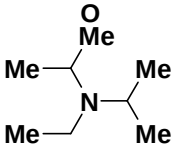

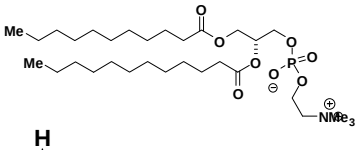

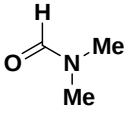

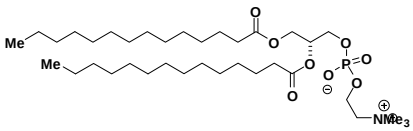

DMSO	Dimethyl sulfoxide
DPPC	1,2-dipalmitoyl-*sn*-glycero-3-phosphocholine
DQF	Double quantum filter
DSPC	1,2-distearoyl-*sn*-glycero-3-phosphocholine
eq	Equatorial
eq	Equivalents
Erg	Ergosterol
ESI	Electrospray ionization
Et	Ethyl
F-erg	5-fluoro-ergosterol
Fmoc-OSu	9-Fluorenylmethyl N-succinimidyl carbonate
gCOSY	gradient correlation spectroscopy
HMBC	Heteronuclear multi-bond coupling
HPLC	High performance liquid chromatography
HRMS	High resolution mass spectrometry
MAS	Magic angle spinning
Me	Methyl
MeAmB	C41-methyl amphotericin B
MeAmdeB	C41-methyl amphoteronolide B
MeOH	Methanol
MIC	Minimum inhibitory concentration
MLV	Multi-lamellar vesicle
MOE	Molecular operating environment
MS	Mass spectrometry

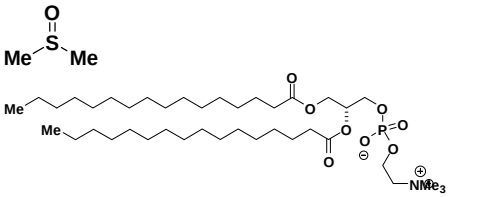

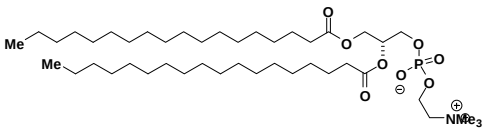

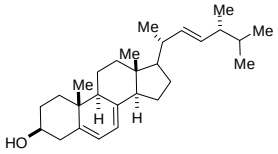

-CH_2CH_3

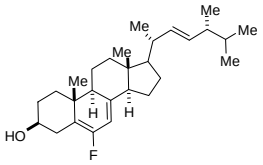

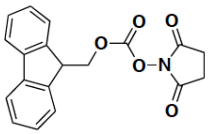

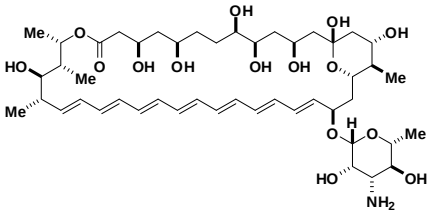

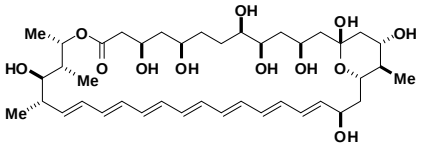

-CH_3

CH_3OH

MSP	Membrane scaffold protein	
NOE	Nuclear overhauser effect	
NOESY	Nuclear overhauser spectroscopy	
OTf	Triflate	$-OS(O_2)CF_3$
Ph	Phenyl	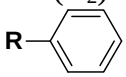
PKS	Polyketide synthase	
POPC	1-palmitoyl-2-oleoyl-*sn*-glycero-3-phospocholine	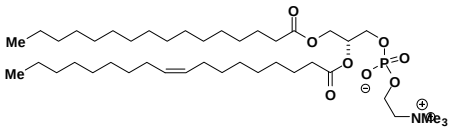
PRE	Paramagnetic relaxation enhancement	
PTFE	Polytetrafluoroethylene	
REDOR	Rotational echo double resonance	
RMS	Root mean square	
RMSD	Root mean square deviation	
ROESY	Rotating frame nuclear Overhauser effect spectroscopy	
RP-HPLC	Reverse phase high performance liquid chromatography	
RT	Room temperature	
SEC	Size exclusion chromatography	
SSNMR	Solid-state nuclear magnetic resonance	
TBDMS	tert-butyldimethylsilyl	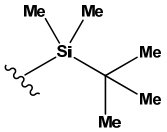
TES	Triethylsilyl	$-Si(CH_2CH_3)_3$
THF	Tetrahydrofuran	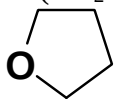
TLC	Thin-layer chromatography	
TMS	Trimethylsilyl	$-Si(CH_3)_3$
U-^{13}C-AmB	Uniformly ^{13}C-labeled AmB	
YPD	Yeast peptone dextrose	

Table of Contents

CHAPTER 1

Amphotericin B: A potent antifungal drug with capacity to perform protein-like function

1-1 AMPHOTERICIN B: DRUG OF LAST RESORT FOR SYSTEMIC FUNGAL INFECTIONS

Amphotericin B (AmB, **1**) is a clinically vital antifungal agent[1] used for treatment of severe fungal infections. Despite an expanding repertoire of antifungal agents in clinical use, life-threatening fungal infections continue to be a threat to hospitalized patients, particularly those who are immunocompromised.[2] The clinical success of AmB is a result of its broad spectrum of activity and infrequent incidence of fungal resistance to AmB–despite over 50 years of clinical use, very few instances of AmB resistance have been documented.[3,4,5,6] The use of AmB is often limited by its severe toxicity, yet it remains the drug of last resort for life-threatening fungal infections. Use of newer antifugnal agents for these infections is often limited due to resistant strains of fungi. This problem is especially pronounced in the hospital setting where treatment-resistant fungal infections are especially common. A recent epidemiological study[7] of 49 U.S. hospitals from 1995 to 2002 found that *Candida* species were the 3rd most common cause of hospital-acquired bloodstream infections, accounting for 10% of such infections. The attributable mortality rate for these infections is reported to be 40%. Thus, there remains a pressing need for safer and more effective antifungal treatments

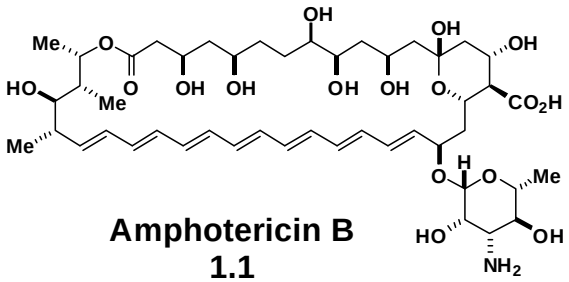

Amphotericin B
1.1

1-2 AMPHOTERICIN B: PROTOTYPE OF A SMALL MOLECULE WITH THE CAPACITY TO PERFORM PROTEIN-LIKE FUNCTION

Lack of fungal resistance to AmB is typically attributed to its unique mechanism of action. For nearly 50 years,[3,4,5,6] the leading model for its mechanism of action has been AmB self-assembly into a membrane-spanning ion channel which disrupts electrochemical gradients, ultimately causing cell death.[2] AmB thus represents a prototype of a small molecule with the capacity to perform protein-like functions. A detailed molecular understanding of AmB channel activity stands to enable efforts to harness this potential and/or improve the poor therapeutic index of AmB. Despite over 50 years of intense research on the biophysical properties of AmB, the fundamental underpinnings of how it exerts its antifungal and channel activities remain

poorly understood.[8] This chapter will detail efforts to understand the biophysical properties of AmB as well as the development and evolution of the ion channel model of AmB.

1-3 EARLY BIOPHYSICAL STUDIES OF AMPHOTERICIN B

First isolated in 1955 from the soil bacterium *Streptomyces nodosus*,[9] AmB emerged at a time when no antifungal agents were available. AmB was thus rapidly investigated for potential clinical use, and in 1958 became the first antifungal drug approved in the United States. For decades, AmB was the treatment of choice for fungal infections, and, despite its toxicity, it remains the drug of last resort for severe fungal infections.

In parallel with clinical investigation of AmB, studies of the biophysical properties of this new natural product were undertaken to determine its structure and mechanism of action. In 1958, Gottlieb[10] and coworkers reported the capacity of hexane extracts from carrots to rescue fungi from the fungicidal activity of AmB. Addition of these extracts to culture medium of *P. oxalicum* rendered these fungi resistant to AmB. Purification and analysis of a white solid from these carrot extracts identified a C_{29} sterol and it was proposed that sterols were involved in this protective mechanism. The authors thus hypothesized that AmB either inhibited the synthesis of membrane sterols or replaced sterol in a physiologically critical reaction.

Shortly after publication of this report, alternative hypotheses were proposed to explain the connection between sterols and AmB antifungal activity. Feingold demonstrated that AmB is lethal to the archaebacterium *Mycoplasma laidlawii.*[11] These bacteria have no cell wall and no membrane sterols. When grown in media containing sterol, however, the cells incorporate this sterol into their membrane. *M. laidlawii* grown in sterol-rich media were sensitive to AmB, whereas cells grown in sterol-free media were refractory to AmB. Furthermore, inoculation of refractory cells from the sterol-free culture to sterol-rich media rendered these cells sensitive to AmB. Conversely, those cells grown in the presence of sterol became refractory to AmB when subsequently cultured in sterol-free media. These experiments demonstrated the requirement of membrane sterol for cytotoxic activity of AmB, but did not illuminate the specific role of sterols in facilitating AmB cytotoxicity.

Follow-up studies in *Acheloplasma laidlawii* by DeKruijff[12] and coworkers further probed the sterol-dependence of AmB. Sterol-dependent permeabilization of model membranes by AmB had been reported (see below), and DeKruijff tested in *A. laidlawii* the hypothesis that AmB would similarly permeabilize cellular membranes in sterol-dependent fashion. Addition of

AmB to suspensions of *A. laidlawii* grown in the presence of cholesterol resulted in rapid, robust efflux of K^+ from the cells. In contrast, when AmB was added to suspensions of *A. laidlawii* grown under sterol-free conditions, no permeability was observed. A variety of sterols were then screened, and it was discovered that a 3β-hydroxyl group and a hydrophobic side chain at C17 were required for permeability, implying a direct role of sterol in mediating cell membrane permeability.

This membrane-permeabilizing activity of AmB garnered significant attention, yet the specifics of how AmB induces ion permeability remained unclear. Three possible mechanisms for this membrane-permeabilizing activity were explored in planar lipid bilayer conductance studies: physical destruction of the phospholipid bilayer, ionophoric transport, and discrete single ion channel formation. Planar lipid bilayers provided means to study AmB-induced conductance on small patches of membrane while also giving the researcher the ability to carefully control the composition of the membrane.

Andreoli and Monahan[13] studied the effects of AmB on planar lipid bilayers formed from sheep erythrocyte lipids. Upon addition of AmB, the resistance of the membrane decreased by 6 orders of magnitude without disrupting the integrity of the membrane. When lipids used to form the membrane were sterol-depleted, AmB had no effect on membrane resistance or stability. This membrane stability in the presence of AmB argued strongly against membrane disruption as a mechanism through which AmB exerts its membrane permeabilizing activity.

To investigate the possibility that AmB acts via ionophoric transport, Cass et al.[14] characterized the membrane conductance properties of AmB in comparison to the ionophoric peptide valinomycin. This protein acts as a carrier to bind and transport one potassium ion at a time across the membrane. Two key experiments identified fundamental differences in how these molecules create ion conductance. First, the relationship between concentration and conductance was measured. For valinomycin, conductance was directly proportional to concentration of valinomycin. The conductance in the presence of AmB increased as a function of $[AmB]^n$, with $n > 4$. Temperature dependence of conductance was also measured. In the case of valinomycin, conductance increased with increasing temperature. For AmB, however, increases in temperature resulted in marked decrease in conductance. The stark contrast between these observations for valinomycin and AmB strongly support the conclusion that AmB does not function via an ionophoric mechanism. The properties of AmB-impregnated membranes in these experiments

are, however, consistent with a self-assembled supramolecular complex stabilized by non-covalent interactions.

In 1976, Ermishkin and coworkers[15] reported single ion channel recordings produced by AmB in planar lipid bilayer experiments. This report marked the first definitive evidence for a discrete AmB ion channel with distinct electrophysiological properties. Strikingly, these channel recordings clearly displayed defined open and closed states, with a step function of constant amplitude for the open state just as would be observed for a protein ion channel (Figure 1-1). Moreover, events were observed in which the current doubled, consistent with opening of a second identical ion channel. Follow-up studies demonstrated that this ion channel could be blocked with tetraethylammonium cations, a property that has also been reported for some protein ion channels. While this discovery represented a major breakthrough in the understanding of the biophysical properties of AmB, the role of the AmB ion channel in antifungal activity, if any, remained unknown. However, this theory quickly took hold, and over 30 years later, the AmB ion channel remains the leading model for the antifungal activity of AmB.

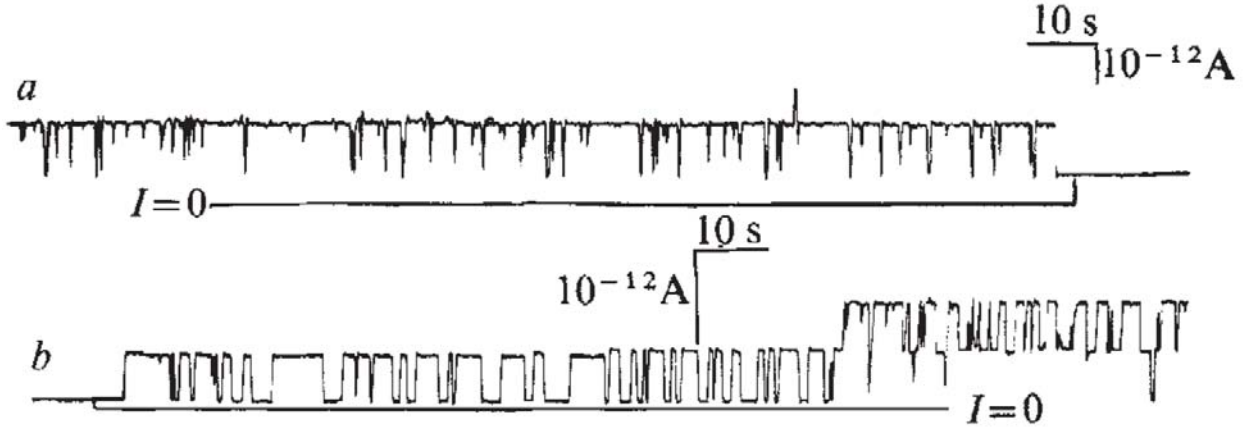

Figure 1-1. Membrane current in the presence of 3 x 10^{-8} M AmB (A) and 1 x 10^{-7} M AmB (B). These single ion channel recordings of AmB in planar lipid bilayers provided the first direct evidence that AmB forms discrete ion channels with defined electrophysiological properties. Used with permission from Ermishkin et al. *Nature* **1976**, *262*, 698-699. ©Nature Publishing Group

1-4 DEVELOPMENT OF THE BARREL-STAVE MODEL FOR THE AMPHOTERICIN B ION CHANNEL

The discovery of AmB also sparked the interest of natural products chemists, and efforts to elucidate the structure of AmB rapidly followed. Elucidating even the primary structure of complex natural products in the 1950s and 1960s was a long and laborious process, relying on

tedious attempts at crystallization and degradation to less complex products which could be fully characterized to draw conclusions about the structure of the parent natural product. Then, as if putting together a jigsaw puzzle of chemical structures, proposals were made for the structure of the natural product. Iterative application of this process by several research groups (including Dutcher,[16] Cope,[17] and Borowski[18]) culminated in the 1970 report of the full structure of AmB by Borowski and coworkers.[18] That same year, the stereochemical assignments of the 19 stereocenters of AmB were reported by Ganis and coworkers[19] on the basis of crystallographic analysis of *N*-iodoacetyl AmB, and the full crystal structure, confirming Borowski's structure, was reported the following year. Borowski later confirmed[20] by solution NMR conformational analysis that the solution conformation of the AmB monomer in pyridine/MeOH matched that observed in the crystal structure.

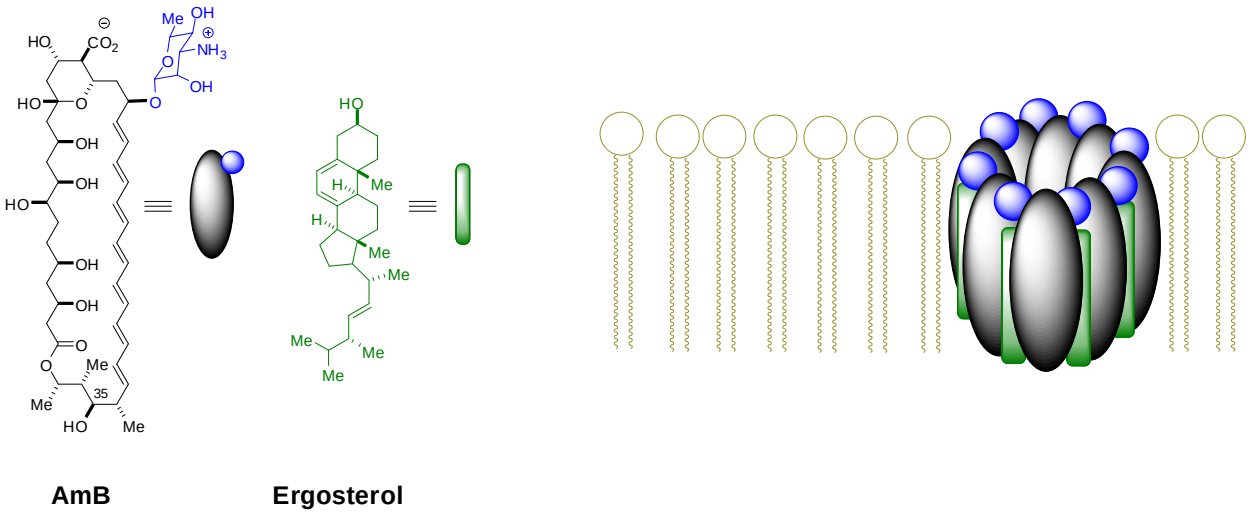

Figure 1-2. Schematic representation of the barrel stave AmB ion channel model.

The discovery of the chemical structure of AmB directly enabled proposal of the now classic barrel-stave model of the self-assembled AmB ion channel (Figure 1-2). In 1973-74, Andreoli,[21] de Kruijff,[12] and Finkelstein[22] each proposed very similar structural models for the AmB ion channel, and elements of each contributed to the current leading model of the AmB ion channel. These models were based on the known biophysical properties of AmB in phospholipid bilayers, and yet are strikingly similar given that they were proposed in parallel. Each model included the same general features:

1. AmB assembles vertically (parallel to the bilayer normal) to form a pore such that the hydrophobic polyene is oriented toward the channel periphery, thus enabling van der

2. The AmB polyol is thus oriented inward toward the conductive portion of the channel, allowing water, ions, and small polar molecules to pass through.
3. The assembled pore interacts with one leaflet of the bilayer. Conspicuously, AmB is ~24 Å in length, or approximately one-half the length of a physiological bilayer (ref. Andreoli 1974).
4. The pore has an interior diameter of approximately 7-10 Å.[12] This feature is based on the observations that glucose permeability through AmB-impregnated membranes is very low and sucrose has no permeability through such membranes.

The model proposed by de Kruijff and Demel was based primarily on these 4 postulates and was constructed from CPK models of AmB and cholesterol (Figure 1-3) to form a barrel-stave pore. In addition, the authors proposed that either one of these ion channel pores spanned just one bilayer leaflet, and thus two adjacent pores were required to span the full bilayer or that the membrane dimples to match the length of a single AmB aggregate (Figure 1-4).[23]

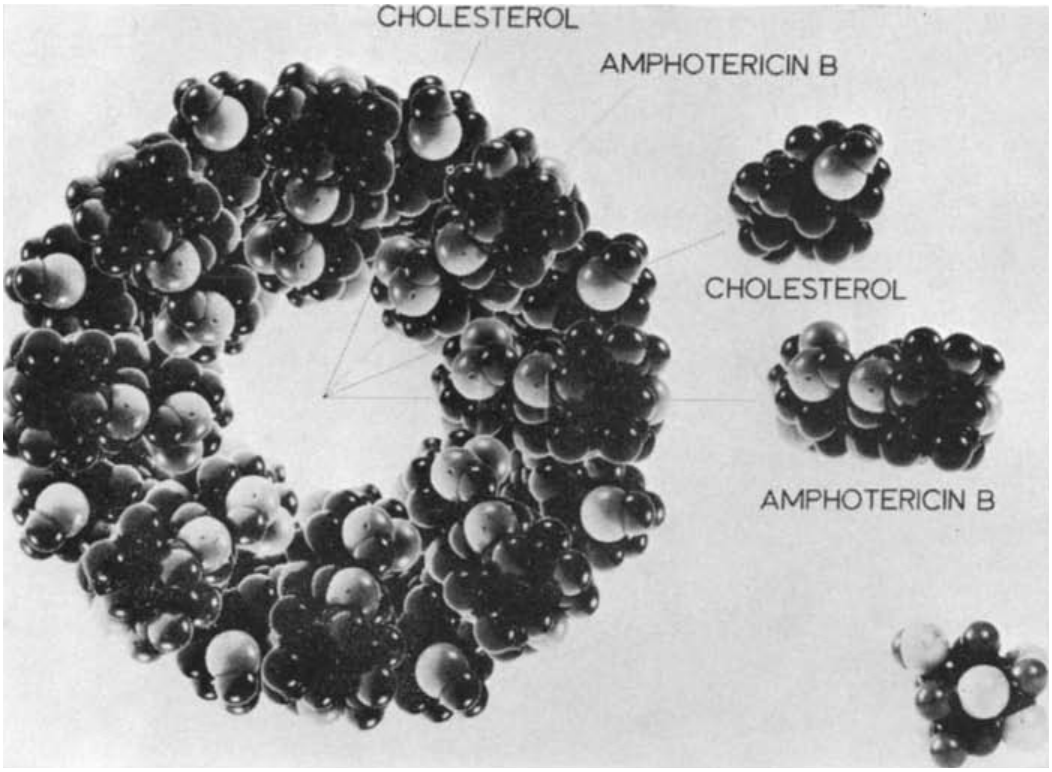

Figure 1-3. CPK model of the AmB ion channel reported by DeKruijff and Demel. Used with permission from de Kruijff and Demel R.A. *Biochim. Biophys. Acta* **1974**, *339*, 57-70. ©1974 Elsevier B.V. ©Elsevier

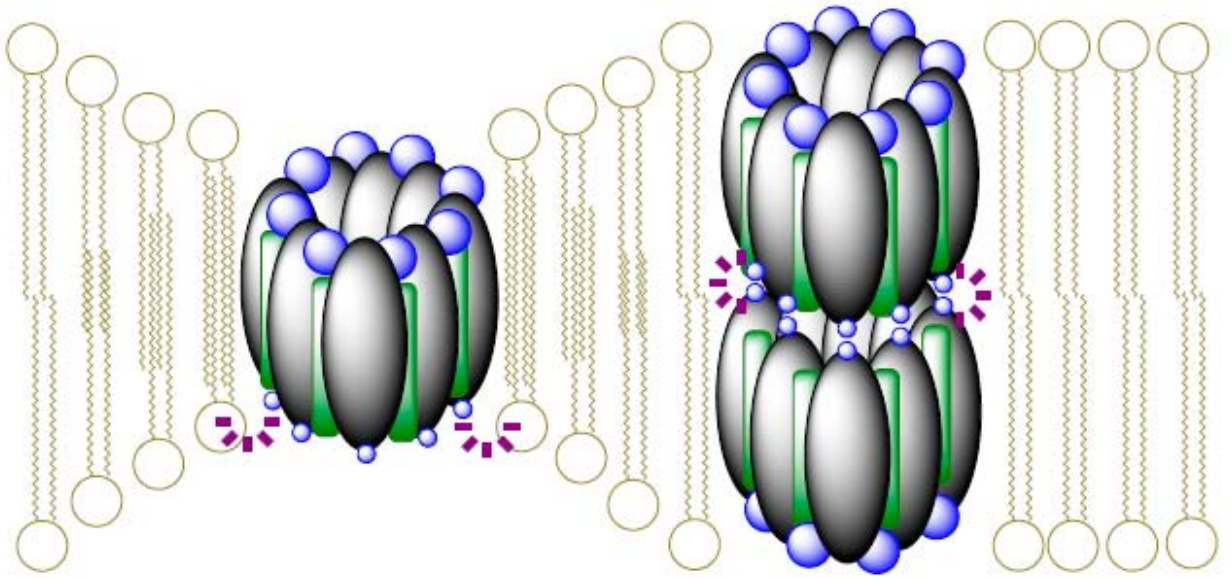

Figure 1-4. DeKruijff and coworkers proposed two possible models for AmB pores in phospholipid membranes: either two pores are required to span the bilayer (right) or the bilayer dimples to match the length of a single pore. Used with permission from Gray, K.C.; Palacios, D.S.; Dailey, I.; Endo, M.M.; Uno, B.E.; Wilcock, B.C.; Burke, M.D. *Proc. Natl. Acad. Sci. USA,* **2012**, *109*, 2234-2239. ©2012 National Academy of Sciences of the United States of America

Andreoli proposed a two-dimensional cross-sectional model which incorporated the additional observation that sterols with a 3β hydroxyl are required for AmB to induce membrane permeability (Figure 1-5) (ref Andreoli and de Kruijff). Specific hydrogen-bonding interactions were proposed, one involving the sterol hydroxyl proton and the carbonyl of the C41 carboxylate (Figure 1-5, left) and the other involving the sterol hydroxyl oxygen and the C17 hydroxyl proton. Interestingly, included in this report was the observation that the methyl ester of AmB induced membrane permeability and thus the proposed interaction to sterol involved the carbonyl, and not the -OH, of the C41 carboxyl group (see below for further discussion of the carboxyl and amine). Andreoli specifically commented that other polar interactions between the sterol and AmB were possible. This structural model did not go so far as to propose a channel stoichiometry or a 3-dimensional channel structure, stating simply, "it is amusing to note that a cylindrical structure…can be constructed from eight space-filling models of ampohotericin B that alternate with cholesterol models."

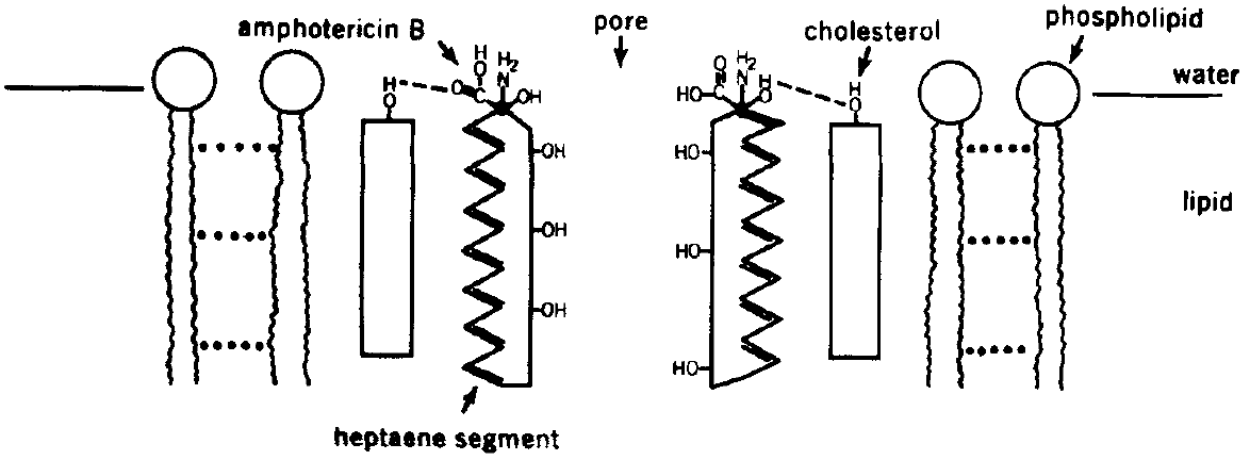

Figure 1-5. Cross sectional view of the model of the AmB ion channel proposed by Andreoli. Used with permission from Andreoli, T. *Ann. N.Y. Acad. Sci.* **1974**, *235*, 448-468. ©John Wiley & Sons, Inc.

1-5 SALT BRIDGE MODEL OF CHANNEL STABILIZATION

The now classic barrel-stave model was further refined in subsequent years to include a proposed intermolecular ring of stabilization of the AmB ion channel by polar interactions between the functional groups at C41 and C3'. Kasumov et al.[24] proposed these polar interactions on the basis of single ion channel recordings of AmB and two derivatives covalently modified at either C41 or C3', AmB methyl ester (AmE), and *N*-acyl AmB. These derivatives gave rise to a much shorter active channel lifetime, and thus there was a much lower probability that these channels were conducting ions at any given time. Moreover, both AmE and *N*-acyl AmB required much higher concentrations to form ion channels. Interestingly, the conductance of the three ion channel recordings did not vary significantly among the three molecules. The authors concluded that the loss of charged groups at the C41 and C3' positions led to a less stable ion channel due to a loss of electrostatic stabilization. Thus, the stability of the native AmB ion channel was assumed to be associated with electrostatic interactions between C41 and C3'.

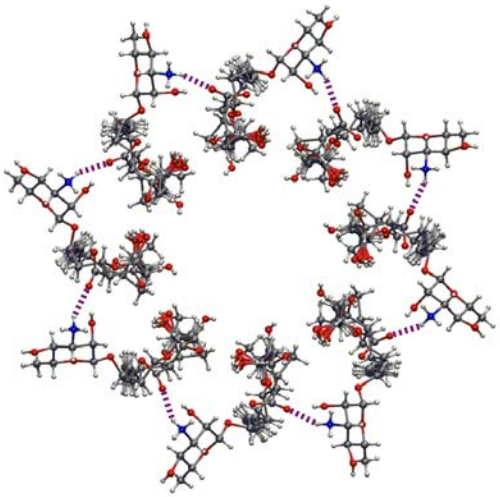

Figure 1-6. Schematic "top-down" view of the barrel-stave ion channel model with intermolecular salt bridges marked with purple dashes. Adapted with permission from Palacios, D.S.; Anderson, T.M.; Burke, M.D. J. Am. Chem. Soc. 2007, 129, 13804-13805. ©2007 American Chemical Society.

Two considerations complicate interpretation of structure/function data for covalently modified

AmB derivatives. First, self-assembly of small molecules is remarkably sensitive to steric perturbations.[25,26] As a result, discriminating between steric effects and disruption of hydrogen bonding is challenging. Second, as noted by Borowski et al.,[27] AmB derivatives esterified at C41 retain a polar carbonyl and still possess the ability to form polar interactions with mycosamine. Borowski specifically proposed that the carbonyl of the methyl ester of AmB retains this capacity and therefore retains capacity for channel formation and fungicidal activity.

Conspicuously, the carboxyl and amine groups proposed to be critical for channel stabilization are installed biosynthetically as post-polyketide synthase (PKS) modifications of the macrolide core (Figure 1-7)[28,29]. PKS enzymes assemble this core structure of AmB, after which tailoring enzymes complete the biosynthesis: AmphL cytochrome P450, AmphN cytochrome P450, and AmphDI glycosyl transferase enzymes catalyze installation of the C8 alcohol, exhaustive oxidation at C41, and attachment of mycosamine to the C19 alcohol, respectively.

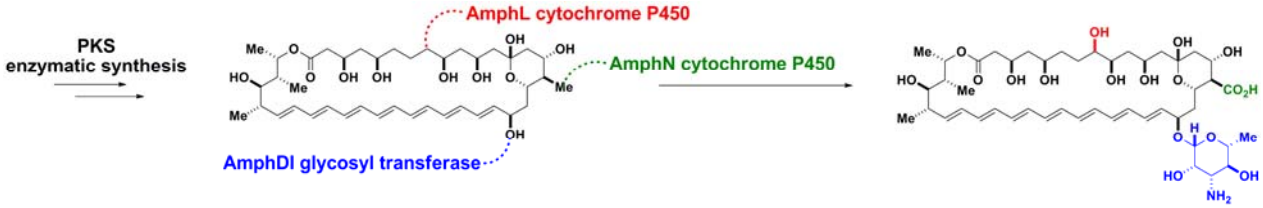

Figure 1-7. AmB is biosynthesized via PKS enzymes. Post-PKS tailoring modificatins install the C41 carboxyl and mycosamine, the 2 functional groups predicted to be critical for stabilizing the active ion channel.

The salt bridge hypothesis was further supported by computational modeling studies. The first of these studies was a molecular mechanics study.[30] These calculations predicted a 4.6 Å distance between the carboxyl and amine, and the stabilization of the complex was attributed primarily to these 8 salt bridge interactions. Subsequently, molecular dynamics simulations were performed by McCammon and coworkers.[31] These calculations similarly predicted intermolecular hydrogen bonding between adjacent carboxylate and amine groups as the primary force for stabilizing the channel complex. A second molecular dynamics study by Baginski and coworkers[32] again predicted this ring of hydrogen bond stabilization. Interestingly, these interactions were calculated to be stronger in the presence of ergosterol than when cholesterol was used as the sterol between AmB molecules. The authors emphasized that derivatives that modify the amine likely perturb this hydrogen bonding interaction leading to an inactive compound. A major limitation of computational studies such as those discussed here is that they are designed to study the AmB ion channel and starting conditions for the calculations arrange

AmB in a channel-like AmB assembly. Thus, the results are biased toward the existing ion channel and salt bridge model.

Many studies have probed contributions of the C41 carboxylate and C3' ammonium to AmB channel and antifungal activity by covalent modification at these positions.[8e,33,34,35] Briefly, *N*-acylated AmB derivatives are inactive, whereas esterification at C41 produces derivatives which are roughly equipotent to AmB itself. Borowski and coworkers[33] have reported an extensive series of derivatives esterified at C41 and/or alkylated/acylated at C3' that demonstrated this trend. It was reported that a positive charge at the amine was required to maintain antifungal and K^+ efflux activity, while a variety of ester substituents were tolerated at C41 without a significant decrease in activity.

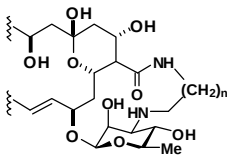

1.3 n=3
1.4 n=5
1.5 n=7

Another example[36] is the report by Murata and coworkers in which intramolecular bridges were used to link the C41 carboxylate directly to the C3' amine (**1.3-1.5**). These compounds had markedly diminished antifungal and K^+ efflux activity, with the exception of **1.4** with n=5 which had good efflux activity but poor antifungal activity. Based on modeling of this compound, the authors drew conclusions about the active conformation of AmB.

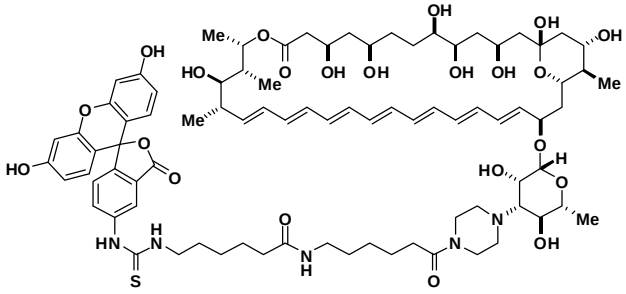

1.6

Another example[8e] of the covalent modifications approach is the AmB-fluorescein conjugate (**1.6**) synthesized by Carreira and coworkers. This compound displayed K^+-efflux activity but was completely inactive in antifungal assays. Fluorescence and microscopy studies of this compound in yeast and mammalian cells showed that the molecule localized inside mammalian cells but was localized at the membrane in yeast cells.

1-6 SOLUTION NMR STUDIES OF AMPHOTERICIN B

Due to inherent size limitations, solution NMR has been of limited utility to study the function of AmB. However, this technique has proved useful for studying the structure of monomeric AmB in solution. In 1992, Borowski[20] and coworkers reported a solution NMR conformational analysis of AmB protected at C41 as the methoxycarbonylmethylamide. ^1H

coupling constants were used to calculate dihedral angles according to Karplus relationships,[37] and ROESY studies were employed to identify proximal protons. From these data, a structure was proposed. This structure was in very good agreement with the *N*-iodoacetyl AmB crystal structure, thus demonstrating that AmB derivatives bearing covalent modifications at C41 or C3' have the same ground state conformation.

1-7 SOLID-STATE NMR STUDIES OF AMPHOTERICIN B

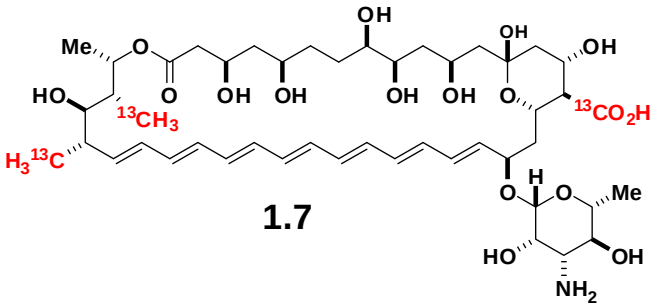

1.7

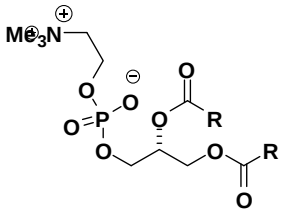

R = $-(CH_2)_nCH_3$

DLPC, n = 10
DMPC, n = 12
DPPC, n = 14
DSPC, n = 16

In attempts to study the AmB ion channel, Murata and coworkers[38] employed rotational echo double resonance[39] (REDOR) SSNMR experiments for AmB in the presence of lipid bilayers. The REDOR experiment identifies ^{13}C nuclei proximal to phospholipid ^{31}P nuclei by taking advantage of the dipolar coupling interaction between these nuclei. It is thus possible to assess whether a nucleus resides proximal to the phospholipid head group. Biosynthetically prepared[28] tri-^{13}C-AmB (**1.7**) was used in this initial report. In this study, multi-lamellar vesicles (MLVs) composed of **1.7** and the fully saturated lipids 1,2-dimyristoyl-sn-glycero-3-phosphocholine (DMPC) or 1,2-distearoyl-sn-glycero-3-phosphochiline (DSPC) were analyzed for REDOR dephasing of AmB ^{13}C nuclei by lipid ^{31}P nuclei. Modest dephasing was observed for all three ^{13}C labels of tri-^{13}C-AmB in the presence of DMPC. In the presence of DSPC, dephasing was observed only at the carboxyl carbon. From these results, it was concluded that AmB inserts vertically in bilayer membranes and forms a double pore channel in the presence of DSPC and a single pore channel in the presence of the shorter DMPC. These results are depicted in Figure 1-8.

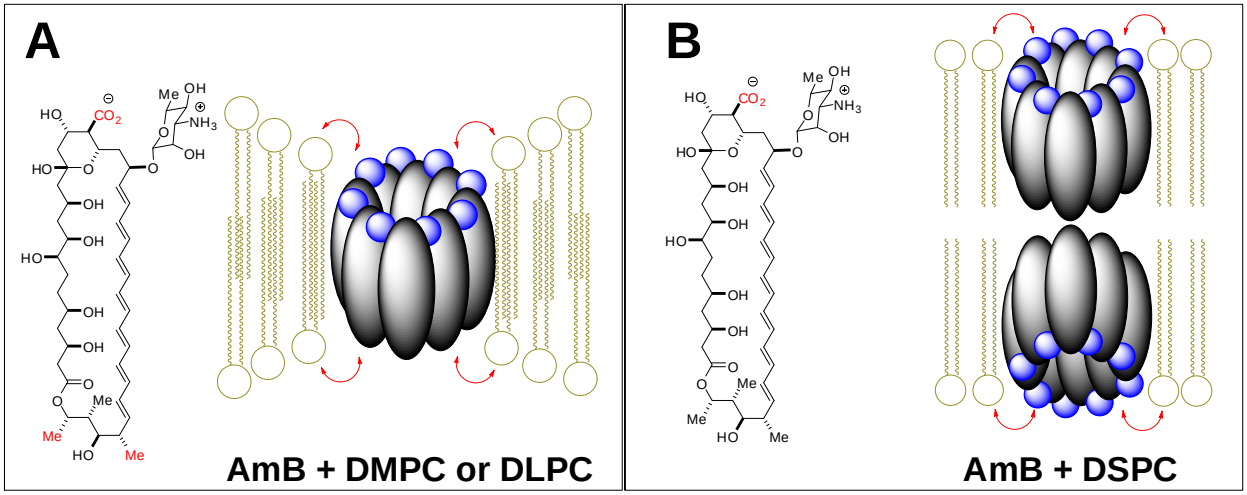

Figure 1-8. Visual depiction of REDOR dephasing and subsequent interpretation. A) In the presence of DMPC or DLPC (no sterol present), the nuclei shown in red are moderately dephased. This was interpreted as evidence for a single pore membrane-spanning channel, depicted schematically with red arrows indicating sites of REDOR dephasing. B) When longer DSPC lipids are used, only C41 (red) is moderately dephased. This was interpreted as evidence for a double pore channel..

Two limitations of these experiments are noteworthy. First, the lipid system was devoid of sterol, yet AmB is known to manifest its biological activity only in membranes containing sterols.[40] Second, the lipids used in these studies were fully saturated, whereas biological membranes contain a substantial proportion of unsaturated lipids. As described in Chapter 3, this distinction has important biophysical consequences that impact the activity of AmB.

A follow-up study[41] examined uniformly ^{13}C-labelled AmB (~15% ^{13}C incorporation) in vesicles comprised of an alternative phospholipid, 1,2-dilauroyl-*sn*-glycero-3-phosphochline, which possess very short (C12) and fully saturated acyl chains.. Modest REDOR dephasing was again observed for the C41 and C38/C39 sites, but no REDOR dephasing was reported for carbons comprising the polyene region. From these data, it was concluded that, in this bilayer comprised of very short lipids, AmB is inserted into the membrane and a single barrel spans the entire membrane. Again, the use of sterol-free unsaturated lipids compromise the significance of these studies. The use of C12 acyl chains, which are rarely observed in natural systems, raises further questions regarding the physiological relevance of these findings. These results are also depicted in Figure 1-8.

Another SSNMR study[42] by Murata and coworkers analyzed a fluorinated ergosterol derivative (F-erg, **1.8,** Figure 1-9A) in the presence of U-^{13}C-AmB in DMPC MLVs. ^{13}C-^{19}F REDOR studies were performed, but no REDOR dephasing of AmB was observed. A tethered F-erg / AmB conjugate (**1.9**, Figure 1-9B) was synthesized and REDOR studies were performed on this molecule. REDOR dephasing of AmB C1' and the AmB polyene were observed. It was concluded due to the lack of intermolecular ^{13}C-^{19}F REDOR effects that ergosterol may be surrounding the AmB ion channel, rather than interdigtiated with AmB.

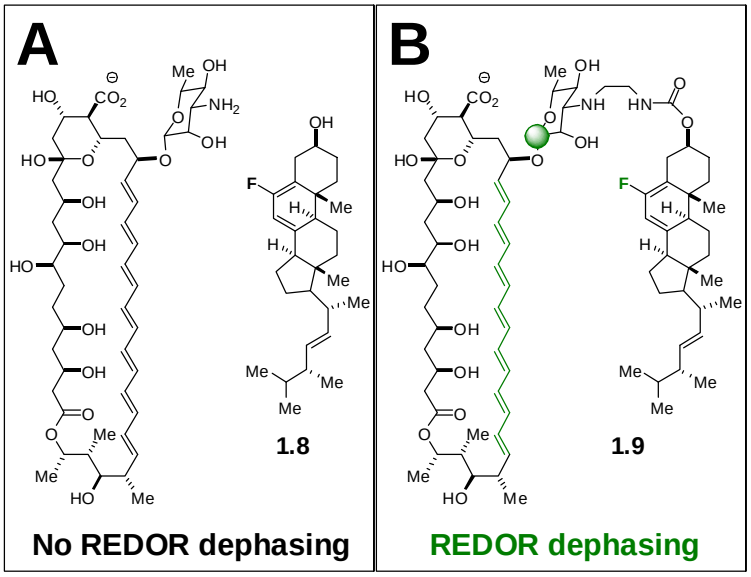

Figure 1-9. A) No REDOR dephasing was observed for AmB in the presence of F-erg. B) When F-erg was tethered to AmB, REDOR dephasing was observed to C1' and the AmB polyene.

In another series of studies,[43] Murata and coworkers studied orientation effects of the sugar. To do this, tethered molecules were synthesized in which the C41 carboxyl was tethered to the amine through an intramolecular bridge. One such compound (**1.10**, Figure1.10), contained a 1-^{13}C-, ^{15}N-glycine linker. This compound was incorporated into DMPC MLVs containing ergosterol for SSNMR analysis. The dipolar coupling for this ^{13}C-^{15}N pair was measured to be ~200 Hz, and from this it was concluded that the molecule was immobilized on a timescale of >5 ms (1/200 Hz). The authors thus concluded that this derivative existed in a rigid limit and therefore was part of a complex greater than 20 nm in diameter.

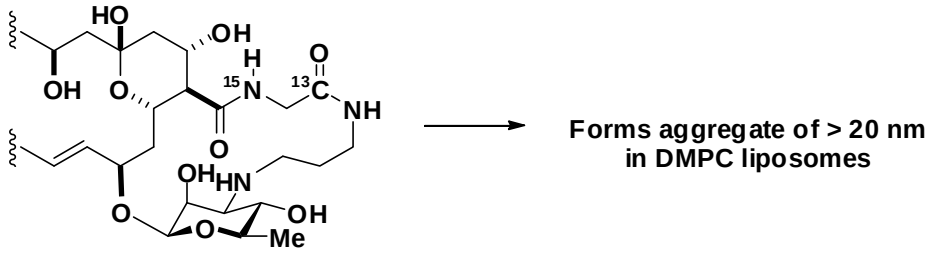

1.10

Figure 1-10. An intramolecularly bridged derivative was judged to immobilize as part of a >20 nm complex in DMPC liposomes on the basis of a C-N dipolar coupling of 200 Hz.

The Murata group has more recently reported some SSNMR studies in MLVs derived from the mixed saturated, unsaturated lipid POPC (**1.11**). The first of these studies[44] sought to more fully characterize the AmB ion channel by mixing 14-fluoro-AmB (**1.12**) and tri-^{13}C-AmB in POPC liposomes. ^{13}C-^{19}F REDOR was thus used to measure the intermolecular ^{13}C-^{19}F dephasing at AmB C41. In POPC MLVs lacking sterol as well as those incorporating cholesterol, the ^{13}C-^{19}F distance was calculated to be 10.3 Å. In ergosterol-containing POPC MLVs, the calculated distance increased to 12.1 Å. The authors concluded that ergosterol increases the distance between adjacent AmB molecules in the channel complex. In contrast to the model proposed in their study of the F-erg-AmB conjugate, it was now proposed that ergosterol does intercalate between adjacent AmB molecules.

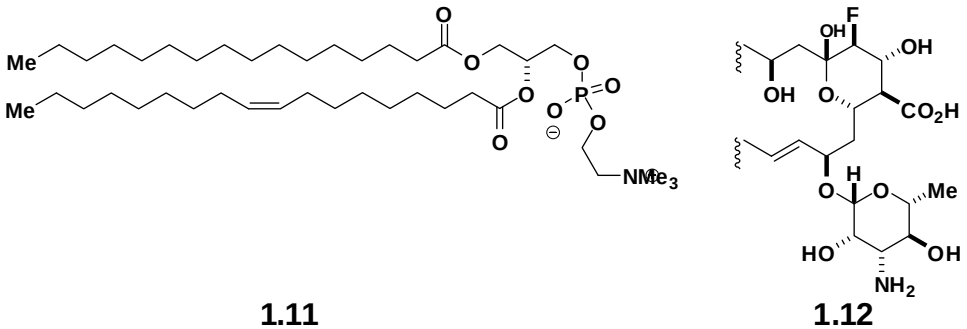

1.11 **1.12**

A ^{2}H-NMR study[45] of a deuterated AmB derivative, AmB-d_6 **1.13** and deuterated sterols ergosterol-d_1 **1.14** and cholesterol-d_1 **1.15** further supported a model in which AmB interacts more closely with ergosterol than with cholesterol. This study was based on the work of Dufourc[46] showing that the ^{2}H spectrum of cholesterol-d_1 was not significantly perturbed by AmB. Murata and coworkers performed similar experiments on cholesterol-d_1 and ergosterol-d_1 in POPC MLVs in the presence of increasing amounts of AmB. Conversely, the spectrum of

AmB-d_6, was analyzed for the same series of AmB/ergosterol ratios. Deuterium powder spectra for each molecule were analyzed for changes in the presence of AmB. The cholesterol-d_1 spectrum was not substantially perturbed by AmB, whereas the spectrum of ergosterol-d_1 coalesced toward the isotropic center peak. It was concluded that the fast axial diffusion of ergosterol was inhibited by AmB. Based on the spectra of AmB-d_6, it was concluded that AmB is also immobilized under the same conditions. From the similar mobility of AmB and ergosterol, it was concluded that these two molecules have a direct interaction in POPC vesicles. Lack of perturbation of the cholesterol-d_1 spectrum led the authors to conclude that AmB has a weaker intermolecular interaction with cholesterol. Importantly, in other studies Murata and coworkers concluded that AmB does not bind cholesterol.[47] In addition, it had remained controversial whether AmB binds directly to ergosterol[3,12,27,30,31,32,42,45,48,49,50,51] or whether AmB's sterol-dependence was an indirect consequence of membrane sterol content,[47,52,53,54,55,56,57,58,59,60] and Baginski recently reported[47] that this issue remained unresolved.

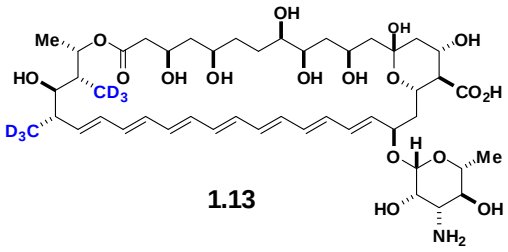

1.13

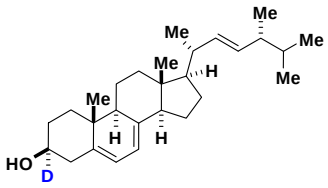

1.14

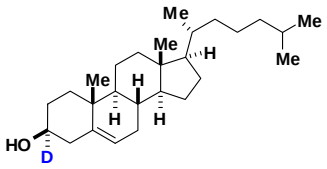

1.15

The Murata group also recently reported ^{13}C-^{19}F REDOR studies of 14-fluoro-AmB and a skipped ^{13}C-labeled ergosterol (**1.16**, Figure 1-11) in POPC MLVs.[48] These experiments revealed dephasing of ergosterol C19, C21, C26, and C27 in the presence of 14-fluoro-AmB. In addition, ^{13}C-^{31}P REDOR revealed dephasing of ergosterol C26 and C27 by ^{31}P of POPC. Viewed through the lens of the leading ion channel model for the mechanism of action of AmB and the previously described REDOR studies in saturated lipids, it was concluded based on these latest REDOR results that the AmB ion channel is comprised of both "head-to-head" and "head-to-tail" orientation of AmB and ergosterol. Importantly, however, the ^{13}C-^{31}P REDOR experiments that were previously performed in saturated lipids devoid of ergosterol were not repeated in this POPC-based system. Also significantly, to the best of our knowledge, direct ^{13}C-^{31}P REDOR dephasing between AmB and POPC or any other unsaturated lipid has not been reported.

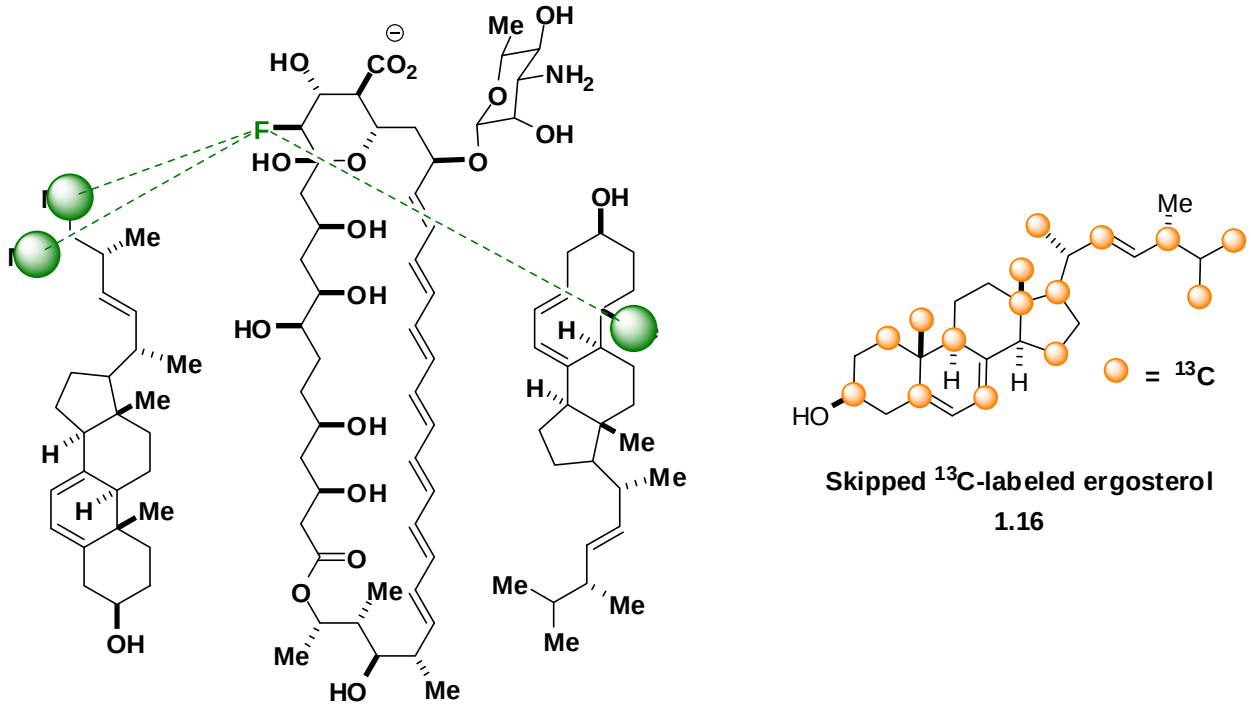

Figure 1-11. Shown at right is the skipped 13C-labeled ergosterol used for 13C-19F REDOR experiments. At left, green spheres indicate nuclei dephased by 19F. The authors proposed both head-to-tail and head-to-head interactions of AmB with ergosterol.

As described above, we recognized limitations with the aforementioned studies that complicated interpretation of the reported results. Most importantly, no functional validation of the liposome system was reported. In particular, the MLVs composed of saturated lipids (DMPC, DLPC, DSPC) contained no sterol. The functional relevance of studying AmB in this type of system remains controversial. As will be described in chapter 3, POPC/AmB/Ergosterol MLVs have been found to be a physiologically relevant bilayer system. However, interpreting the above data through the lens of the prior studies with saturated lipids complicates collective data interpretation. Moreover, as will be described in chapter 3, studies from our group have revealed that AmB primarily kills yeast by simply binding ergosterol – channel formation is actually not required.

1-8 SUMMARY

For nearly 40 years, two hypotheses have been the driving force for experiments probing the activity of AmB: 1) AmB primarily inserts in membranes to form discrete ion channel pores, and 2) these ion channel pores are stabilized primarily by a ring of polar interactions between the C41 carboxylate and the C3' amine. This dissertation describes experiments that test both of these hypotheses. We have developed an alternative to the covalent modification strategy for studying the functional groups of AmB which involves synthetically deleting the functional group in question, determining the conformation of the resulting compound, and determining the biophysical and biological consequences of this deletion. This method is analagous to the protein technique of alanine scanning which determines the functional role of individual amino acids by systematically replacing them with alanine. In this type of an approach, conformational analysis is critical to rule out the possibility that conformational changes are responsible for observed changes in function.

Applying this functional group deletion strategy to AmB, we synthesized C41-methyl amphotericin B, amphoteronolide B, and C41-methyl amphoteronolide B (**1.7** through **1.9**) lacking either one (**1.7** and **1.8**) or both (**1.9**) of the functional groups predicted to be critical for stabilizing the amphotericin B ion channel. In stark contrast to the leading hypothesis of AmB antifungal activity, C41-methyl AmB, which lacks the capacity to form the predicted ring of channel stabilizing polar interactions, is equipotent to the natural product. This work will be detailed in Chapter 2.

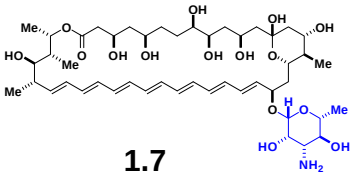

1.7

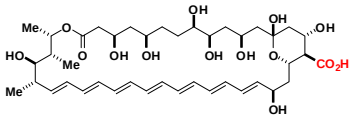

1.8

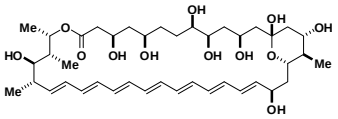

1.9

Moreover, we have developed a SSNMR method for probing the primary location of AmB in phospholipid bilayers using paramagnetic spin-labeled phospholipids. These paramagnetic probe reagents have a dramatic impact on T1 relaxation of POPC ^{13}C nuclei. Strikingly, no such perturbation was observed for AmB ^{13}C nuclei, indicating that the majority of AmB is not localized within the phospholipid bilayer. Moreover, additional experiments have revealed that extramembranous aggregates of AmB extract ergosterol from bilayer membranes, providing both a structural and functional foundation for our observations that sterol binding is in

fact the primary mechanism by which AmB kills yeast. This work will be detailed in Chapters 3 and 4.

REFERENCES

1) Kontoyiannis, D.P.; Lewis R.E. *Lancet* **2002**, *359*, 1135-1144.
2) Snydman, D.R. *Chest* **2003**, *123*, 500S-503S.
3) Bolard, J. *Biochim. Biophys. Acta* **1986**, *864*, 257-304.
4) Hartsel, S.D.; Hatch, C.; Ayenew, W. *J. Liposome Res.* **1993**, *3*, 377-408.
5) Cereghetti, D.M.; Carreira, E.M. *Synthesis* **2006**, *6*, 914, 942.
6) Hartsel, S.; Bolard, J. *Trends Pharm. Sci.* **1996**, *17*, 445-449.
7) Wisplinghoff, H.; Bischoff, T.; Tallent, S.M.; Seifert, H.; Wenzel, R.P.; Edmond, M.B.; *Clin. Infect. Dis.* **2004**, *39*, 309-317.
8) (a) HsuChen, C.C.; Feingold, D.S. *Nature* **1974**, *251*, 656-659. (b) Chen, W.C.; Chou, D.-L.; Feingold, D.S. *Antimicrob. Agents Chemother.* **1978**, *13*, 914-917. (c) Brajtburg, J.; Powderly, W.G.; Kobayashi, G.S.; Medoff, G. *Antimicrob. Agents Chemother.* **1990**, *34*, 183-188. (d) Beggs, W.H. *Antimicrob. Agents Chemother.* **1994**, *38*, 363-364. (e) Zumbuehl, A.; Jeannerat, D.; Martin, S.E.; Sohrmann, M.; Stano, P.; Vigassy, T.; Clark, D.D.; Hussey, S.L.; Peter, M.; Peterson, B.R.; Pretsch, E.; Walde, P.; Carreira, E.M. *Angew. Chem. Int. Ed.* **2004**, *43*, 5181-5185.
9) (a) Sternberg, T.H.; Wright, E.T. Oura, M. *Antibiot. Ann.* **1955-1956**, 566-573; (b) Steinberg, B.A.; Jamber, W.P.; Suydam, L.O. *Antibiot. Ann*. **1955-1956**, 574-578; (c) Gold, W.; Stout, H.A.; Pagano, J.F.; Donovick, R. Antibiot. Ann. 1955-1956, 579-586; (d) Vandeputte, J.; Wachtel, J.L.; Stiller, E.T. Antibiot. Ann. 1955-1956, 587-591.
10) Gottleib, D.; Carter, H.E.; Sloneker, J.H.; Amman, A. *Science* **1958**, *128*, 361.
11) Feingold, D.S. *Biochem. Biophys. Res. Commun*. **1965**, *19*, 261
12) DeKruijff, B.; Demel R.A.; *Biochim. Biophys. Acta* **1974**, *339*, 57-70
13) Andreoli, T.E.; Monahan, M. *J. Gen. Physiol.* **1968**, *52*, 300-325
14) Cass, A.; Finkelstein, A.; Krespi, V. *J. Gen. Physiol.* **1970**, *56*, 100-124
15) Ermishkin, L.N.; Kasumov, K.M.; Potzuleyev, V.M. *Nature* **1976**, *262*, 698-699
16) Dutcher, J.D.; Walters, D.R.; Wintersteiner, O. *J. Org. Chem.* **1963**, *28,* 995-999.
17) Cope, A.C.; Axen, U.; Burrows, E.P.; Weinlich, J. *J. Am. Chem. Soc.* **1966**, *88,* 4228-4235.
18) Borowski, E.; Zieliński, J.; Ziminski, T.; Falkowski, L.; Kołodziejczyk, P.; Golik, J.; Jereczek, E. *Tetrahedron Lett.* **1970**, *11,* 3909-3914.
19) Mechlinski, W.; Shaffner, C.P.; Ganis, P.; Avitabile, G. *Tetrahedron Lett.* **1970**, *11,* 3873-3876.
20) Sowinski, P.; Pawlak, J.; Borowski, E.; Gariboldi, P. *Magn. Res. Chem.* **1992**, *30*, 275-279.
21) Andreoli, T.E. *Ann. N.Y. Acad. Sci.* **1974**, *235*, 448-468.
22) Finkelstein, A.; Holz, R. in *Membranes* vol. 2. Lipid Bilayers and Antibiotics. Eisenman, G. Editor, Marcel Dekker, Inc., New York, **1973**, 377-408.
23) Hoogevest, P.V.; de Kruijff, B. *Biochim. Biophys. Acta* **1978**, *511*, 397-407.
24) Kasumov, Kh.M.; Borisova, M.P.; Ermishkin, L.N.; Potseluyev, V.M.; Silbershtein, A. Y. *Biochim. Biophys. Acta* **1979**, *551*, 229-237
25) Umegawa, Y.; Matsumori, N.; Oishi, T.; Murata, M. *Tetrahedron Lett.* **2007**, *48*, 3393-3396.
26) Matsumori, N.; Sawada, Y.; Murata, M. *J. Am. Chem. Soc.* **2005**, *127*, 10667-10675
27) Mazerski, J.; Bolard, J.; Borowski, E. *Biochim. Biophys. Acta* **1995**, *1236*, 170-176
28) McNamara, C.M.; Box, S.; Crawforth, J.M.; Hickman, B.S.; Norwood, T.J.; Rawlings, B.J. *J. Chem. Soc. Perkin Trans. 1* **1998**, 83-87.
29) Caffrey, P.; Lynch, S.; Flood, E. Finnan, S.; Oliynyk, M. *Chem. Biol.* **2001**, *8*, 713-723.

30) Khutorsky, V.E. *Biochim. Biophys. Acta* **1992**, *1108*, 123-127.
31) Baginski M.; Resat, H.; McCammon, J.A. *Mol. Pharmacol.* **1997**, *52*, 560-570.
32) Baginski, M.; Resat, H.; Borowski, E. *Biochim. Biophys. Acta* **2002**, *1567*, 63-78.
33) Chéron, M.; Cybulska, B.; Mazerski, J.; Grzybowska, J.; Czerwinski, A.; Borowski, E. *Biochem. Pharmacol.* **1988**, *37*, 827-836.
34) Matsumori, N.; Yamaji, N.; Matsuoka, S.; Oishi, T.; Murata, M. *J. Am. Chem. Soc.* **2002**, *124*, 4180-4181.
35) Mathias, J.P.; Simanek, E.E.; Whitesides, G.M. *J. Am. Chem. Soc.* **1994**, *116*, 4326-4340
36) Görbitz, C.H.; Etter, M.C. *J. Am. Chem. Soc.* **1992**, *114*, 627-631.
37) Haasnoot, C. A. G.; de Leeuw, F. A. A. M.; Altona, C. *Tetrahedron*, **1980**, *36*, 2783-2792
38) Matsuoka, S.; Ikeuchi, H.; Matsumori, N.; Murata, M. *Biochemistry* **2005**, *44*, 704-710
39) Gullion, T.; Schaefer, J. *J. Magn. Reson.* **1989**, *81*, 196-200.
40) Gray, K.C.; Palacios, D.S.; Dailey, I.; Endo, M.M.; Uno, B.E.; Wilcock, B.C.; Burke, M.D. *Proc. Natl. Acad. Sci. USA,* **2012**, *109*, 2234-2239.
41) Matsuoka, S.; Ikeuchi, H.; Umegawa, Y.; Matsumori, N.; Murata, M. *Bioorg. Med. Chem.* **2006**, *14*, 6608-6614
42) Kasai, Y.; Matsumori, N; Umegawa, Y.; Matsuoka, S.; Ueno, H.; Ikeuchi, H.; Oishi, T.; Murata, M. *Chem. Eur. J.* **2008**, *14*, 1178-1185
43) Matsumori, N.; Sawada, Y.; Murata, M.; *J. Am. Chem. Soc.* **2006**, *128*, 11977-11984.
44) Umegawa, Y.; Matsumori, N.; Oishi, T.; Murata, M. *Biochemistry* **2008**, *47*, 13463-13469.
45) Matsumori, N.; Tahara, K.; Yamamoto, H.; Morooka, A.; Doi, M.; Oishi, T.; Murata, M. *J. Am. Chem. Soc.* **2009,** *131*, 11855-11860.
46) Dufourc, E.J.;Parish, E.J.; Chitrakorn, S.; Smith, I.C.P. *Biochemistry* **1984**, *23*, 6062-6071.
47) Matsuoka, S.; Murata, M. *Biochim. Biophys. Acta* **2002**, *1564*, 429-434.
48) de Kruijff, B.; Gerritsen, W.J.; Oerlemans, A.; Demel, R.A.; van Deenen, L.L.M. *Biochim. Biophys. Acta*, **1974**, *339*, 30-43
49) de Kruijff, B.; Gerritsen, W.J.; Oerleman, A.; Van Dijck, Demel, R.A.; Van Deenen L.L.M. *Biochim. Biophys. Acta.***1974**, *33*, 44-56
50) Herve, M.; Debouzy, J.C.; Borowski, E.; Cybulska, B.; Gary-Bobo, C.M. *Biochim. Biophys. Acta*, **1989**, *980*, 261-272.
51) Mickus, D.E.; Levitt, D.G.; Rychnovsky,S.D. *J. Am. Chem. Soc.* **1992**, 359-360.
52) Feingold, D.S. *Biochem. Biophys. Res. Commun.* **1973**, *51*, 972-978
53) Hartsel, S.C. *Biochim. Biophys. Acta* **1995**, *1238*, 156-162
54) Cotero, B.V.; Rebolledo-Antunez, S.; Ortega-Blake, I. *Biochim. Biophys. Acta* **1998**, *1375*, 43-51;
55) Lopes, S.; Castanho, M.A.R.B. *J.Phys. Chem. B*, **2002**, *106*, 7278-7282.
56) Matsuoka, S.; Murata, M. *Biochim. Biophys. Acta* **2002**, *1564*, 429-434
57) Venegas, B.; González-Damian, J.; Celis, H.; Ortega-Blake, I. *Biophys. J.* **2003**, *85*, 2323-2332
58) Coutinho, A.; Silva, L.; Fedorov, A.; Prieto, M. *Biophys. J.* **2004**, *87*, 3264-3276
59) Zumbuehl, A.; Stano, P.; Heer, D.; Walde, P.; Carreira, E.M. *Org. Lett.* **2004**, *6*, 3683-3686.
60) Baginski, M. *J. Phys. Chem. B* **2006**, *110*, 16743-16753.
61) Neumann, A.; Baginski, M.; Czub, J. *J. Am. Chem. Soc.* **2010**, *132*, 18266-18272
62) Umegawa, Y.; Nakagawa, Y.; Tahara, K.; Tsuchikawa, H.; Matsumori, N.; Oishi, T.; Murata, M.; *Biochemistry* **2012**, *51*, 83-89

CHAPTER 2

Degradative synthesis, NMR conformational analysis, and evaluation of antifungal activity of C41-methyl amphotericin B, amphoteronolide B, and C41-methyl amphoteronolide B

ABSTRACT

As discussed in Chapter 1, past efforts toward understanding the structure/function relationships underlying the AmB ion channel have focused on covalent modification of the natural product. An alternative strategy developed in our group is to synthetically delete protic functional groups from the AmB skeleton and determine the functional consequences. This strategy circumvents the inherent shortcomings of the covalent modification approach since no steric bulk is added to the molecular scaffold and these derivatives lack the ability to hydrogen bond at the site of deletion. However, a new consideration is introduced by this functional group deletion approach–conformation of the macrolide skeleton. While it has been demonstrated that AmB derivatives with covalent modifications of the carboxylic acid or amine functional groups have the same ground-state conformation as judged by NMR[1] or X-ray crystallographic[2] analysis, respectively, the effect of functional group deletion on AmB conformation has not been studied. To address this question, we have employed Monte Carlo methods constrained by phase-sensitive COSY and NOESY NMR data to determine the conformations of AmB, C41-methyl amphoteronolide B, amphoteronolide B, and C41-methyl amphotericin B. Through this approach we have demonstrated that the conformation of the AmB macrolactone remains unchanged upon deletion of appended functional groups. Thus, our conformational analysis has enabled the unambiguous interpretation of functional data obtained for these derivatives, leading to the striking observation that, contrary to the current channel model, oxidation at C41 is not required for potent antifungal activity.

Daniel Palacios optimized conditions for reduction of the C41 carboxyl group to the corresponding C41 methyl, developed the flexible synthetic pathway to **2.2-2.4**, and contributed to preliminary NMR conformational analysis studies. Portions of this chapter are taken with permission from Palacios, D.S.; Anderson, T.M.; Burke, M.D. *J. Am. Chem. Soc.* **2007**, *129*, 13804-13805.

2-1 SYNTHESIS OF AMPHOTERICIN DERIVATIVES

Manipulation of AmB is challenging due to its light, oxygen, and acid sensitivity as well as its poor solubility in water and most common organic solvents. Nevertheless, we have developed a flexible, modular synthesis which allows for reversal of either[3] one or both of the two post-PKS modifications predicted to be critical for self-assembly of the AmB ion channel. The two key transformations in this synthesis are reduction of the C41 carboxyl group to the corresponding methyl and oxidative removal of the mycosamine sugar. Conditions for reduction of the C41 carboxylic acid and oxidative deglycosidation of the amphotericin B macrolide were optimized in the context of degradative syntheses of C41-methyl AmB **2.4** and amphoteronolide B **2.3**, respectively.

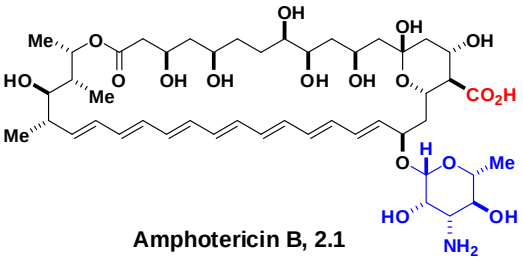

Amphotericin B, 2.1

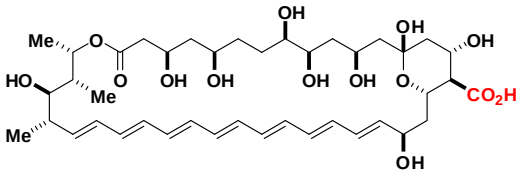

Amphoteronolide B, 2.3

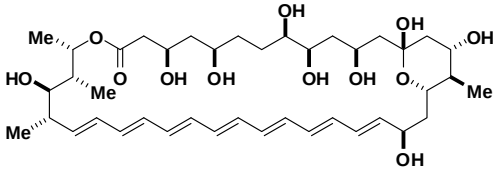

C41-Methyl Amphoteronolide B, 2.2

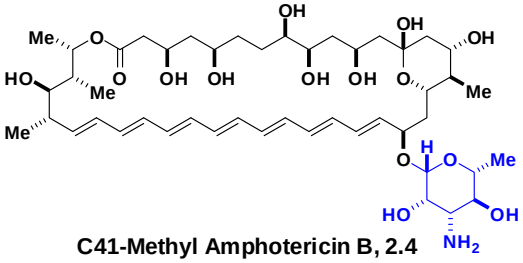

C41-Methyl Amphotericin B, 2.4

Our first synthesis of amphoteronolide B (Scheme 2.1) built on the degradative synthesis reported by Nicolaou.[3a] For the key deglycosidation reaction, we opted for Masamune's higher-yielding deglycosidation[4] under the action of 2,3-dichloro-5,6-dicyano-1,4-benzoquinone (DDQ). However, several problems were encountered which rendered this synthetic route infeasible for synthesis of **2.3** in quantities sufficient for the intended assays and NMR studies. The primary difficulty was the sensitive nature of the trimethylsilyl protected intermediate **2.6**, which did not tolerate reaction conditions of the oxidative deglycosidation to enone **2.7** (TLC of the reaction mixture indicated formation of numerous inseparable byproducts). Purification of **2.7** by flash chromatography proved excessively challenging, presumably due to the acid-labile

nature of the trimethylsilyl protecting group. Both Masamune's and Nicolaou's conditions resulted in prohibitively low yields (<15%) for this key transformation.

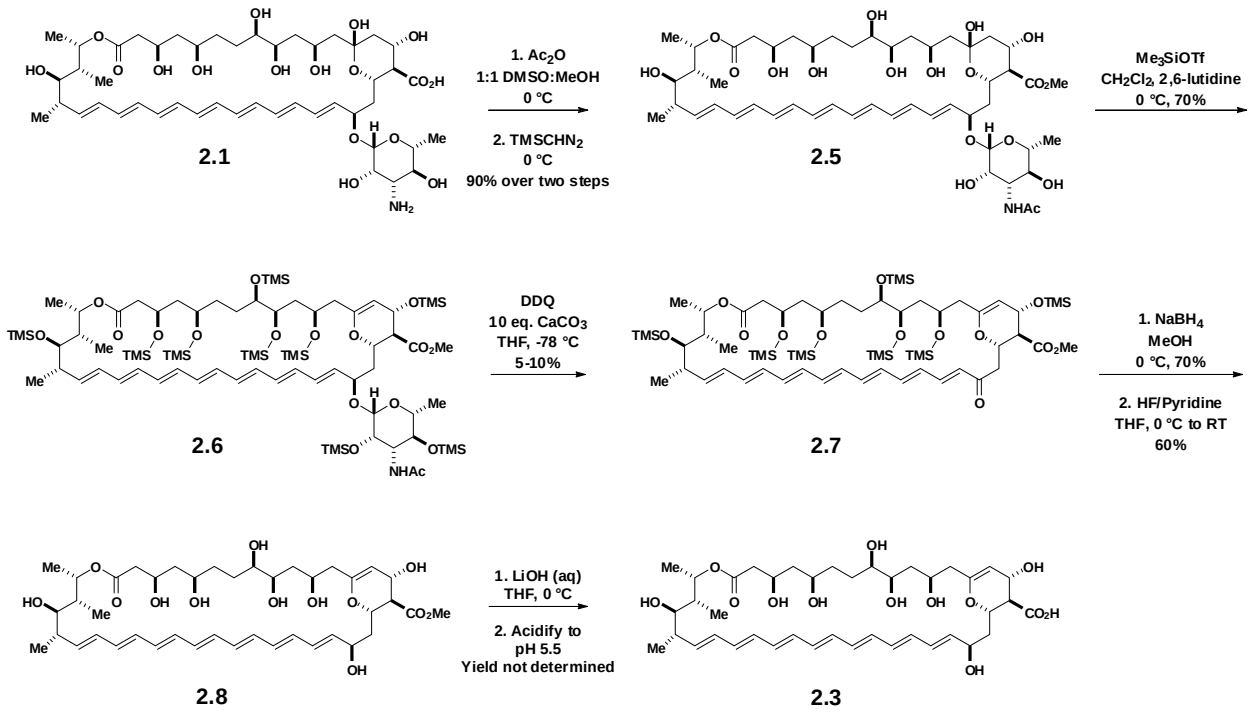

Scheme 2.1 1st generation synthesis of amphoteronolide B

Faced with these challenges, we devised a synthesis that would provide a more robust, high-yielding deglycosidation. Noting that Masamune's substrate for the deglycosidation contained tert-butyldimethylsilyl (TBDMS) and acetonide protecting groups, and that MacPherson et al.[3c] chose triethylsilyl protecting groups for degradative syntheses of AmB derivatives, the more robust triethylsilyl group was chosen for our studies.

The second-generation synthesis of amphoteronolide B (Scheme 2.2) proceeded via protection of the C3' amine as the corresponding 9-(fluoreneyl)-methoxycarbonyl (Fmoc) carbamate followed by protection of the anomeric hydroxyl as a methyl ketal. Protection of the C41 carboxyl as an allyl ester and global triethylsilyl (TES) hydroxyl protection yielded the deglycosidation precursor **2.10**.

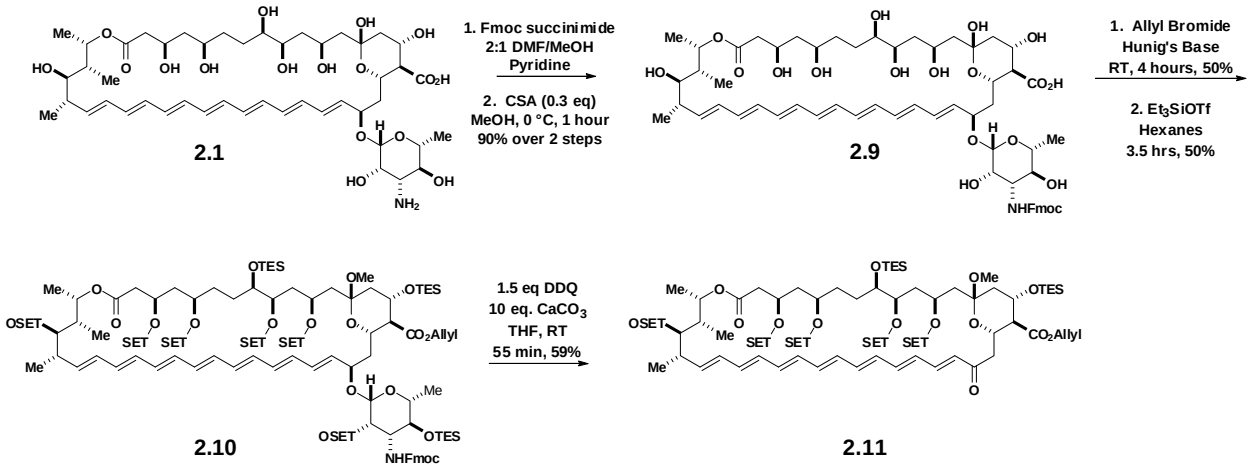

Scheme 2.2. Second generation synthesis of allyl heptaenone intermediate en route to amphoteronolide B

A screen of reaction conditions for deglycosidation of **10** revealed a strong temperature dependence for conversion to heptaenone **2.11**. **S**urprisingly, at -78 ºC, 58% starting material was recovered, while 5% of the desired enone was isolated (Table 2-1, entry 1). Repeating the reaction at 0 ºC (entries 2-4) and room temperature (entries 5-6) resulted in higher isolated yields of **2.11**, with reproducible yields at room temperature between 55-60% This represents the highest yield ever reported for deglycosidation of an amphotericin derivative to the corresponding heptaenone.[3a, 4]

Entry	DDQ eq	Temperature	Time	Yield	Recovered Starting Material
1	0.95	-78 °C	25 min	5%	58%
2	0.95	0 °C	30 min	49%	24%
3	1.5	0 °C	10 min	48%	18%
4	1.5	0 °C	50 min	48%	-
5	1.5	23 ºC	60 min	59%	-
6	1.5	23 ºC	55 min	57%	-

Table 2-1. Optimization of conditions for DDQ-mediated oxidative deglycosidation of **10**.

With the enone in hand, amphoteronolide B was accessible via four deprotection steps (Scheme 2.3). $NaBH_4$ reduction of **11** proceeded in 78% yield followed by desilylation to form **2.12** as a single diastereomer[3a] in 84% yield. The methyl ketal **2.12** was hydrolyzed in 76% yield, and Pd-mediated deallylation yielded amphoteronolide B in 16% yield after HPLC purification. The optimized deglycosidation conditions were incorporated by Dan Palacios into a flexible synthetic pathway which afforded **2.2**-**2.4** in quantities and purities sufficient for antifungal assays (>10 mg of each compound was obtained in >90% purity as measured by HPLC).[5]

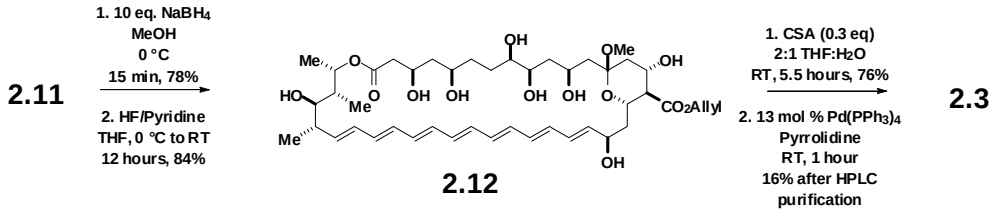

Scheme 2.3. Second generation synthesis of amphoteronolide B.

2-2 NMR-BASED CONFORMATIONAL ANALYSIS

Conformational analysis of **2.1**-**2.4** was critical for enabling interpretation of functional data generated by biophysical assays of these derivatives. Because the AmB macrolactone is known to be rigid,[1] we hypothesized that the ground-state conformation would be unchanged by these functional group deletions. To test our hypothesis, we employed Monte Carlo methods constrained by phase-sensitive COSY (COSYPS) and NOESY NMR data to determine the solution conformation of **2.1**-**2.4**. Compounds **2.1**, **2.3**, and **2.4** were not amenable to high resolution solution NMR analysis due to their poor solubilities in appropriate NMR solvents. Therefore, we chose the suitably protected analogs *N*-acyl AmB methyl ester **2.13**,[3a] AmdeB allyl ester **2.14**, and *N*-Fmoc MeAmB **2.15** for the conformational analysis of **2.1**, **2.3**, and **2.4**, respectively. MeAmdeB **2.2** was used directly in our NMR studies.

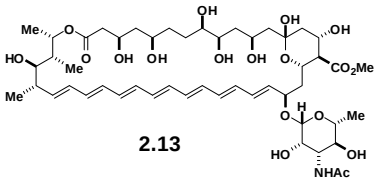

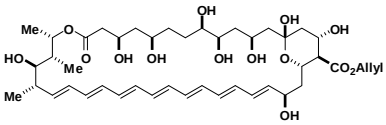

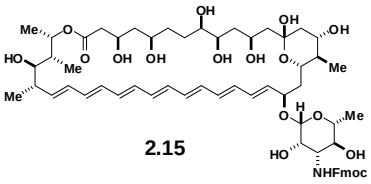

To obtain dihedral constraints for conformational analysis, coupling constants for each compound were extracted from COSYPS spectra using amplitude-constrained multiplet evaluation (ACME) in nmrPipe.[6] The ACME method for determining *J* values from COSYPS spectra is described in detail by Delaglio et al.[6b] Briefly, nmrPipe can accurately model the crosspeaks of a COSYPS spectrum provided the spectrum is acquired with interscan delay time sufficient for the spins to fully relax. A peak-fitting algorithm fits spectrum crosspeaks and calculates coupling constants for the corresponding spins.

Raw COSYPS data were acquired and processed as described by Delaglio[6b] to produce a diagonal-suppressed spectrum[7] and a diagonal-only spectrum (Figure 2-1 depicts representative spectra for the AmdeB allyl ester **2.14**). ACME integrates selected peaks from the diagonal-only

spectrum and the average integration value is used for peak-fitting of crosspeaks in the diagonal-suppressed spectrum. Figure 2-2 shows the results of fitting two peaks from the COSYPS diagonal of AmdeB allyl ester **2.15**. Panels A, B, and C contain; A) the selected region of the spectrum (with peaks for fitting labeled 1 and 2), B) simulated peaks calculated in the fitting process, C) the residual between the experimental and calculated peaks. Therefore, in an accurate simulation, no residual is present for the selected peaks. Through this process, the average integration of diagonal peaks can be applied to peak-fitting of crosspeaks in the diagonal-suppressed spectrum.

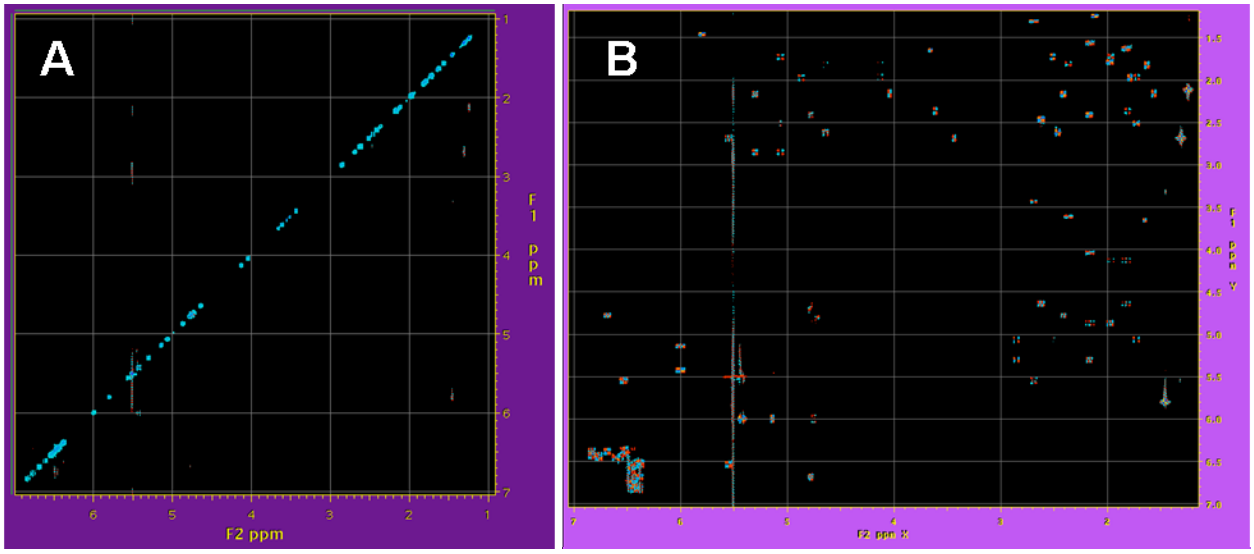

Figure 2-1. **A.** Diagonal-only COSYPS spectrum of AmdeB allyl ester **2.14**. **B.** Diagonal-only COSYPS spectrum of **2.14**. Adapted with permission from Palacios, D.S.; Anderson, T.M.; Burke, M.D. *J. Am. Chem. Soc.* **2007**, *129*, 13804-13805. Copyright 2007 American Chemical Society.

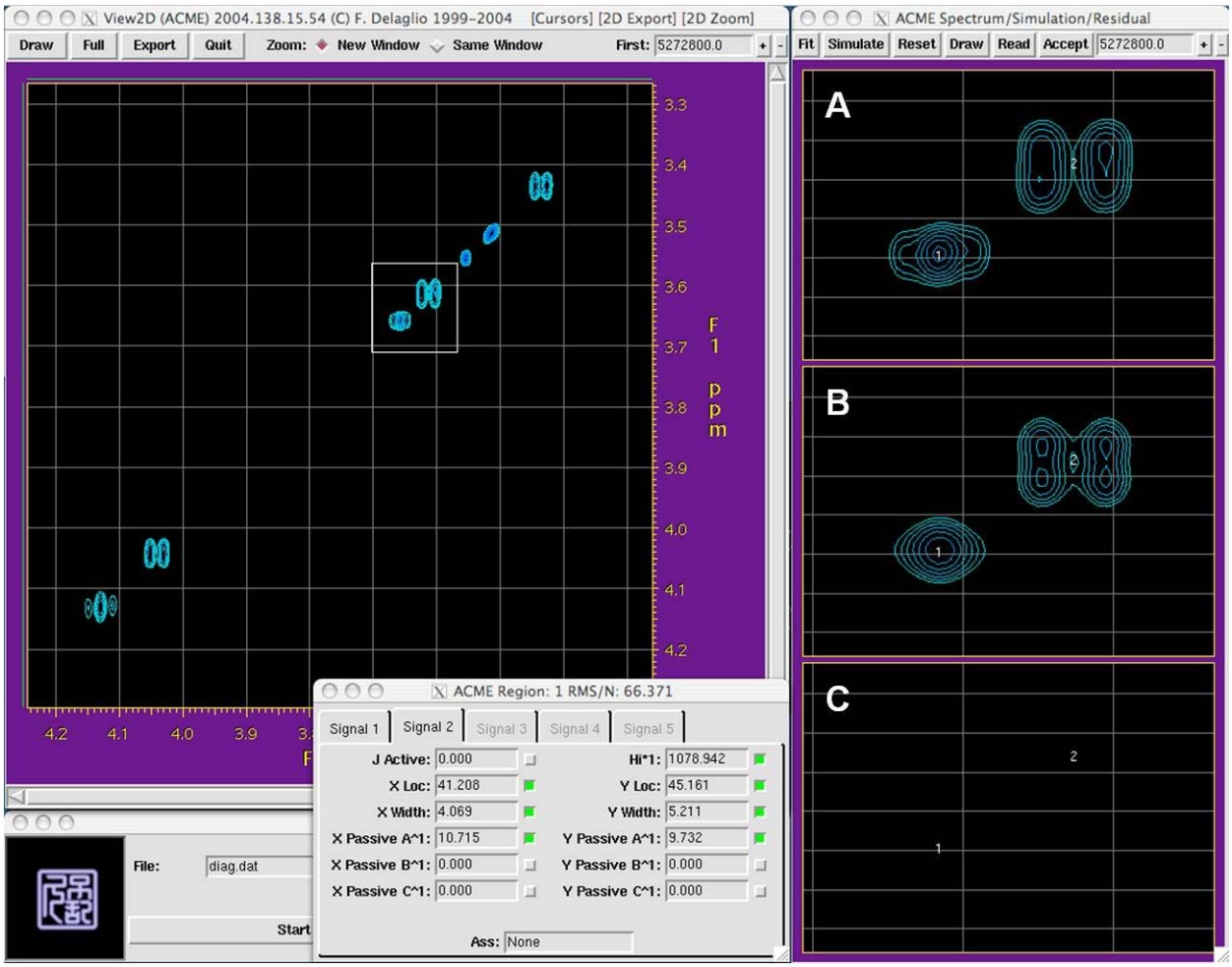

Figure 2-2. ACME results for fitting the AmdeB allyl ester **2.14** diagonal. **A.** The selected spectral region with peaks for fitting labeled 1 and 2. **B.** Simulated peaks calculated in fitting process. **C.** Residual between panels A) and B). Adapted with permission from Palacios, D.S.; Anderson, T.M.; Burke, M.D. *J. Am. Chem. Soc.* **2007**, *129*, 13804-13805. Copyright 2007 American Chemical Society.

The fine structure of crosspeaks in a COSYPS spectrum provides coupling constant data[8] in a manner analogous to obtaining coupling constants from a one-dimensional multiplet. In a two-dimensional crosspeak, the spacing between antiphase portions of the crosspeak corresponds to the *J* value for the associated spins. The ACME method employs the reference integration from the diagonal in a peak-fitting algorithm that fits selected crosspeaks and calculates coupling constants. Figure 2-3 shows the results of the fitting algorithm applied to the cross-peak corresponding to protons H-18 and H-17 in AmdeB allyl ester **2.14**. Panel A again contains the selected peak from the spectrum, Panel B depicts the simulated crosspeak, and Panel C displays the residual. The lack of any significant residual is consistent with accurate reproduction of the multiplet fine structure in the fitting process. Similar analysis for each crosspeak in the spectra of

compounds **2.2**, **2.13**, **2.14**, and **2.15** was used to derive the coupling constants from which dihedral constraints were calculated (see Table 2-2 for a compilation of these data).

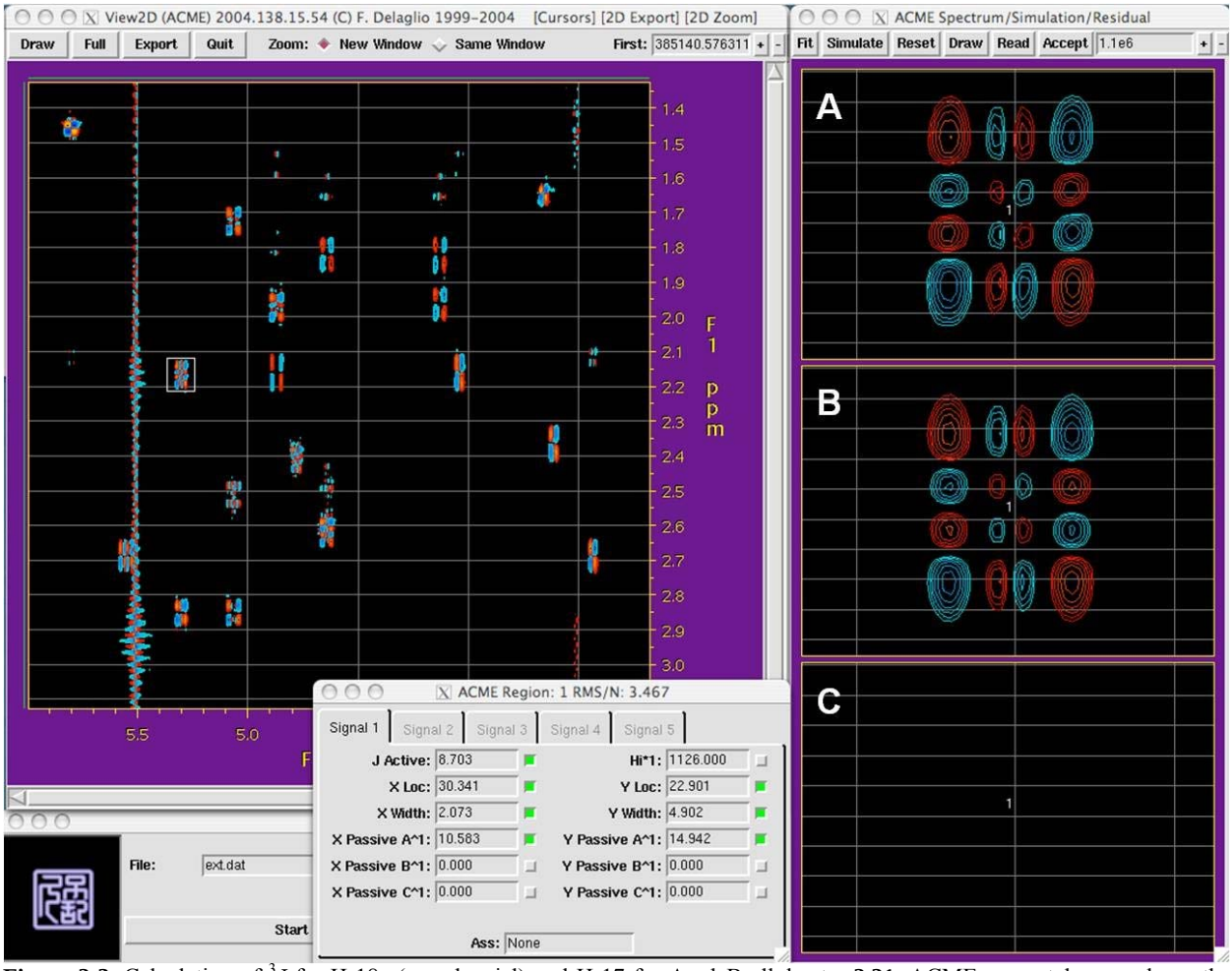

Figure 2-3. Calculation of ^{3}J for H-18a (pseudoaxial) and H-17 for AmdeB allyl ester **2.21**. ACME accurately reproduces the fine structure of the multiplet with no residual between the experimental and calculated peaks. Adapted with permission from Palacios, D.S.; Anderson, T.M.; Burke, M.D. *J. Am. Chem. Soc.* **2007**, *129*, 13804-13805. Copyright 2007 American Chemical Society.

Dihedral angles were calculated from ^{1}H-^{1}H ^{3}J values according to Altona's extended Karplus[9] equation using the MestReJ software.[10] However, each ^{3}J gives rise to 4 possible solutions to the Karplus equation. Methods for choosing the appropriate value are well-precedented. For example, in the context of conformational analysis of the erythronolide B lactone, Aurichio[11] and Egan[12] chose dihedral values consistent with NOE data and the erythronolide B crystal structure, respectively. For our analyses, we chose angles consistent with both NOESY data and the AmB crystal structure.[2] In some cases, two solutions to the Karplus equation were consistent with both NOESY and crystal structure data, and both solutions were included.

Consistent with protein structural analysis techniques,[8] each H-H dihedral was constrained to the selected value ± 30º. When two solutions to the Karplus equation were selected, both values (± 30º) were allowed. Table 2-2 lists the *J* values and corresponding dihedral constraints used in the conformational searching. Consistent with the known *trans*-configuration of the seven double bonds of the polyene moiety,[2] the π-bonds were constrained to 180º ± 10°.Interproton distances were constrained for proton pairs exhibiting NOE correlations, with the lower limit set at 1.8 Å (twice the hydrogen van der Waals radius), and the upper limit set at 5.0 Å.[8] Table 2-3 lists the NOE correlations used for conformational searching, and Figures 2-4 through 2-7 depict these correlations (red lines indicate NOE correlations). *Notably, all four compounds contain a series of transannular NOEs between protons of the polyol and those of the polyene*.

All NMR-derived distance and dihedral constraints were enforced in Monte Carlo conformational searches. This type of conformational search probes conformational space by randomly perturbing all dihedral angles in the molecule and then minimizing the resulting structures (with constraints enforced). Conformational searches were performed using the Molecular Operating Environment program (MOE),[13] with an empirical MMFF94x force field and a Born solvation model. 3500 conformations were generated and minimized for each compound, and each lowest energy conformation was used for root-mean-square (RMS) atom alignment of the four macrolactone rings.

	N-Acyl AmB Methyl Ester			*N*-Fmoc C41-Me AmB			AmdeB Allyl Ester			C41-Me AmdeB		
		θ constraint (degrees)			θ constraint (degrees)			θ constraint (degrees)			θ constraint (degrees)	
Protons	**J (Hz)**	**Lower**	**Upper**	**J (Hz)**	**Lower**	**Upper**	**J (Hz)**	**Lower**	**Upper**	**J (Hz)**	**Lower**	**Upper**
2ax - 3	**3.1**	-81	-21	**1.8**	-89	-29	**4.7**	-72	-12	**ND**[a]		
2eq -3	**10.0**	129	-120	**9.1**	123	-115	**9.2**	126	-174	**9.2**	124	-115
3 - 4ax	**2.9**	21	81	**2.0**	28	88	**3.9**	15	75	**4.3**	12	72
3 - 4eq	**9.9**	123	-133	**10.1**	124	-134	**10.1**	124	-134	**10.9**	133	-142
4ax - 5	**2.9**	-81	-21	**1.0**	-127	-37	**4.4**	-72	-12	**1.8**	-89	-29
4eq - 5	**9.6**	131	-120	**9.6**	132	-120	**9.5**	130	-120	**10.3**	136	-126
5 - 6ax	**1.3**	35	95	**1.8**	30	90	**5.4**	5	65	**1.1**	37	97
5 - 6eq	**10.6**	133	-145	**10.7**	137	-148	**10.3**	129	-141	**11.5**	150	-150
6eq - 7eq	**13.9**	150	-150	**13.4**	139	-139	**ND**[a]			**13.5**	141	-140
6eq - 7ax	**8.1**	5	65	**4.4**	22	82	**ND**[a]			**5.7**	16	76
6ax - 7ax	**12.1**	129	-129	**12.7**	133	-133	**ND**[a]			**10.6**	120	-120
6ax - 7eq	**ND**[a]			**ND**[a]			**ND**[a]			**ND**[a]		
7ax - 8	**10.7**	129	-140	**10.6**	128	-139	**11.2**	135	-147	**11.3**	138	-150
7eq - 8	**2.7**	23	83	**2.5**	24	84	**2.8**	22	82	**2.4**	25	85
8-9	**3.1**	-65	-5	**3.4**	-63	-3	**3.0**	-66	-6	**3.2**	-64	-4
9 - 10ax	**1.8**	29	89	**2.6**	24	84	**3.3**	19	79	**2.3**	33	93
9 - 10eq	**11**	128	-139	**10.7**	126	-136	**10.7**	126	-136	**11.7**	129	-128
10ax - 11	**2.3**	-85	-25	**NA**[a]	NA	NA	**3.1**	-80	-20	**1.3**	-94	-34
10eq - 11	**10.0**	134	-123	**10.4**	137	-131	**10.3**	136	-126	**10.9**	142	-132
11 - 12ax	**2.7**	23	83	**ND**[a]			**3.4**	19	79	**1.2**	35	95
11 - 12eq	**11.3**	132	-142	**11.0**	128	-138	**11.3**	132	-142	**10.7**	126	-136
14ax - 15	**11.6**	144	-134	**11.8**	147	-137	**11.0**	138	-127	**11.5**	143	-133
14eq - 15	**4.5**	24	84	**2.6**	35	95	**3.5**	29	89	**2.1**	39	99
15 - 16	**10.4**	132	-141	**11.2**	150	-150	**10.7**	148	-152	**10.8**	150	-150
16 - 17	**10.8**	130	-130	**10.4**	135	-144	**10.6**	165	-148	**10.8**	150	-150
17 - 18ax	**8.8**	124	-115	**7.5**	120	-120	**8.7**	123	-177	**8.1**	120	180
17 - 18eq	**1.0**	-98	-67	**ND**[a]			**0.9**	-99	-39	**ND**[a]		
18ax - 19	**2.0**	28	88	**2.5**	24	84	**ND**[a]			**3.9**	15	75
18eq - 19	**4.5**	-72	-12	**4.6**	-82	-22	**6.0**	-74	-14	**5.5**	-64	-4
19 - 20	**8.8**	120	180	**8.0**	120[b]	-120[b]	**8.8**	120[b]	-120[b]	**8.9**	120[b]	-120[b]
21 - 22	**ND**			**ND**			**11.0**	150[b]	-150[b]	**10.8**	150[b]	-150[b]
23 - 24	**ND**			**ND**			**11.0**	150[b]	-150[b]	**10.8**	150[b]	-150[b]
25 - 26	**ND**			**ND**			**11.5**	150[b]	-150[b]	**ND**		
33 - 34	**10.2**	133	-167	**10.0**	120[b]	-120[b]	**10.1**	120[b]	-120[b]	**9.9**	120[b]	-120[b]
34 - 35	**9.6**	125	-138	**9.6**	125	-138	**9.8**	128	-140	**10.0**	130	-143
35 - 36	**2.3**	-85	-25	**2.5**	-84	-24	**2.6**	-83	-23	**2.6**	-83	-23
36 - 37	**4.2**	-82	-22	**1.8**	-93	-33	**1.9**	-100	-40	**3.1**	-90	-30
1'-2'	**1.0**	34	118	**1.6**	24	84	**NA**			**NA**		
2'-3'	**3.0**	-82	-22	**ND**[a]			**NA**			**NA**		
3'-4'	**10.5**	152	-135	**9.7**	142	-124	**NA**			**NA**		
4'-5'	**9.2**	150	-150	**9.1**	150	-150	**NA**			**NA**		

[a]Associated cross peak was either too close to the diagonal or too weak to achieve an acceptable peak-fit.

[b]The generalized Karplus equation was utilized to determine dihedral constraint (Karplus, M.; *J. Phys. Chem.* **1959**, *30*, 11-15.).

Table 2-2. Dihedral constraints used in conformational searches using MOE. Also shown are the coupling constants (calculated by ACME) from which the dihedral constraints were derived. See supporting information for a description of the axial (ax) and equatorial (eq) convention for AmB. Adapted with permission from Palacios, D.S.; Anderson, T.M.; Burke, M.D. *J. Am. Chem. Soc.* **2007**, *129*, 13804-13805. Copyright 2007 American Chemical Society.

Proton	N-Acyl AmB Methyl Ester	N-Fmoc C41-Me AmE	AmdeB Allyl Ester	C41-Me AmdeE
	NOE with proton(s)	NOE with proton(s)	NOE with proton(s)	NOE with proton(s)
3	**5, 28**	**5, 28**	**5, 28**	**5, 28**
5	3, 28	3, 28	3, 26, 28	3, 28
7eq	**9, 24, 26**	–	–	–
8	10ax	–	–	–
9	**7eq, 11, 22, 24**	**11, 22**	**11, 20, 22, 24, 26**	**11**
10ax	8	–	–	12ax
11	**9, 20, 22**	**9, 20, 22**	**9, 20, 22, 24**	**9, 20**
12ax	14ax	–	–	10ax
14ax	**12ax**	–	**16**	–
15	17	–	–	–
16	**14ax**	–	**14ax, 18ax**	–
17	15, 20	20	20	20
18ax	–	–	**16**	–
19	21, 1'	21	21	21
20	**11, 17**	**11, 17**	**9, 11, 17, 22**	**11, 17, 22**
21	19	19	19	19
22	**9, 11**	–	**9, 11, 20, 24**	**20**
24	7eq, 9	–	9, 11, 22, 26	–
26	**7eq**	–	**5, 9, 24**	–
28	3, 5	3, 5	–	3, 5
31	**33**	**33**	–	**33**
32	34, 37	34, 37	34, 37	34, 37
33	**31, 35, 36**	**31, 36**	**31, 35**	**31, 35**
34	32, 37	32	32, 37	32, 37
35	**33**	–	**33**	**33**
36	33	33	–	–
37	**34, 32**	**32**	**34, 32**	**34, 32**
1'	3', 5'	3', 5'	NA	NA

Table 2-3. Observed NOE correlations used to derive distance constraints in conformational searches using MOE. Adapted with permission from Palacios, D.S.; Anderson, T.M.; Burke, M.D. *J. Am. Chem. Soc.* **2007**, *129*, 13804-13805. Copyright 2007 American Chemical Society.

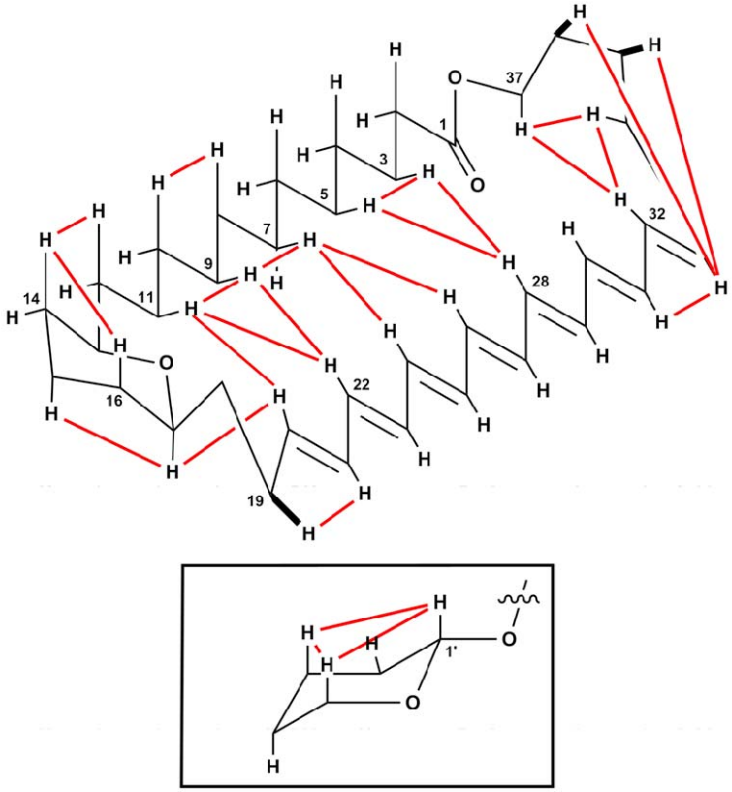

Figure 2-4. NOE correlations for N-acyl AmB Methyl ester **2.13**. For clarity, appendages other than protons have been removed from the macrolide skeleton. Selected carbon atoms are numbered. Adapted with permission from Palacios, D.S.; Anderson, T.M.; Burke, M.D. *J. Am. Chem. Soc.* **2007**, *129*, 13804-13805. Copyright 2007 American Chemical Society.

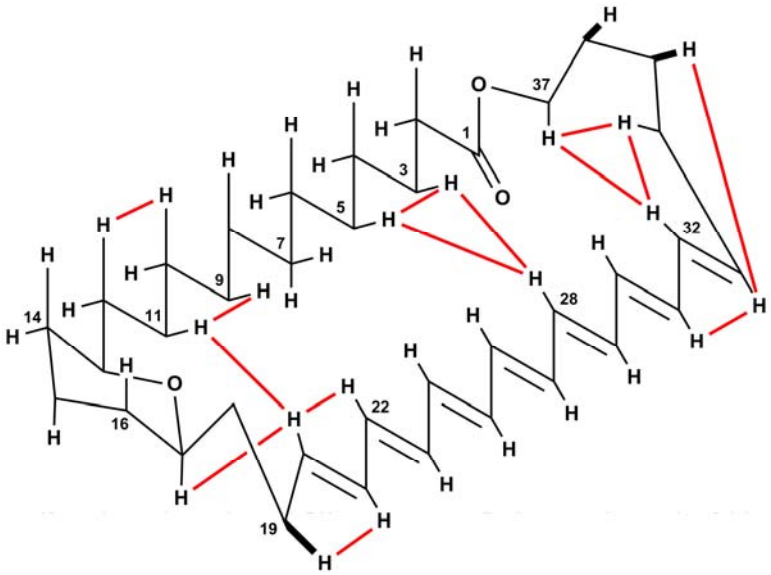

Figure 2-5. NOE correlations for MeAmdeB **2.2**. For clarity, appendages other than protons have been removed from the macrolide skeleton. Selected carbon atoms are numbered. Adapted with permission from Palacios, D.S.; Anderson, T.M.; Burke, M.D. *J. Am. Chem. Soc.* **2007**, *129*, 13804-13805. Copyright 2007 American Chemical Society.

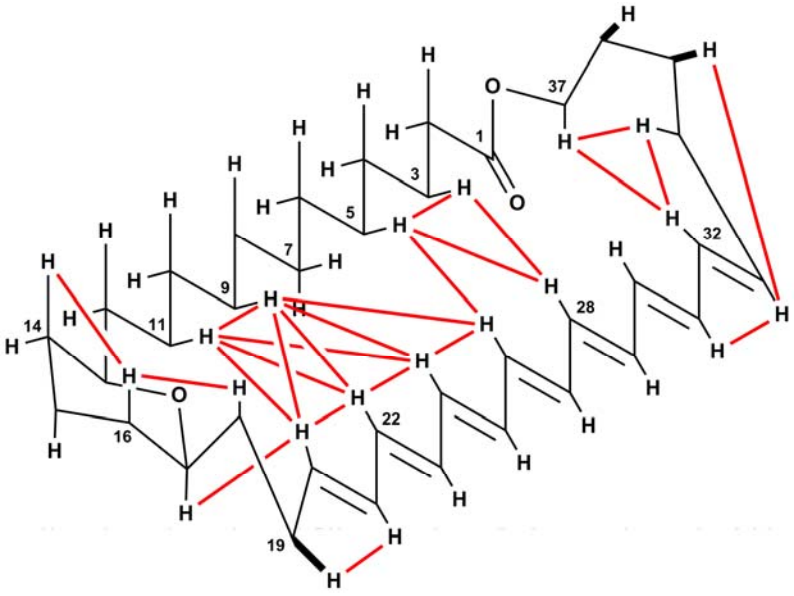

Figure 2-6. NOE correlations for AmdeB allyl ester **2.14**. For clarity, appendages other than protons have been removed from the macrolide skeleton. Selected carbon atoms are numbered. Adapted with permission from Palacios, D.S.; Anderson, T.M.; Burke, M.D. *J. Am. Chem. Soc.* **2007**, *129*, 13804-13805. Copyright 2007 American Chemical Society.

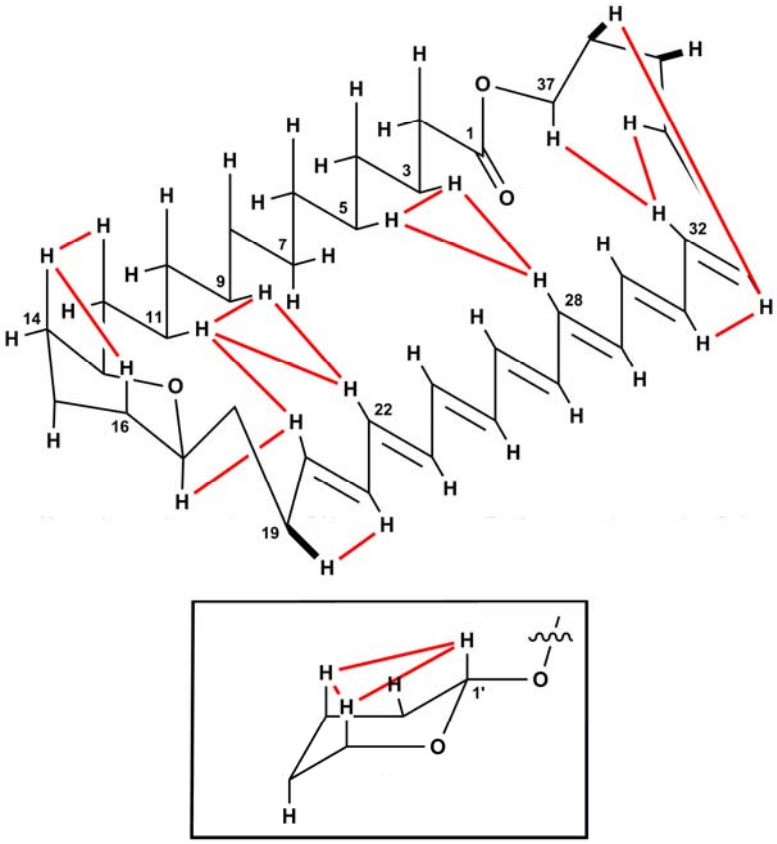

Figure 2-7. NOE correlations for *N*-Fmoc MeAmB **2.15**. For clarity, appendages other than protons have been removed from the macrolide skeleton. Selected carbon atoms are numbered. Adapted with permission from Palacios, D.S.; Anderson, T.M.; Burke, M.D. *J. Am. Chem. Soc.* **2007**, *129*, 13804-13805. Copyright 2007 American Chemical Society.

Only the atoms of the macrolactone ring and the cyclic hemiketal were used for RMS alignment. All other atoms were deleted from the lowest-energy conformers and the four resulting macrolide skeletons representing the ground-state conformations of AmB **2.1**, MeAmB **2.2**, AmdeB **2.3**, and MeAmdeB **2.4** were used for alignment. Rigid RMS atom alignment revealed RMS deviation (RMSD) of 0.081 Å for the four structures (Figure 2-8). Thus, functional group deletion does not change the conformation of the AmB macrolide skeleton.

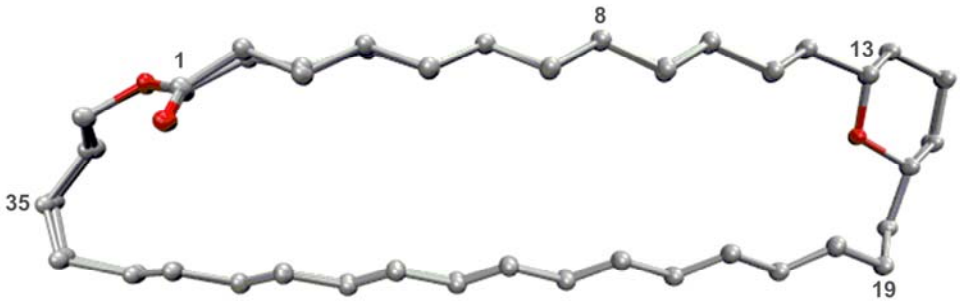

Figure 2-8. Superposition of the ground-state conformation of the macrolactone skeletons of compounds **2.1** - **2.4** (or their more soluble analogs). Rigid RMS atom alignment revealed RMSD = 0.081 Å for the four structures. Adapted with permission from Palacios, D.S.; Anderson, T.M.; Burke, M.D. *J. Am. Chem. Soc.* **2007**, *129*, 13804-13805. Copyright 2007 American Chemical Society.

2-3 ANTIFUNGAL ASSAYS

The impact of our functional group deletions on antifungal activity was evaluated in a disc diffusion assay[14] of each compound against *Saccharomyces cerevisiae*. As shown in Figure 2-9, MeAmdeB **2.2** and AmdeB **2.3** were inactive. *In contrast, and contrary to the current channel model for AmB antifungal activity, MeAmB **2.4** was found to possess activity similar to AmB.* This result was confirmed quantitatively in a broth dilution assay[15] to determine the minimum inhibitory concentration (MIC) for each compound (Figure 2-9). Similar results were observed in both assays for the clinically relevant yeast *Candida albicans* (see supporting information for full details). Because each compound occupies the same conformation, these results cannot be attributed to conformational changes. Clearly, oxidation at C41 is not required for potent antifungal activity.

	AmB 2.1	MeAmdeB 2.2	AmdeB 2.3	MeAmB 2.4
A. Disc diffusion *S. cerevisiae*	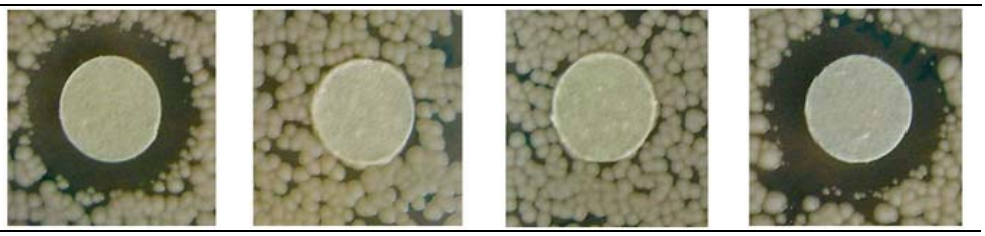			
B. MIC (μM)				
S. cerevisiae	2	>10	>10	1
C. albicans	1	>10	>10	1

Figure 2-9. (A) Disc diffusion assay with *S. cerevisiae* (40 μg of compound per disc). Similar results were achieved with *C. albicans*. (Supporting Information). (B) Broth dilution assays. Adapted with permission from Palacios, D.S.; Anderson, T.M.; Burke, M.D. *J. Am. Chem. Soc.* **2007**, *129*, 13804-13805. Copyright 2007 American Chemical Society.

2-4 DISCUSSION

The work described in this chapter demonstrates a new approach for studying AmB structure/function relationships via functional group deletion and studying the functional consequences of each deletion. Solution NMR conformational analysis directly enabled unambiguous interpretation of our functional studies of **2.2**, **2.3**, and **2.4**. Having determined that functional group deletion did not change the conformation of the macrolactone, we were confident that the observed changes in function were a direct result of functional group deletion. Systematic application of the functional group deletion strategy is currently underway in our laboratories to dissect the structure/function relationships underlying the activity of AmB. Most notably, Kaitlyn Gray et al.[25] have applied the functional group deletion strategy to synthesize C35-deoxy-AmB (**2.16**) and study its biophysical properties.

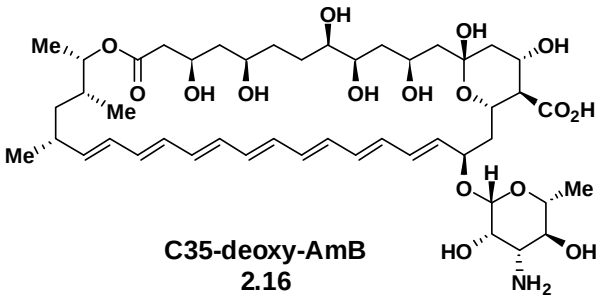

C35-deoxy-AmB
2.16

The discoveries presented in this chapter strongly contradict the current model for AmB antifungal activity – salt bridge stabilization is not required for AmB antifungal activity. There are at least two possible explanations for this phenomenon. Oxidation at C41 may not be required for channel activity and/or channel activity may not be required for antifungal activity. To address the first of these possibilities, extensive biophysical studies of **2.1**-**2.4** performed in our laboratories by Daniel Palacios et al.[26] have confirmed that C41-methyl amphotericin B **2.4** retains full channel and activity while amphoteronolide B **2.3** and C41-methyl amphoteronolide B **2.2** have no channel activity in liposome K efflux and planar lipid bilayer assays. Thus,

oxidation at C41 is not required for AmB channel activity. The work of Kaitlyn Gray et al.[25] on C-35-deoxy-AmB addressed the second possibility. C-35-deoxy AmB was found to have no channel activity while retaining potent antifungal activity against *S. cerevisiae* and *C. albicans.* Thus, channel activity is not required for antifungal activity. These studies and their impact on the experiments described in this dissertation will be discussed further in Chapter 3.

2-5 EXPERIMENTAL SECTION

Part 1. General Methods

Materials. Commercially available materials were purchased from Aldrich Chemical Co. (Milwaukee, WI), Fisher Scientific (Hampton, NH), Lipoid (Luwigshafen, Germany) and Silicycle (Quebec, Canada) and used without further purification unless noted otherwise. Amphotericin B was a generous gift from Bristol-Myers Squibb Company. All solvents were dispensed from a solvent purification system that passes solvents through packed columns according to the method of Pangborn and coworkers[16] (THF, Et_2O, CH_2Cl_2 : dry neutral alumina; DMSO, DMF, CH_3OH : activated molecular sieves). Hexanes, 2,6-lutidine, triethylamine, and pyridine were freshly distilled under nitrogen from CaH_2. Camphorsulfonic acid was recrystallized from ethyl acetate. Water was doubly distilled or obtained from a Millipore (Billerica, MA) Gradient A10 MilliQ water purification system.

Reactions. Due to the light and air sensitivity of amphotericin B, all manipulations were carried out under low light conditions and compounds were stored under an anaerobic atmosphere. All reactions were performed in oven- or flame-dried glassware under an atmosphere of argon unless otherwise indicated. Reactions were monitored by analytical thin layer chromatography performed using the indicated solvent on E. Merck silica gel 60 F_{254} plates (0.25mm). Compounds were visualized using a UV (λ_{254}) lamp or stained by an acidic solution of *p*-anisaldehyde. Alternatively, reactions were monitored by RP-HPLC using an Agilent 1100 Series HPLC system equipped with a Sunfire^{TM} C_{18} 5 micron 10 x 250 mm column (Waters Corp. Milford, MA) with UV detection at 406 nm and the indicated eluent and flow rate.

Purification and Analysis. Flash chromatography was performed as described by Still and coworkers[16] using the indicated solvent on E. Merck silica gel 60 230-400 mesh or on Silicycle 17% carbon C_{18} 230-400 mesh reverse phase silica gel. ^1H NMR spectra were recorded at 23 °C on a Varian Unity Inova Narrow Bore spectrometer operating at a ^1H frequency of 500 MHz with a Varian 5 mm $^1H\{^{13}C/^{15}N\}$ pulsed-field gradient Z probe or a Varian Unity Inova spectrometer operating at a ^1H frequency of 600 MHz with a Varian 5 mm $^1H\{^{13}C/^{15}N\}$ pulsed-field gradient X,Y,Z probe. Chemical shifts (δ) are reported in parts per million (ppm) downfield from tetramethylsilane and referenced internally to the residual protium in the NMR solvent (CHD_2OD, δ = 3.31, center line, $CD_3C(O)CHD_2$, δ = 2.05, center line) or to added tetramethylsilane. Data are reported as follows: chemical shift, multiplicity (s = singlet, d =

doublet, t = triplet, dd = doublet of doublets, m = multiplet, b = broad, app = apparent), coupling constant (*J*) in Hertz (Hz) and integration. For compounds **2.13** (a more soluble derivative of **2.1**), **2.2**, **2.14** (a more soluble derivative of **2.3**), and **2.15** (a more soluble derivative of **2.4**), proton and coupling constant assigments were made using a variety of two-dimensional NMR techniques including phase-sensitive COSY experiments combined with amplitude constrained multiplet evaluation (ACME)[6b] (see Part III for a detailed discussion). ^{13}C spectra were recorded at 23 °C with a Varian Unity Inova spectrometer operating at a ^{13}C frequency of 125 MHz with a 5 mm Nalorac gradient $\{^{13}C/^{15}N\}^{1}H$ quad probe or a Varian Unity Inova spectrometer operating at a ^{13}C frequency of 150 MHz and equipped with a Varian 5 mm 600 DB Auto X probe. Chemical shifts (δ) are reported downfield of tetramethylsilane and are referenced to the carbon resonances in the NMR solvent (CD_3OD, δ = 49.0, center line, $CD_3C(O)CD_3$, δ = 29.8, center line) or to added tetramethylsilane (δ = 0.00). MS analysis was performed with an Applied Biosystems Micromass Ultima system with ESI ionization. High resolution mass spectra (HRMS) were obtained at the University of Illinois mass spectrometry facility. All synthesized compounds gave HRMS within 5 ppm of the calculated values. The purity of amphotericin B and its derivatives was determined by HPLC analysis using a Waters SunFire Prep C_{18} OBD 5 micron 30 x 150 mm Lot # 168I161701 column with detection at 406 nm and an eluent of acetonitrile and aqueous ammonium acetate unless otherwise indicated.

Part 2. Synthesis of AmB derivatives

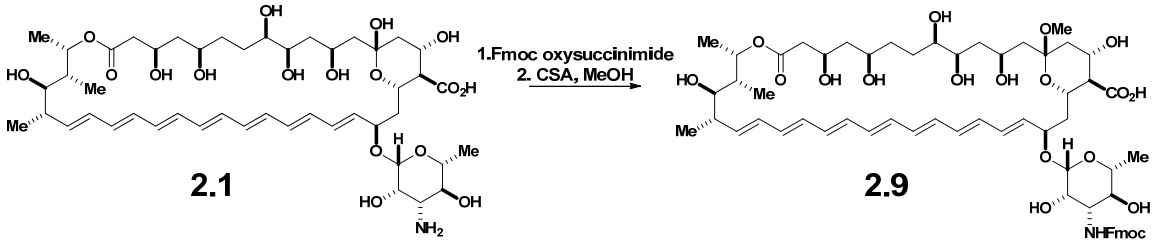

13-O-Methyl *N*-Fmoc Amphotericin B (2.9)

The following procedure was followed twice in parallel: Amphotericin B (1.5 g, 1.46 mmol) was dissolved in a mixture of DMF (70 mL) and methanol (35 mL) in a round-bottom flask with magnetic stirring under argon in the dark. Pyridine (840 μL, 10.22 mmol, freshly distilled over CaH_2) was added followed by *N*-(9-fluorenylmethoxycarbonyl)oxysuccinimide (840 mg, 2.48 mmol). The resulting solution was stirred for 13 hours at which point the reaction flask was poured into 1.8 L cold (0 °C) diethyl ether. The resulting yellow precipitate was stirred at 0 °C

for 30 minutes. The precipitate from both reaction flasks was collected by vacuum filtration. The filter cake was washed with cold diethyl ether, collected, and placed under high vacuum overnight. The yellow *N*-Fmoc amphotericin B (2.84 g, 2.5 mmol) was dissolved in 1:1 THF/Methanol (84 mL) in a round-bottom flask with magnetic stirring under argon in the dark. The reaction flask was cooled to 0 °C, (±)-10-camphorsulfonic acid (174 mg, 0.75 mmol) was added, and the reaction was stirred for 1 hour at 0 °C. Triethylamine (105 μL, 0.75 mmol) was added and the flask contents were filtered through filter paper to remove precipitated salt. The solution was concentrated *in vacuo* until precipitate began to form, at which point flask contents were poured into 800 mL 1:1 hexanes/diethyl ether, rinsing the flask with a small amount of 1:1 THF/diethyl ether. The resulting yellow precipitate was filtered and washed with 1:1 diethyl ether/ethyl acetate (250 mL). The filter cake was collected and placed under high vacuum overnight to furnish **2.9** as a yellow solid (3.04 g, 2.6 mmol, 90% from **2.1**) which was used without further purification.

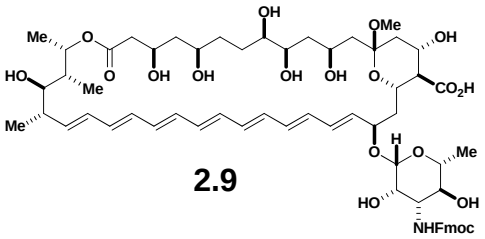

2.9

^{1}H NMR (400 MHz, DMSO *d*-5), selected resonances

δ 7.88 (d, *J* = 7.6 Hz, 2H), 7.76 (dd, *J* = 2.8, 4.4 Hz, 2H), 7.41 (t, *J* = 7.6 Hz, 2H), 7.32 (dd, *J* = 4.8, 7.2 Hz, 2H), 6.49-5.84 (m, 13H), 5.42 (dd, *J* = 4, 10.4 Hz, 1H), 5.19 (app d, *J* = 4.4 Hz, 1H), 4.82 (app t, *J* = 6.4 Hz, 3H), 4.77 (d, *J* = 4 Hz, 1H), 4.67 (m, 2H), 4.45 (d, *J* = 6 Hz, 1H), 4.21 (app t, *J* = 8.8 Hz, 1H), 4.10-3.92 (m, 2H), 3.58 (m, 1H), 3.55-3.30 (m, 5H), 3.21-3.01 (m, 4H), 2.35-2.21 (m, 1H), 2.14 (app d, *J* = 5.6 Hz, 2H), 1.96 (t, *J* = 11 Hz, 2H), 1.86 (d, *J* = 8 Hz, 1H), 1.70 (d, *J* = 6.8 Hz, 1H), 1.65-1.19 (m, 10H), 1.15 (d, *J* = 4.8 Hz, 3H), 1.09 (d, *J* = 6.0 Hz, 3H), 1.02 (d, *J* = 6.0 Hz, 3H), 0.90 (d, *J* = 7.2 Hz, 3H).

HRMS (ESI)

calculated for $C_{63}H_{85}NO_{19}$ $(M + Na)^+$: 1182.5614

found: . 1182.5608

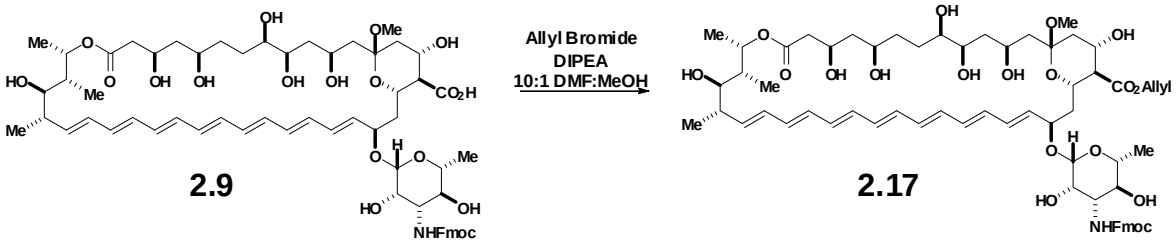

13-O-Methyl *N*-Fmoc Amphotericin B Allyl Ester (2.17)

Compound **2.9** (1.69 g, 1.46 mmol) was dissolved in 50 mL DMF with magnetic stirring under argon in the dark. Methanol (5 mL), Hunig's base (1 mL, 5.9 mmol), and allyl bromide (5 mL, 58 mmol) were added sequentially and the reaction was stirred for 4 hours, at which point the flask contents were poured into 2:1 hexanes/diethyl ether (1.8 L). A yellow-brown precipitate formed and settled to the bottom of the Erlenmeyer flask, and the hexanes/diethyl ether is removed via vacuum filtration. The precipitate (still on the bottom of the Erlenmeyer flask) was dissolved in a minimum amount of 1:1 THF/Methanol. The filter paper from the vacuum filtration was rinsed with 1:1 THF/Methanol and the combined crude product was concentrated *in vacuo* to a yellow-brown solid which was washed with water and gravity filtered through fluted filter paper. The solid was collected and coevaporated twice with acetonitrile. The crude solid was purified by flash chromatography (SiO_2, 10% methanol/methylene chloride) to yield **2.17** (1.275 g, 1.06 mmol, 73%) as a yellow solid.

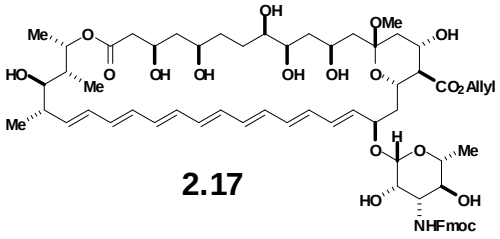

TLC (CH_2Cl_2:MeOH 9:1)

R_f = 0.4, stained by *p*-anisaldehyde

^{1}H NMR (400 MHz, CD_3OD), selected resonances

δ 7.82 (d, *J* = 7.6 Hz, 2H), 7.68 (dd, *J* = 3.2, 4 Hz, 2H), 7.39 (t, *J* = 7.4 Hz, 2H), 7.31 (app t, *J* = 7.4 Hz, 2H), 6.44-6.10 (m, 12H), 6.97 (ddd, *J* = 5.6, 11.2, 16.4 Hz, 1H), 6.85 (dd, *J* = 6.4, 15.2 Hz, 1H), 5.49 (dd, *J* = 9.6, 14 Hz, 1H), 5.40 (dd, *J* = 1,2, 16.8 Hz, 1H), 5.26 (app d, *J* = 10.9 Hz, 1H), 5.19 (app t, *J* = 5.2 Hz, 1H), 4.67 (app ddd, *J* = 6, 13.2, 19.2 Hz, 2H), 4.57 (app t, *J* = 7.2 Hz, 1H), 4.50 (s, 1H), 4.36 (d, *J* = 6.8 Hz, 2H), 4.23 (t, *J* =

6.8 Hz, 1H), 4.20-4.09 (m, 2H), 4.00 (t, *J* = 9.2 Hz, 1H), 3.93 (m, 1H), 3.79 (d, *J* = 2.8 Hz, 1H), 3.70 (m, 1H), 3.58 (app dd, *J*= 3.0, 9.8 Hz, 1H), 3.50 (app dd, *J* = 1.4, 8.6 Hz, 1H), 3.34 (s, 1H), 3.23-3.15 (m, 4H), 2.42-2.15 (m, 5H), 2.00 (m, 1H), 1.90-1.78 (m, 2H), 1.76-1.52 (m, 5H), 1.52-1.31 (m, 7H), 1.27 (d, *J* = 5.2 Hz, 3H), 1.19 (d, *J* = 6.4 Hz, 3H), 1.10 (d, *J* = 6.4 Hz, 3H), 1.00 (d, *J* = 6.8 Hz, 3H)

HRMS (ESI)

calculated for $C_{66}H_{89}NO_{19}$ $(M + Na)^+$: 1222.5927

found: 1222.5876

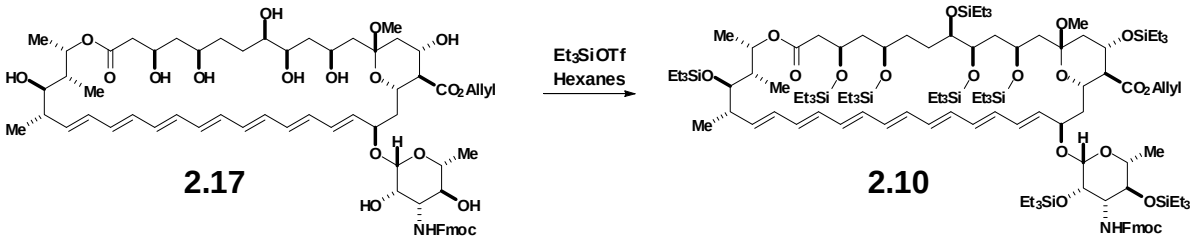

2.17 **2.10**

Nonakis-triethylsilyl 13-O-Methyl-*N*-Fmoc Amphotericin B Allyl Ester (2.10)

Compound **2.17** (535 mg, 0.45 mmol) was suspended in hexanes (15 mL, freshly distilled over CaH_2) with magnetic stirring under argon in the dark. The reaction flask was cooled to 0 °C, and 2,6-lutidine (0.94 mL, 8.1 mmol, freshly distilled over CaH_2) was added, followed by triethylsilyl trifluoromethanesulfonate (1.43 mL, 6.3 mmol, added dropwise), and the reaction was stirred for 2 hours at 0 °C. After two hours, 2,6-lutidine (0.47 ml, 4 mmol, freshly distilled over CaH_2) and triethylsilyl trifluoromethanesulfonate (0.72 mL, 3.15 mmol, added dropwise) were added. Fifteen minutes after completion of this addition, 2,6-lutidine (0.47 mL, 4 mmol, freshly distilled over CaH_2) and triethylsilyl trifluoromethanesulfonate (0.72 mL, 3.15 mmol, added dropwise) were added and the reaction was stirred for one more hour. The reaction was quenched by addition of saturated aqueous $NaHCO_3$ (~50 mL) and flask contents were transfeered to a separatory funnel containing saturated aqueous $NaHCO_3$ (~300 mL). Diethyl ether (~300 mL) was added to the separatory funnel and the crude product was partitioned between the organic and aqueous layers. The organic layer was washed with water (3 x 300 mL), saturated aqueous $CuSO_4$ (2 x 300 mL), and brine (1 x 300 mL). The organic layer was dried over anhydrous Na_2SO_4, gravity filtered through fluted filter paper, and concentrated *in*

vacuo to yield a viscous yellow-orange oil (still containing triethylsilanol). This oil was coevaporated with toluene overnight under high vacuum. A second coevaporation with toluene was performed before purification of the crude oil by flash chromatography (SiO_2, 10% to 25% Ether/Hexanes) to yield **2.10** as a yellow oil (517 mg, 0.23 mmol, 52%).

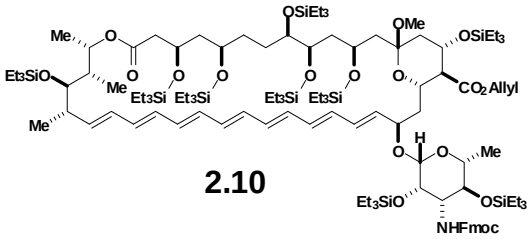

2.10

TLC (Petroleum ether:diethyl ether 4:1)

R_f = 0.6, stained by *p*-anisaldehyde

^{1}H NMR (Acetone-d_6, 500 MHz)

δ 7.64 (d, *J* = 7.5 Hz, 2H, **Fmoc–H**), 7.69, (d, *J* = 7 Hz, 2H, **Fmoc-H**), 7.42, (t, *J* = 7.5 Hz, 2H, **Fmoc–H**), 7.34 (tq, *J* = 7 Hz, 1 Hz, 2H, **Fmoc-H**), 6.56-6.11 (m, 12H, **H-21** through **H-32**), 6.06-5.94 (m, 2H, **H-20**, **H-43**), 5.49 (dd, *J* = 9.5, 15 Hz, 1H, **H-33**), 5.44 (app dd, *J* = 1.5, 17 Hz, 1H, **Allyl-H**), 5.35 (d, *J* = 10 Hz, 1H), 5.29 (dd, *J* = 1.5, 10 Hz, 1H, **Allyl H**), 4.76-4.58 (m, 4H, **Allyl-CH$_2$**, **H-37**, **H-19**), 4.51-4.41 (m, 2H, **H-15**, **Fmoc-H**), 4.47 (app s, 1H, **H-1'**), 4.33 (dd, *J* = 7.5, 10.5 Hz, 1H,**Fmoc–H**), 4.26-4.12 (m, 2H), 4.12 (m, 1H), 3.99 (m, 2H, **H-17**, one unassigned), 3.90 (d, *J* = 3 Hz, 1H, **H-2'**), 3,84 (dd, *J* = 2.5, 9 Hz, 1H, **H-35**), 3.66 (m, 2H, **H-3'**, one unassigned), 3.45 (t, *J* = 9 Hz, 1H, **H-4'**), 3.30 (m, 1H, **H-5'**), 3.13 (s, **C13-O<u>Me</u>**), 2.79 (d, *J* = 16.5 Hz, 1H), 2.57 (app d, *J* = 7 Hz, 2H), 2.43 (m, 1H, **H-34**), 2.36 (t, *J* = 10.25 Hz, 1H, **H-16**), 2.04-1.46 (m, 14H), 1.23 (d, *J* = 6 Hz, 3H, **H-6'**), 1.17 (d, *J* = 6 Hz, 3H, **H-38**), 1.07-0.89 (m, 87H,), 0.78-0.56 (m, 54H)

HRMS (ESI)

calculated for $C_{120}H_{215}NO_{19}Si_9$ $(M + Na)^+$:	2249.3710
found:	2249.3630

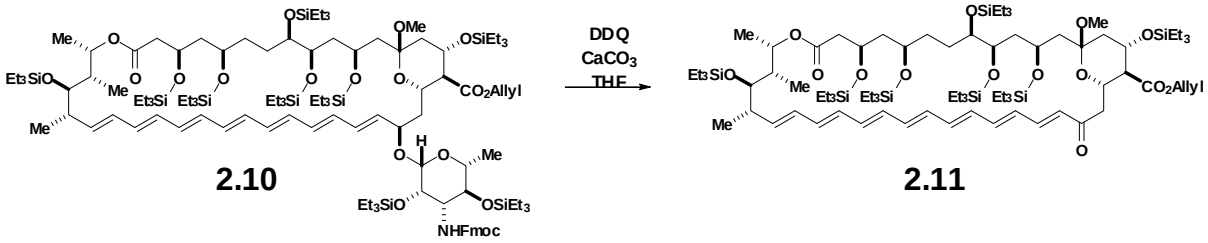

Heptakis-triethylsilyl 13-O-Methyl 20, 22, 24, 26, 28, 30, 32-Heptaen-19-one Amphoteronolide B Allyl Ester (2.11)

Compound **2.10** (1.02 g, 0.46 mmol) was dissolved in THF (23 mL) with magnetic stirring under argon in the dark. $CaCO_3$ (467 mg, 4.7 mmol) was added followed by 2,3-dichloro-5,6-dicyano-1,4-benzoquinone (157 mg, 0.69 mmol) and the reaction stirred at room temperature for 55 minutes over which time the solution color changed from yellow to orange. The reaction was quenched with saturated aqueous $NaHCO_3$, and diethyl ether was added to the reaction flask. Flask contents were transferred to a separatory funnel containing saturated aqueous $NaHCO_3$. Diethyl ether was added and the organic phase was washed twice with saturated aqueous $NaHCO_3$ and twice with brine. Aqueous $NaHCO_3$ phases were back-extracted with diethyl ether (3 times) until nearly colorless. The combined organic phases were dried over anhydrous Na_2SO_4, gravity filtered through fluted filter paper, concentrated in vacuo, and purified by flash chromatography (SiO_2, 10% then 20% ether/petroleum ether) to yield **2.11** as an orange foam (430 mg, 0.26 mmol, 57%).

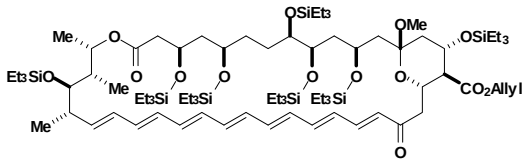

2.11

TLC (Petroleum ether:diethyl ether 4:1)

$R_f = 0.3$

^{1}H NMR (Acetone-d_6, 500 MHz), selected resonances

δ 7.82 (dd, J = 11.25, 15.75 Hz, 1H, **H-21**), 7.11 (dd, J = 11.5, 14.5 Hz, 1H, **H-23**), 6,80 (dd, J = 10.75, 14.75 Hz, 1H, **H-25**), 6.56 (m, 2H, **H-24, H-27**), 6.47-6.12 (m, 7H, **H-22**, **H-26**, **H-28** through **H-32**), 6.03 (d, J = 15.5 Hz, 1H, **H-20**), 6.00 (m, 1H, **Allyl-H**), 5.49 (dd, J = 10.25, 14.75 Hz, 1H, **H-33**), 5.40 (app ddd, J = 1.5, 3, 15.5 Hz 1H, **Allyl-H**),

5.25 (app ddd, *J* = 1.5, 2.5, 10.25 Hz, 1H, **Allyl-H**), 4.66 (app ddd, *J* = 1.5, 3, 5.5 Hz, 2H, **Allyl-CH$_2$**), 4.46 (m, 2H, **H-15**, **H-37**), 4.26 (m, 1H), 4.08 (m, 2H), 3.94 (dd, *J* = 3, 9.5 Hz, 1H, **H-35**), 3.75 (m, 1H, **H-17**), 3.66 (m, 1H), 3.18 (dd, *J* = 10.5, 12 Hz 1H, **H-18**), 2.90 (s, 3H, C13-O**CH$_3$**), 2.99 (m, 1H), 2.64 (m, 1H), 2.44 (m, 1H, **H-34**), 2.38 (t, *J* = 10.25 Hz, 1H, **H-16**), 2.28 (app t, *J* = 10.75 Hz, 1H), 2.12 (d, *J* = 12.5 Hz, 1H, **H-18**), 1.97-1.70 (m, 9H), 1.67-1.46 (m, 1H), 1.16-1.11 (m, 14H), 1.07-0.94 (m, 52H), 0.90-0.83 (m, 14H), 0.76-0.52 (m, 34H)

HRMS (ESI)

calculated for $C_{87}H_{164}O_{14}Si_7$ $(M + Na)^+$: 1652.0404

found: 1652.0308

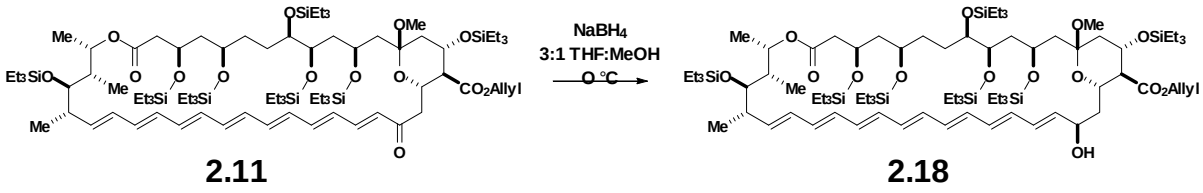

2.11 **2.18**

Heptakis-triethylsilyl-13-O-Methyl Amphoteronolide B Allyl Ester (2.18)

Compound **2.11** (708 mg, 0.43 mmol) was dissolved in a combination of THF (3.3 mL) and methanol (1.1 mL) with magnetic stirring under argon in the dark, and the reaction flask was cooled to 0 °C. $NaBH_4$ (163 mg, 4.3 mmol) was added and the reaction stirred 10 minutes over which time the solution color changed from orange to pale yellow. The flask contents were transferred to a separatory funnel containing saturated aqueous NH_4Cl (~200 mL). Diethyl ether (~200 mL) was added and the organic phase was washed with water (200 mL) and brine (200 mL), dried over anhydrous Na_2SO_4, and gravity filtered through fluted filter paper. The crude product was concentrated *in vacuo* and purified by flash chromatography (SiO_2, 10% then 30% diethyl ether/petroleum ether) to yield **2.18** as a yellow foam (550 mg, 0.34 mmol, 78%).

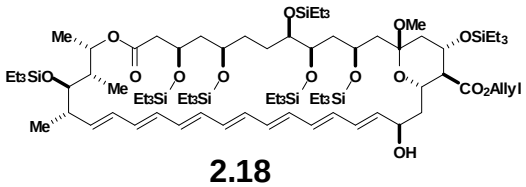

2.18

TLC (Petroleum ether:diethyl ether 7:3)

$R_f = 0.34$

^{1}H NMR (Acetone-d_6, 500 MHz)

δ 6.50-6.11 (m, 13H, **H-20 through H-32**), 5.98 (app ddd, *J* = 6, 11, 16.5 Hz, 1H, **Allyl-H**), 5.52 (dd, *J* = 9.5, 15 Hz, 1H, **H-33**), 5.38 (ddd, *J* = 1.5, 3, 17 Hz, 1H, **Allyl-H**), 5.23 (app dd, *J* = 1.5, 10 Hz, 1H, **Allyl-H**), 4.70 (m, 1H, **H-37**), 4.61 (m, 2H, **Allyl-CH_2**), 4.50 (m, 1H, **H-19**), 4.43 (dt, *J* = 5, 11 Hz, 1H, **H-15**), 4.24 (m, 1H), 4.12 (app t, *J* = 10 Hz, 1H), 4.05 (m, 1H, **H-17**), 3.99 (sep, 4.25 Hz, 1H), 3.93 (d, *J* = 4 Hz, 1H, C19-O**H**), 3.83 (dd, *J* = 3, 9 Hz, 1H, **H-35**), 3.69 (m, 1H), 3.62 (app dd, *J* = 4.5, 10.5 Hz, 1H), 3.15 (s, 3H, C13-O**CH_3**), 2.81 (s, 1H), 2.56 (m, 2H), 2.42 (m, 1H, **H-34**), 2.33 (t, *J* = 10 Hz, 1H, **H-16**), 2.10 (dd, *J* = 4.5, 12.5 Hz, 1H, **H-14**), 1.99 (m, 1H), 1.94-1.57 (m, 14H), 1.51 (m, 1H), 1.17 (d, *J* = 6 Hz, 3H, **H-38**), 1.06-0.93 (m, 69H), 0.76-0.57 (m, 42H).

HRMS (ESI)

calculated for $C_{87}H_{166}O_{14}Si_7$ $(M + Na)^+$: 1654.0560

found: 1654.0493

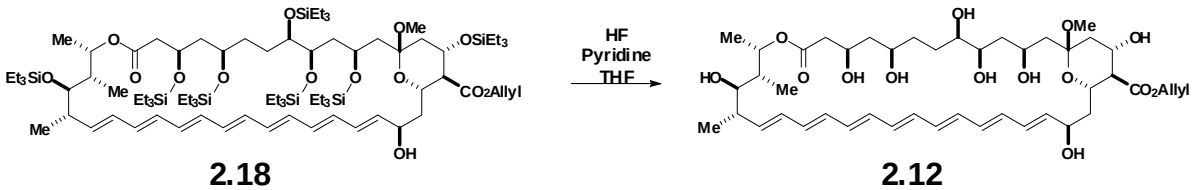

2.18 **2.12**

13-O-Methyl Amphoteronolide B Allyl Ester (2.12)

Compound **2.18** (550 mg, 0.34 mmol) was dissolved in THF (5 mL) in a plastic bottle with magnetic stirring under argon in the dark, and the reaction bottle was cooled to 0 °C. A separate

plastic bottle was charged with THF (3.8 mL) and 70% HF/Pyridine (6.4 mL) and cooled to 0 °C. Pyridine (6.4 mL) was added dropwise to the second bottle over 5 minutes, and the HF/Pyridine solution was cannulated to the plastic bottle containing **2.18**. The reaction was stirred for 12 hours at which time the reaction was quenched with saturated aqueous $NaHCO_3$ and transferred to a separatory funnel containing saturated aqueous $NaHCO_3$ (~200 mL). 20% methanol/methylene chloride was added and the aqueous phase was washed with 20% methanol/methylene chloride until colorless. The combined organic washes were concentrated *in vacuo* to remove approximately one-half of the solvent and benzene (~150 mL) was added to the flask. Flask contents were concentrated in vacuo and the crude product was purified by flash chromatography (SiO_2, 10% methanol/methylene chloride) to yield **2.12** as a yellow-orange solid (239 mg, 0.29 mmol, 84%). HRMS (ESI) calculated for $C_{45}H_{68}O_{14}$ $(M + Na)^+$: 855.46, found: 855.4.

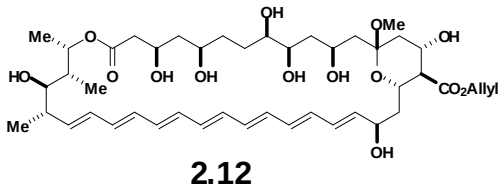

2.12

TLC (CH_2Cl_2:MeOH 4:1)

$R_f = 0.64$

^{1}H NMR (CD_3OD, 400 MHz)

δ 6.46-6.10 (m, 12H), 5.98 (app ddd, *J* = 5.6, 11.2, 16.4 Hz, 1H), 5.80 (dd, *J* = 7.6, 14.8 Hz, 1H), 5.47 (dd, *J* = 9.6, 14 Hz, 1H), 5.38 (ddd, *J* = 1.6, 32., 17.2 Hz, 1H), 5.24 (app dd, *J* = 1.6, 10.4 Hz, 2H), 4.66 (app d, *J* = 5.6 Hz, 2H), 4.47 (dd, *J* = 7.2, 12 Hz, 1H), 4.25-4.14 (m, 5H), 3.99 (m, 1H), 3.90 (app d, *J* = 4.4 Hz, 1H), 3.70 (m, 1H), 3.53 (app d, *J* = 10.8 Hz, 1H), 3.27-3.20 (m, 2H), 3.18 (s, 3H), 2.43-2.16 (m, 5H), 2.11 (dd, *J* = 4.8, 13.2 Hz, 1H), 1.89-1.25 (m, 10H), 1.19 (d, *J* = 6.4 Hz, 3H), 1.11 (d, *J* = 6.4 Hz, 3H), 1.00 (d, *J* = 7.4 Hz, 3H).

HRMS (ESI)

calculated for $C_{45}H_{68}O_{14}$ $(M + Na)^+$: 855.4507

found: 855.4531

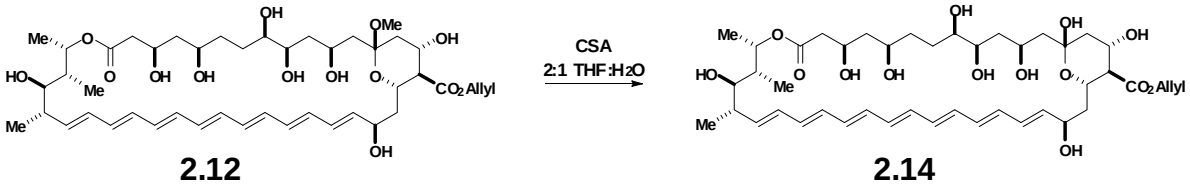

2.12 **2.14**

Amphoteronolide B Allyl Ester (2.14)

Compound **2.12** (68.4 mg, 0.082 mmol) was dissolved in a combination of THF (mL) and water (mL) with magnetic stirring under argon in the dark. (±)-10-camphorsulfonic acid (5.7 mg, 0.025 mmol) was added and the reaction was stirred for 5.5 hours at room temperature. The reaction was quenched with triethylamine and flask contents were concentrated *in vacuo* to remove THF and precipitate the crude product as an aqueous slurry. The yellow precipitate was collected by vacuum filtration. The filter cake was washed with water, the solid collected, and the filter paper washed with THF and acetonitrile. The crude solid was concentrated *in vacuo* to yield **2.14** as a yellow solid (51.4 mg, 0.063 mmol, 77%). The characterization below is of the actual material used in NMR studies (synthesized by Dan Palacios, NMR characterization by the author).

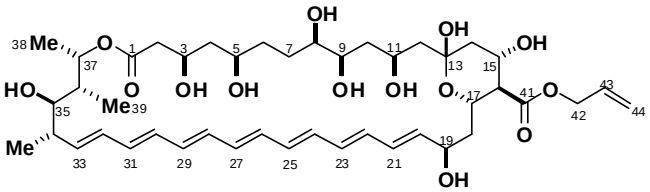

2.14

Proton and coupling constant assignments were made using a variety of two-dimensional NMR techniques including phase-sensitive COSY experiments combined with amplitude constrained multiplet evaluation (ACME).[6b] The polyene macrolide skeletons of **2.1 - 2.4** are quite rigid and hydrogen atoms can be assigned as having pseudoequatorial (e) and pseudoaxial (a) orientations.[2] The labeling scheme used herein is consistent with that utilized by Sowinski et al.[1]

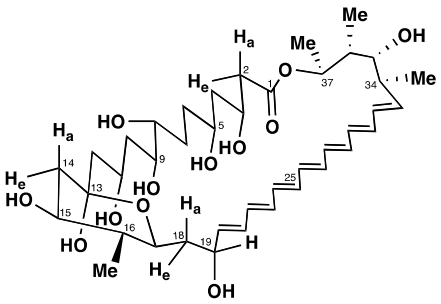

HPLC

tR = 28.6 min; flow rate = 25 mL/min, gradient of 5 → 95% MeCN in H_2O over 25 min.

^{1}H NMR (500 MHz, pyridine *d*-5:CD_3OD 10:1)

δ 6.83 (dd, J = 11, 15 Hz, 1H, **H-22**), 6.77 (dd, J = 11, 15 Hz, 1H, **H-24**), 6.69 (dd, $J_{19,20}$ = 9.5 Hz, $J_{20,21}$ = 15.5 Hz, 1H, **H-20**), 6.61 (dd, J = 14.5, 15 Hz, 1H, **H-26**), 6.54-6.35 (m, 9H), 6.04-5.96 (app ddd, $J_{42,43}$ = 6.5, $J_{43,44cis}$ = 11 Hz, $J_{43,44trans}$ = 17 Hz, 1H, **H-43**), 5.80 (app d, $J_{36,37}$ = 1.9 Hz, 1H, **H-37**), 5.55 (dd, $J_{32,33}$ = 15 Hz, $J_{33,34}$ = 10.1 Hz, 1H, **H-33**), 5.42 (dd, $J_{44cis,44trans}$ = 1.5 Hz, $J_{43,44trans}$ = 17.5 Hz, 1H, **H-44*trans***), 5.30 (app t, $J_{16,17}$ = 10.6 Hz, $J_{17,18e}$ = 0.9 Hz, $J_{17,18a}$ = 8.7 Hz, 1H, **H-17**), 5.14 (dd, $J_{44cis,44trans}$ = 1.5 Hz, $J_{43,44cis}$ = 10.5 Hz, 1H, **H-44*cis***), 5.06 (app dt, $J_{14e,15}$ = 3.5 Hz, $J_{14a,15}$ = 11.0 Hz, $J_{15,16}$ = 10.7 Hz, 1H, **H-15**), 4.87 (t, $J_{10a,11}$ = 3.1 Hz, $J_{10e,11}$ = 10.3 Hz, $J_{11,12a}$ = 3.4 Hz, $J_{11,12e}$ = 11.3 Hz, 1H, **H-11**), 4.80-4.73 (m, $J_{18e,19}$ = 6.0 Hz, $J_{19,20}$ = 8.8 Hz, 3H, **H-19**, **H-42**(2)), 4.64 (app t, $J_{2a,3}$ = 4.7 Hz, $J_{2e,3}$ = 9.2 Hz, $J_{3,4a}$ = 3.9 Hz, $J_{3,4e}$ = 10.1 Hz, 1H, **H-3**), 4.13 (app t, $J_{4a,5}$ = 4.4 Hz, $J_{4e,5}$ = 9.5 Hz, $J_{5,6a}$ = 5.4 Hz, $J_{5,6e}$ = 10.3 Hz, 1H, **H-5**), 4.04 (app d, $J_{8,9}$ = 3.0 Hz, $J_{9,10a}$ = 3.3 Hz, $J_{9,10e}$ = 10.7 Hz, 1H, **H-9**), 3.61 (app d, $J_{7e,8}$ = 2.8 Hz, $J_{7a,8}$ = 11.2 Hz, $J_{8,9}$ = 3.0 Hz, 1H, **H-8**), 3.43 (app d, $J_{34,35}$ = 9.8 Hz, $J_{35,36}$ = 2.6 Hz, 1H, **H-35**), 2.85 (t, $J_{15,16}$ = 10.7 Hz, $J_{16,17}$ = 10.6 Hz, 1H, **H-16**), 2.66 (m, $J_{33,34}$ = 10.1 Hz, $J_{34,35}$ = 9.8 Hz, 1H, **H-34**), 2.61 (dd, $J_{2a,2e}$ = 17 Hz $J_{2e,3}$ = 9.2 Hz, 1H, **H-2e**), 2.51 (dd, $J_{14a,14e}$ = 12 Hz $J_{14e,15}$ = 3.5 Hz, 1H, **H-14e**), 2.46 (dd, $J_{2a,2e}$ = 16.5, $J_{2a,3}$ = 4.7, 1H, **H-2a**), 2.41 (dd, $J_{17,18e}$ = 0.9 Hz, $J_{18a,18e}$ = 14 Hz, $J_{18e,19}$ = 6.0 Hz, 1H, **H-18e**), 2.37 (m, $J_{7e,8}$ = 2.8 Hz, 1H, **H-7e**), 2.19-2.15 (m, $J_{9,10e}$

= 10.7 Hz, $J_{10e,11}$ = 10.3 Hz, $J_{17,18a}$ = 8.7 Hz. 2H, **H-10e**, **H18a**), 2.10 (m, $J_{35,36}$ = 2.6 Hz, $J_{36,37}$ = 1.9 Hz, 1H, **H-36**), 2.00-1.95 (m, $J_{5,6e}$ = 10.3 Hz, $J_{11,12e}$ = 11.3 Hz, 2H, **H-6e**, **H-12e**), 1.85-1.80 (m, $J_{3,4e}$ = 10.1 Hz, $J_{4e,5}$ = 9.5 Hz, $J_{7a,8}$ = 11.2 Hz, $J_{14e,15}$ = 3.5 Hz, 3H, **H-4e**, **H-7a**, **H-14e**), 1.78-1.70 (m, $J_{5,6a}$ = 5.4 Hz, $J_{11,12a}$ = 3.4 Hz, 2H, **H-6a**, **H-12a**), 1.61 (app t, $J_{3,4a}$ = 3.9 Hz, $J_{4a,5}$ = 4.4 Hz, 1H, **H-4a**), 1.56 (app d, $J_{9,10a}$ = 3.3 Hz, $J_{10a,10e}$ = 14.5 Hz, $J_{10a,11}$ = 3.1 Hz, 1H, **H-10a**), 1.46 (d, $J_{37,38}$ = 6.5 Hz, 3H, **H-38**), 1.31 (d, $J_{34,40}$ = 6 Hz, 3H, **H-40**), 1.25 (d, $J_{36,39}$ = 7 Hz, 3H, **H-39**).

^{13}C NMR (150 MHz, pyridine *d*-5:CD_3OD, 10:1)

δ 173.5, 172.2, 140.9, 137.5, 135.0, 134.8, 134.7, 134.1, 133.7, 133.5, 133.4, 133.3, 133.2, 133.1, 132.9, 132.8, 129.1, 118.0, 98.6, 78.8, 76.3, 75.2, 72.2, 71.1, 70.4, 69.7, 68.5, 68.1, 67.0, 66.7, 65.4, 59.0, 47.6, 45.9, 45.1, 43.8, 43.0, 42.8, 41.1, 41.0, 39.4, 36.6, 31.8, 30.2, 29.5, 26.0, 24.4, 23.5, 19.1, 17.4, 12.9.

HRMS (ESI)

calculated for $C_{44}H_{66}O_{14}$ $(M+Na)^+$: 841.4350

found: 841.4369

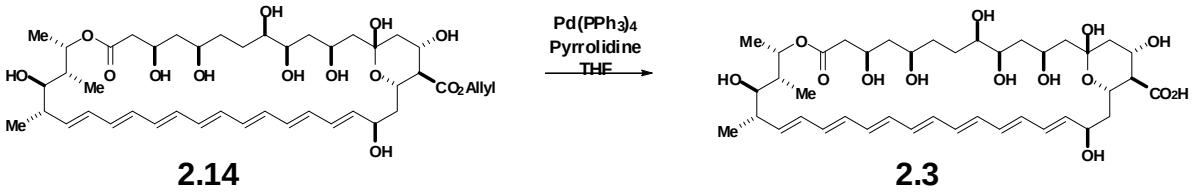

2.14 **2.3**

Amphoteronolide B (2.3)

Compound **2.14** was dissolved in THF (3.9 mL) with magnetic stirring under argon in the dark. Pyrrolidine (16 μL) followed by $Pd(PPh_3)_4$ (0.5 mL of a 0.017 M solution in THF, 0.008 mmol) were added sequentially. The crude product precipitated immediately and the reaction was stirred for 30 minutes. Flask contents were diluted with ether and the precipitate was collected by vacuum filtration, washing the filter cake with ether. The yellow solid was collected and acetonitrile added to coevaoporate residual THF/ether/pyrrolidine. The crude product was dissolved in 1:1 THF/methanol, filtered through a 0.2 micron syringe filter and purified by

HPLC (10 x 250 SunFire C18 ODS column) to yield **2.3** as a pale yellow solid (40 mg, 16 %). In the initial synthesis of **2.3**, a clean NMR spectrum was not obtained due to decomposition. Full characterization of **2.3** was accomplished by Dan Palacios. As **2.3** was also used in yeast assays, full characterization is shown below.

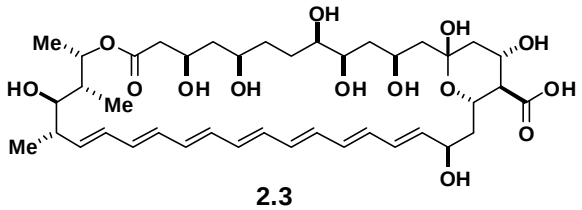

2.3

HPLC

tR: 21.6 min; flow rate = 25 mL/min, gradient of 0 → 75% MeCN in 10 mM ammonium acetate over 25 min.

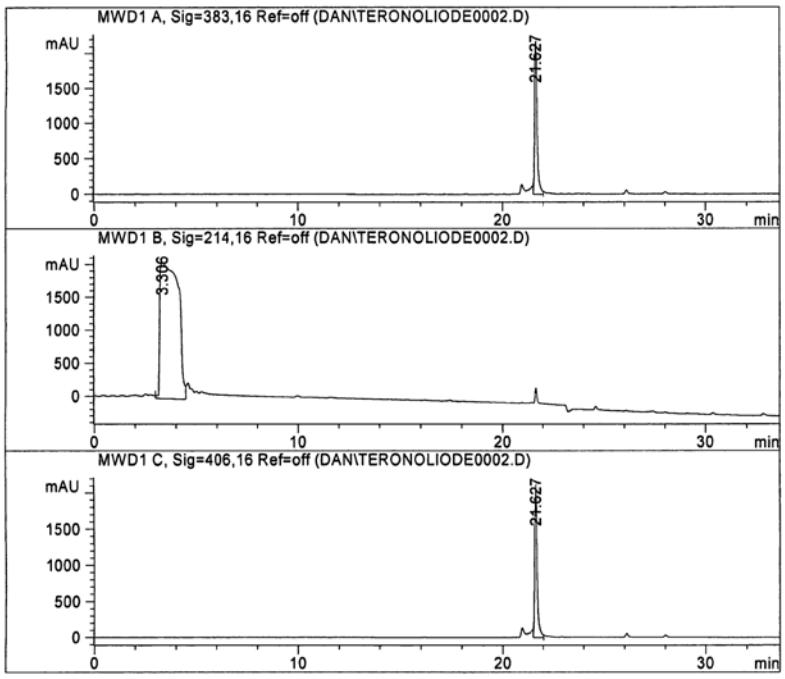

^{1}H NMR (pyridine *d*-5:CD_3OD 10:1)

δ 6.76-6.67 (m, 2H), 6.59-6.55 (m, 2H), 6.45-6.35 (m, 10H), 5.72 (app d, *J* = 5 Hz, 1H), 5.16 (app t, *J* = 10 Hz, 1H), 4.92 (bs, 1H), 4.78 (bs, 2H), 4.57 (app t, *J* = 10 Hz, 1H), 4.05 (app t, 9.5 Hz, 1H), 3.95 (app d, *J* = 10.5 Hz, 1H), 3.65 (app d, *J* = 4 Hz, 1H), 3.52 (app d, *J* = 10.5 Hz, 1H), 3.41 (app d, *J* = 9 Hz, 1H), 2.64 (bs, 2H), 2.56 (dd, *J* = 10, 16.5 Hz, 1H), 2.43-2.40 (m, 2H), 2.24 (bs, 2H), 2.10-2.05 (m, 2H), 1.95-1.90 (m, 2H), 1.79-1.65

(m, 5H), 1.58 (app d, J = 13.5 Hz, 1H), 1.51 (app d, J = 11 Hz, 1H), 1.41 (d, J = 6.5 Hz, 3H), 1.28 (d, J = 6.5 Hz, 3H), 1.21 (d, J = 7 Hz, 3H).

HRMS

Calculated for $C_{41}H_{62}O_{14}$ $(M+Na)^+$: 801.4037

found: 801.4039

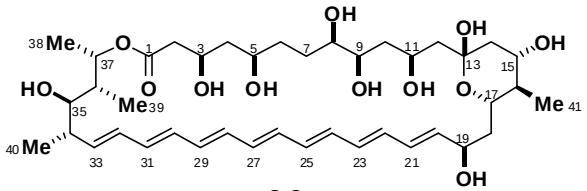

2.2

C41-Methyl amphoteronolide B (2.2)

Compound **2.2** was synthesized and purified by Dan Palacios for use in NMR and yeast studies as was recently described.[5] Full NMR characterization was completed by the author.

HPLC

tR = 24.9 min, flow rate = 25 mL/min, gradient of 5 → 95% MeCN in H_2O over 25 min.

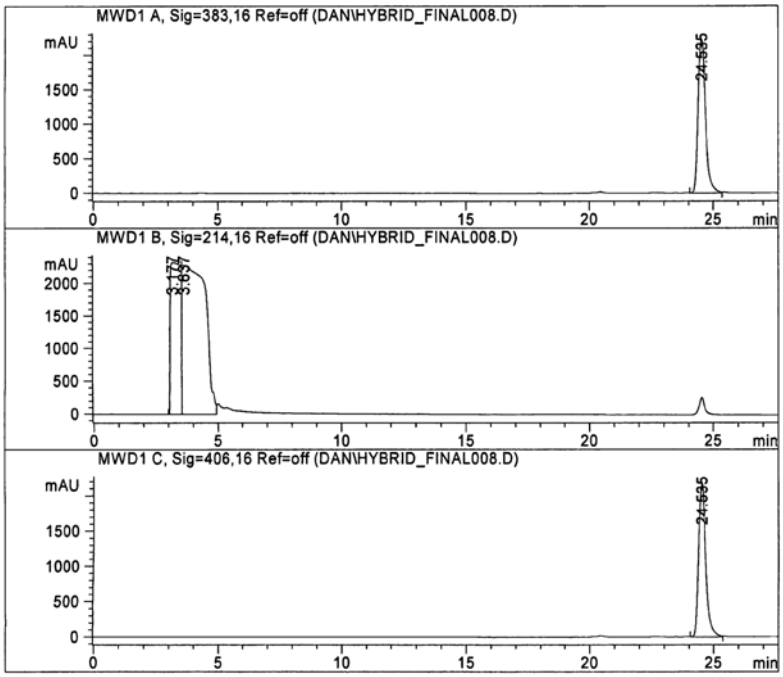

^{1}H NMR (600 MHz, pyridine *d*-5, CD_3OD 10:1)

δ 6.83 (dd, J = 10.8, 14.7 Hz, 1H, **H-22**), 6.77 (dd, J = 10.8, 15 Hz, 1H, **H-24**), 6.70 (dd, $J_{19,20}$ = 8.9 Hz, $J_{20,21}$ = 15 Hz, 1H, **H-20**), 6.60 (dd, J = 11.4, 14.4 Hz, 1H, **H-23**), 6.55-6.35 (m, 9H), 5.79 (app d, $J_{36,37}$ = 3.1 Hz, 1H, **H-37**), 5.55 (dd, $J_{32,33}$ = 15.6, $J_{33,34}$ = 9.9 Hz, 1H, **H-33**), 4.87 (app t, $J_{10a,11}$ = 1.3 Hz, $J_{10e,11}$ = 10.9 Hz, $J_{11,12a}$ = 1.2 Hz, $J_{11,12e}$ = 10.7 Hz, 1H, **H-11**), 4.77 (m, $J_{18a,19}$ = 3.9, $J_{18e,19}$ = 5.5 Hz, $J_{19,20}$ = 8.9 Hz, 1H, **H-19**), 4.65 (m, $J_{2e,3}$ = 9.2 Hz, $J_{3,4a}$ = 4.3, $J_{3,4e}$ = 10.9 Hz, $J_{16,17}$ = 10.8 Hz, $J_{17,18a}$ = 8.1 Hz, 2H, **H-3**, **H-17**), 4.20 (app dt, $J_{14e,15}$ = 2.1, $J_{14a,15}$ = 11.5 Hz, $J_{15,16}$ = 10.8 Hz, 1H, **H-15**), 4.12 (app t, $J_{4a,5}$ = 1.8, $J_{4e,5}$ = 10.3 Hz, $J_{5,6a}$ = 1.1, $J_{5,6e}$ = 11.5 Hz, 1H, **H-5**), 4.03 (app dd, $J_{8,9}$ = 3.2 Hz, $J_{9,10a}$ = 2.3, $J_{9,10e}$ = 11.7 Hz, 1H, **H-9**), 3.60 (app dd, $J_{7e,8}$ = 2.4, $J_{7a,8}$ = 11.3 Hz, $J_{8,9}$ = 3.2 Hz, 1H, **H-8**), 3.44 (app d, $J_{34,35}$ = 10.0 Hz, $J_{35,36}$ = 2.6 Hz, 1H, **H-35**), 2.68 (m, $J_{33,34}$ = 9.9 Hz, $J_{34,35}$ = 10.0 Hz, 1H, **H-34**), 2.62 (dd, $J_{2a,2e}$ = 16.2 Hz, $J_{2e,3}$ = 9.2 Hz, 1H, **H-2e**), 2.49-2.44 (m, $J_{14e,15}$ = 2.1 Hz, $J_{18e,19}$ = 5.5 Hz, 3H, **H-2a**, **H-14e**, **H-18e**), 2.37-2.34 (m, $J_{6a,7a}$ = 10.6 Hz, $J_{6e,7a}$ = 5.7 Hz, $J_{7a,8}$ = 11.3, 1H, **H-7a**), 2.19-2.15 (m, $J_{9,10e}$ = 11.7 Hz, $J_{10e,11}$ = 10.9 Hz, 1H, **H-10e**) 2.13-2.10 (m, $J_{35,36}$ = 2.6 Hz, $J_{36,37}$ = 3.1 Hz, 1H, **H-36**), 2.02 (ddd, $J_{17,18a}$ = 8.1 Hz, $J_{18a,18e}$ = 14.4 Hz, $J_{18a,19}$ = 3.9 Hz, 1H, **H-18a**), 1.99-1.95 (m, $J_{5,6e}$ = 11.5 Hz, $J_{6e,7a}$ = 5.7 Hz, $J_{6e,7e}$ = 13.5 Hz, $J_{11,12e}$ = 10.7 Hz, 2H, **H-6e**, **H-12e**), 1.85-1.74 (m, $J_{3,4e}$ = 10.9 Hz, $J_{4e,5}$ = 10.3 Hz, $J_{6e,7e}$ = 13.5 Hz, $J_{7e,8}$ = 2.4 Hz, $J_{11,12a}$ = 1.2 Hz, $J_{14a,15}$ = 11.5 Hz, 4H, **H-4e**,

H-7e, **H-12a**, **H-14a**), 1.72-1.66 (m, $J_{5,6a}$ = 1.1 Hz, $J_{6a,7a}$ = 10.6 Hz, $J_{15,16}$ = 10.8 Hz, 2H, **H-6a**, **H-16**), 1.63 (app dt, $J_{3,4a}$ = 4.3 Hz, $J_{4a,4e}$ = 14.1 Hz, $J_{4a,5}$ = 1.8 Hz, 1H, **H-4a**), 1.56 (app dd, $J_{9,10a}$ = 2.3Hz, $J_{10a,10e}$ = 14.4 Hz, $J_{10a,11}$ = 1.3 Hz, 1H, **H-10a**), 1.45 (d, $J_{37,38}$ = 6.6 Hz, 3H, **H-38**), 1.34 (d, $J_{16,41}$ = 6 Hz, 3H, **H-41**), 1.31 (d, $J_{34,40}$ = 6 Hz, 3H, **H-40**), 1.24 (d, $J_{36,39}$ = 7.2 Hz, 3H, **H-39**).

^{13}C NMR (150 MHz, pyridine *d*-5 : CD_3OD, 10:1)

δ 172.1, 141.4, 137.5, 135.1, 134.8, 134.2, 133.6, 133.4, 133.1, 132.8, 132.7, 129.1, 98.3, 78.7, 76.3, 75.3, 75.2, 72.2, 71.4, 70.4, 69.7, 68.5, 48.2, 46.7, 45.1, 44.4, 43.8, 43.0, 41.5, 41.2, 41.0, 36.6, 31.9, 30.2, 29.8, 19.1, 17.4, 14.1, 12.8.

HRMS (ESI)

calculated for $C_{41}H_{64}O_{12}$ $(M + Na)^+$: 771.4295

found: 771.4268

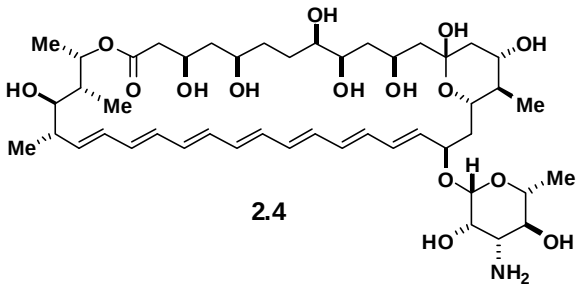

2.4

C41-Methyl amphotericin B (2.4)

Compound **2.4** was synthesized, purified, and characterized by Dan Palacios for use in yeast studies as was recently described.[5]

HPLC

tR = 21.7 minutes; flow rate = 25 mL/min, gradient of 5 → 95% MeCN in 5 mM ammonium acetate over 25 min.

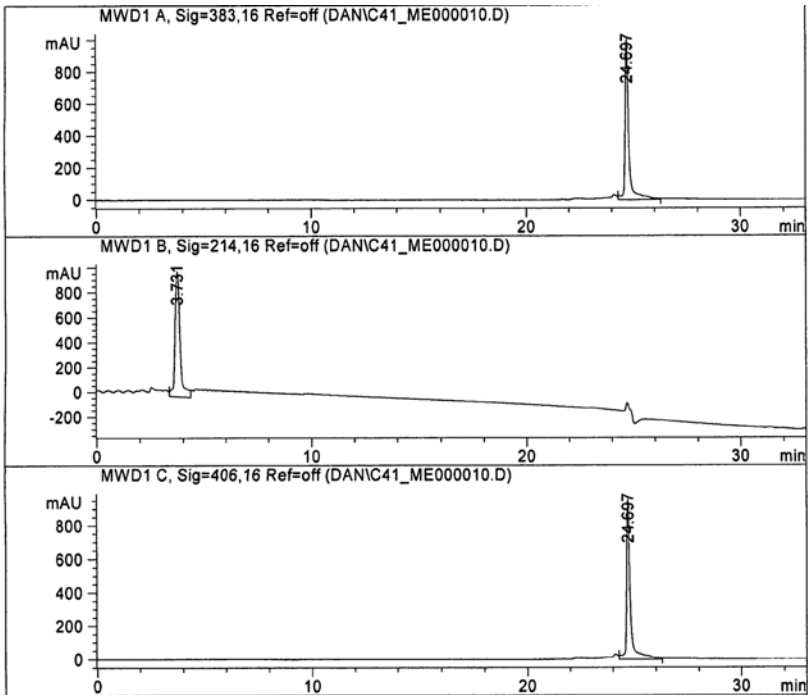

^{1}H NMR (500 MHz, pyridine *d*-5:CD_2OD 10:1)

δ 6.78-6.71 (m, 2H), 6.58-6.37 (m, 9H), 6.43-6.35 (m, 2H), 5.77 (app d, *J* = 5.5 Hz, 1H), 5.54 (dd, *J* = 10, 15 Hz, 1H), 4.95 (s, 1H), 4.81-4.77 (m, 2H), 4.61 (dt, *J* = 3, 12.5 Hz, 1H), 4.45-4.40 (m, 2H), 4.35 (d, *J* = 2.5 Hz, 1H), 4.11-4.03 (m, 2H), 4.00 (app d, *J* = 11 Hz, 1H), 3.77 (t, *J* = 9 Hz, 1H), 3.66-3.58 (m, 2H), 3.57 (app d, *J* = 11 Hz, 1H) 3.42 (app d, *J* = 9.5 Hz, 1H), 2.66 (app dd, *J* = 7, 9.5 Hz, 1H), 2.60 (dd, *J* = 9.5, 16.5 Hz, 1H), 2.49 (dd, *J* = 5.5, 14.5 Hz, 1H), 2.41 (app dd, *J* = 7.5, 12 Hz, 2H), 2.39-2.35 (m, 1H), 2.10 (app dd, *J* = 7.5, 15.5, 2H), 1.95-1.88 (m, 3H), 1.81-1.72 (m, 3H), 1.70-1.67 (m, 2H), 1.66-1.59 (m, 2H), 1.52 (d, *J* = 6 Hz, 3H), 1.44 (d, *J* = 6.5 Hz, 3H), 1.30 (d, *J* = 6.5 Hz, 3H), 1.24 (d, *J* = 7 Hz, 3H), 1.22 (d, *J* = 6.5 Hz, 3H).

HRMS (ESI)

calculated for $C_{47}H_{75}NO_{15}$ $(M + Na)^+$: 894.5191

found: 894.5182

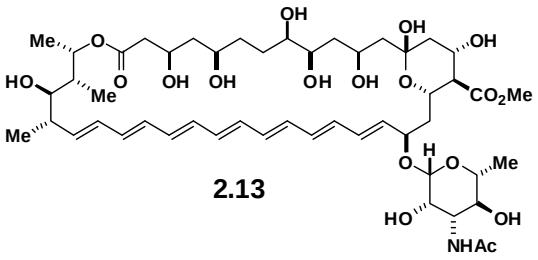

2.13

***N*-acyl amphotericin B methyl ester (2.13)**

Compound **2.13** was prepared as described by Nicolaou et al.[3a]

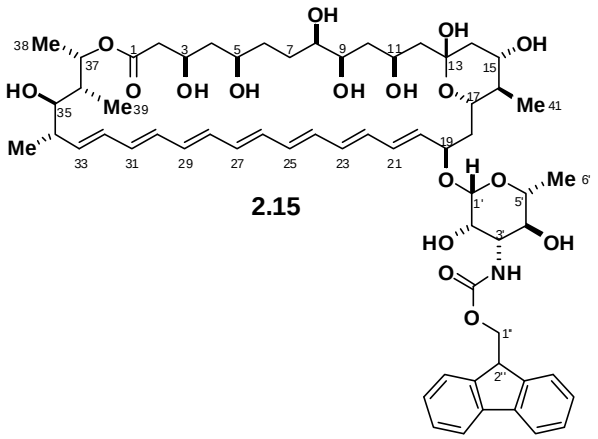

2.15

N-Fmoc-41-methyl amphotericin B (2.15)

Compound **2.15** was synthesized and purified by Dan Palacios for use in NMR studies as was recently described.[5] Full NMR characterization was completed by the author.

HPLC

tR = 25.1 minutes; flow rate = 25 mL/min, gradient of 5 → 95% MeCN in 5 mM ammonium acetate over 25 min.

^{1}H NMR (600 MHz, pyridine *d*-5:CD_3OD 10:1)

δ 7.85 (d, J = 7.2 Hz, 2H), 7.71 (dd, J = 6, 8.5 Hz, 2H), 7.41 (t, J = 7.2 Hz, 2H), 6.74 (m, 2H), 6.60-6.34 (m, 11H), 5.77 (app d, $J_{36,37}$ = 1.8 Hz, 1H, **H-37**), 5.54 (dd, $J_{32,33}$ = 15 Hz $J_{33,34}$ = 10.0, 1H, **H-33**), 4.97 (app s, $J_{1',2'}$ = 1.6 Hz, 1H, **H-1'**), 4.82-4.78 (m, $J_{10e,11}$ = 10.4 Hz, $J_{11,12e}$ = 11.0 Hz, $J_{18a,19}$ = 2.5 Hz, $J_{18e,19}$ = 4.6 Hz, $J_{19,20}$ = 8.0 Hz, 2H, **H-11**, **H-19**), 4.62 (app t, $J_{2a,3}$ = 1.8 Hz, $J_{2e,3}$ = 9.1 Hz, $J_{3,4a}$ = 2.0 Hz, $J_{3,4e}$ = 10.1 Hz, 1H, **H-3**), 4.51-4.43 (m, $J_{16,17}$ = 10.4 Hz, $J_{17,18a}$ = 7.5 Hz, 3H, **H-17**, **H-1''**(2)), 4.39 (app d, $J_{1',2'}$ = 1.6 Hz, 1H, **H-2'**), 4.34 (dd, $J_{2',3'}$ = 3 Hz, $J_{3',4'}$ = 9.7 Hz, 1H, **H-3'**), 4.29 (t, J = 7.2 Hz, 1H, **H-2''**), 4.12-4.07 (m, $J_{4a,5}$ = 1.0 Hz, $J_{4e,5}$ = 9.6 Hz, $J_{5,6a}$ = 1.8 Hz, $J_{5,6e}$ = 10.7 Hz, $J_{14e,15}$ = 2.6 Hz, $J_{14a,15}$ = 11.8 Hz, $J_{15,16}$ = 11.2 Hz, 2H, **H-5**, **H-15**), 4.02-3.99 (m, $J_{8,9}$ = 3.4 Hz, $J_{9,10a}$ = 2.6 Hz, $J_{9,10e}$ = 10.7 Hz, $J_{3',4'}$ = 9.7 Hz, $J_{4',5'}$ = 9.1 Hz, 2H, **H-9**, **H-4'**), 3.73 (app dd, $J_{4',5'}$ = 9.1 Hz, $J_{5',6'}$ = 6.6 Hz, 1H, **H-5'**), 3.58 (app d, $J_{7e,8}$ = 2.5 Hz, $J_{7a,8}$ = 10.6 Hz, $J_{8,9}$ = 3.4 Hz, 1H, **H-8**), 3.43 (app d, $J_{34,35}$ = 9.6 Hz, $J_{35,36}$ = 2.5 Hz, 1H, **H-35**), 2.67 (app dd, $J_{33,34}$ = 10.0 Hz, $J_{34,35}$ = 9.6 Hz, 1H, **H-34**), 2.60 (dd, $J_{2a,2e}$ = 16.8 Hz, $J_{2e,3}$ = 9.1 Hz, 1H, **H-2e**),

2.46 (app dd, $J_{18a,18e}$ = 16.8 Hz, $J_{18e,19}$ = 4.6 Hz, 1H, **H-18e**), 2.44-2.40 (m, $J_{2a,3}$ = 1.8 Hz, $J_{14e,15}$ = 2.6 Hz, 2H, **H-2a**, **H-14e**), 2.36-2.33 (m, $J_{6e,7e}$ = 13.4 Hz, $J_{7e,8}$ = 2.5 Hz, 1H, **H-7e**), 2.17-2.07 (m, $J_{9,10e}$ = 10.7 Hz, $J_{10e,11}$ = 10.4 Hz, $J_{35,36}$ = 2.5 Hz, $J_{36,37}$ = 1.8 Hz, 2H, **H-10e**, **H-36**), 2.02-1.90 (m, $J_{5,6e}$ = 10.7 Hz, $J_{6e,7a}$ = 4.4 Hz, $J_{6e,7e}$ = 13.4 Hz, $J_{11,12e}$ = 11.0 Hz, $J_{17,18a}$ = 7.5 Hz, $J_{18a,19}$ = 2.5 Hz, 3H, **H-6e**, **H-12e**, **H-18a**), 1.81-1.76 (m, $J_{3,4e}$ = 10.1 Hz, $J_{4e,5}$ = 9.6 Hz, $J_{6e,7a}$ = 4.4 Hz, $J_{6a,7a}$ = 12.7 Hz, $J_{7a,8}$ = 10.6 Hz, 3H, **H-4e**, **H-7a**, **H12a**), 1.73-1.69 (m, $J_{5,6a}$ = 1.8 Hz, $J_{6a,7a}$ = 12.7 Hz, $J_{14a,15}$ = 11.8 Hz, 2H, **H-6a**, **H-14a**), 1.62-1.60 (m, $J_{3,4a}$ = 2.0 Hz, $J_{4a,5}$ = 1.0 Hz, $J_{15,16}$ = 11.2 Hz, $J_{16,17}$ = 10.4 Hz, 2H, **H-4a**, **H-16**), 1.56 (d, $J_{5',6'}$ = 6.6 Hz, 3H, **H-6'**), 1.55-1.52 (m, $J_{9,10a}$ = 2.6 Hz, 1H, **H-10a**), 1.44 (d, $J_{37,38}$ = 6.6 Hz, 3H, **H-38**), 1.30 (d, $J_{34,40}$ = 6.6 Hz, 3H, **H-40**), 1.24 (d, $J_{36,39}$ = 7 Hz, 3H, **H-39**), 1.23 (d, $J_{16,41}$ = 5.2 Hz, 3H, **H-41**). One of the Fmoc proton resonances was obscured by a solvent peak.

^{13}C NMR (150 MHz, pyridine *d*-5:CD_3OD 10:1)

δ 172.2, 158.0, 145.1, 144.9, 142.0, 141.9, 138.2, 137.6, 134.9, 134.8, 134.5, 134.1, 133.7, 133.5, 133.4, 133.2, 132.9, 130.3, 128.3, 127.8, 126.1, 123.6, 126.0, 120.7, 108.6, 99.6, 98.3, 78.8, 78.1, 76.3, 75.3, 75.0, 72.2, 71.9, 71.5, 70.4, 69.7, 69.5, 68.5, 67.6, 67.1, 58.7, 48.1, 45.1, 44.2, 43.1, 41.1, 36.6, 30.3, 19.1, 18.8, 17.5, 14.1, 12.8.

HRMS (ESI)

calculated for $C_{62}H_{85}NO_{17}$ $(M + Na)^+$:	1138.5715
found:	1138.5734

Part 2: 2-D NMR Acquisition and Data Processing

gCOSY NMR spectra. 500 MHz and 600 MHz gCOSY NMR spectra were acquired at 30 °C with 2048 points, 256 or 512 increments and 1, 4, or 8 transients. Spectra were processed on a SUN Microsystems SPARCstation Ultra 5 computer using Varian VNMR software, version 6.1, revision C, with zero-filling to 4096 x 4096 and sine bell apodization such that sb = at/2 and sb1 = ni/(2*sw1).

H-H NOESY NMR spectra. Samples for NOESY NMR experiments were prepared in an Innovative Technologies, Inc. glove box using a NMR tube sealed with a PTFE screw cap. Sealed ampoules of pyridine *d*-5 and CD_3OD with 0.03% tetramethylsilane were used as solvents for these experiments. 600 MHz NOESY spectra were acquired at 30 °C with 2048 points, 256 increments, 8 transients per increment, τ_{mix} = 0.7 s, and an interscan delay (d1) of 3*T1 (standard T1 relaxation experiments were performed for each compound). Spectra were processed using nmrPipe as follows: 1) 4 points back prediction, 2) 90° shifted sinebell apodization, 3) zero-filling to 8192 points, 4) Fourier transformation and phasing, 5) linear prediction to 512 points, 6) 90° shifted sinebell apodization, 7) zero-filling to 2048 points, and 8) Fourier transformation and phasing. The Sparky program,[18] version 3.113 was used for peak-picking and integration of crosspeaks. Distance restraints were derived and enforced in conformational searches as described in the text.

Phase-sensitive COSY (COSYPS) NMR spectra. 500 MHz COSYPS spectra were acquired at 30 °C with 2048 points, 256 increments, and 4 transients per increment. 600 MHz COSYPS spectra were acquired at 30 °C with 2458 points, 308 increments and 8 transients per increment. All COSYPS spectra were acquired with sufficient interscan delay to allow for full spin-relaxation (d1 = 23.2 seconds, as determined by T1 relaxation experiments, was sufficient for all compounds). Coupling constants and associated dihedral angles were determined as described in the text.

Gradient HMBC NMR spectrum. A gradient HMBC spectrum of *N*-acyl AmB methyl ester **2.13** was acquired at 23 °C with 2048 points, 280 increments, and 128 transients. Parameters for C-H coupling were set such that j1xh = 140 Hz and jnxh = 8 Hz. The spectrum was processed on a SUN Microsystems SPARCstation Ultra 5 computer using Varian VNMR software, version 6.1 revision C, with zero-filling to 1024 points in the indirect dimension and sinebell apodization such that sb = at/2 and sb1 = ni/(2*sw1).

Part 3. Conformational searches and RMS atom alignment

NMR-Restrained Model Structures. Monte Carlo conformational searches were performed using the Molecular Operating Environment program (MOE), Version 2006.08,[19] with the empirical MMFF94x force field and a Born solvation model with no distance cutoffs for non-bonded interactions. Initial atomic coordinates and structure files were generated from the AmB crystal structure using MOE. NMR-derived distance and dihedral constraints were set with a weighting factor of 200. 3500 random conformations were generated and minimized with Gaussian distribution of dihedrals biased towards multiples of 30°, dihedral minimization (RMS = 100), 0.001 Cartesian minimization RMS gradient, 0.0001 Cartesian perturbation, 0.1 RMS tolerance, a maximum of 2000 energy minimization steps for each minimization, a failure limit of 5000, no chiral inversion, no rotation about π bonds or amide bonds, and an energy cutoff of 5 kcal/mol. Force field partial charges were calculated before each minimization. Default values were used for all other parameters.

Rigid RMS atom alignment for NMR-restrained model structures. The macrolactone and hemiketal atoms from each lowest energy conformation were saved as MDL MOL files (*.mol) and imported into the Cerius^2 program, Version 4.11,[20] with no energy minimization or calculation of charges. After rigid RMS atom alignment, the aligned structures were saved as PDB files (*.pdb), and the overlay image (Figure 2-9) was generated using Visual Molecular Dynamics (VMD).[21]

Part 4. Antifungal Assays

Growth conditions for *Saccharomyces cerevisiae*. *S. cerevisiae* (ATCC 9763) cultures were incubated at 30 ºC on yeast peptone dextrose (YPD) agar plates or in YPD liquid cultures with rotary shaking. For liquid YPD medium, yeast extract (5 g), Bacto peptone (10 g), and MilliQ H_2O (475 mL) were combined and autoclaved at 250 ºC for 15 minutes. Sterile 40% w/v aqueous glucose (25 mL) was subsequently added (sterile glucose solutions were prepared by dissolving glucose in MilliQ water and autoclaving at 250 ºC for 12 min). For agar plates, the same procedure was used except using only 225 mL of water and combining with 250 mL sterile 4% w/v aqueous agar solution (sterile 4% w/v agar was prepared by adding agar to MilliQ water and autoclaving at 250 ºC for 15 min). Agar plates were prepared by pouring the hot YPD/agar mixture into sterile 15 mm x 100 mm culture dishes. The plates were allowed to cool at room temperature until the agar had solidified.

Growth conditions for *Candida albicans.* *C.albicans* (ATCC 90028) were cultured in the same manner as *S. cerevisiae* except the cells were incubated at 37 °C rather than 30 °C.

Disk Diffusion Assay. Protocols for disk diffusion assays were adapted from the National Committee of Clinical Laboratory Standards document M2-A8.[22] Yeast were streaked on YPD agar plates with a sterile toothpick and incubated at 30 ºC (*S. cerevisiae*) or 37 °C (*C. albicans*) until individual colonies could be identified by eye (~ 24 h). Five individual colonies were transferred from the agar plate with an inoculating loop to the liquid YPD medium. The liquid culture was incubated overnight at 30 °C (*S. cerevisiae*) or 37 °C (*C. albicans*) in a shaker incubator (200 rpm). The saturated cell culture was diluted with YPD medium to an OD_{600} of 0.1 (~ 3 x 10^7 cells/mL) as measured on a Shimadzu PharmaSpec UV-1700 UV/Visible spectrophotometer. This culture was used to inoculate an YPD plate by streaking the entire plate with a sterile cotton tip applicator three times, turning the plate approximately 60 ° after each application and finishing by swabbing the rim of the agar. The plate was allowed to dry for approximately 2 to 3 minutes before application of paper disks impregnated with compounds **2.1**-**2.4**. The disks were prepared in the following manner: 10 microliters of a 4 mg/ml (*S. cerevisiae*) or a 2 mg/mL (*C. albicans*) solution of each compound in DMSO was added to an 8 mm disk of Whatman 4 filter paper. Controls were prepared in a similar manner using only DMSO. The disks were then placed on the agar and gently pressed with forceps. All disks, including DMSO controls, were added within 15 minutes of inoculation. After disks were added to the plate the plate was inverted and incubated at 30 °C (*S. cerevisiae*) or 37 °C (*C. albicans*) for 36 to 48 hours prior to assessment. Those compounds which showed a visible zone of growth inhibition were judged to be active. This experiment was repeated for each yeast strain and yielded the same results. See Figure 2-10

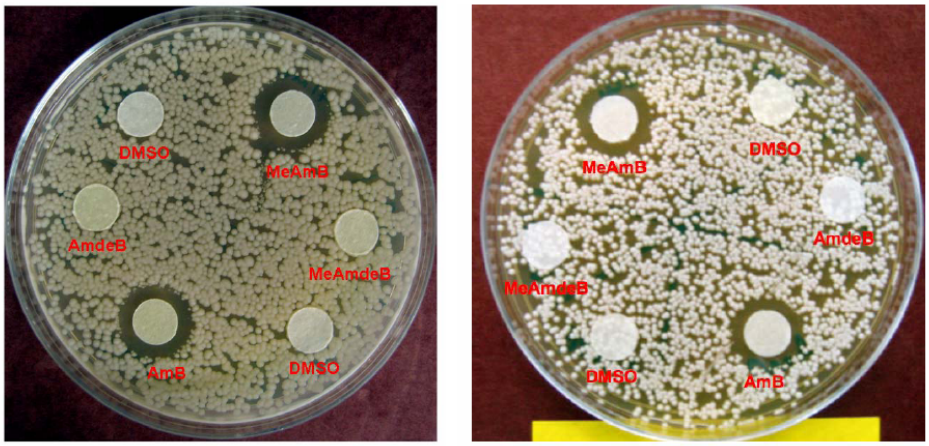

Figure 2-10. Representative results of disk diffusion assays for *S. cerevisiae* (left) and *C. albicans.* Adapted with permission from Palacios, D.S.; Anderson, T.M.; Burke, M.D. *J. Am. Chem. Soc.* **2007**, *129*, 13804-13805. Copyright 2007 American Chemical Society.

Broth microdilution minimum inhibitory concentration (MIC) assays. Protocols for broth microdilution assays were adapted from the National Committee of Clinical Laboratory Standards document M27-A2[23] and from the protocol reported by Paquet and Carreira.[24] Yeast were streaked on YPD agar plates with a sterile toothpick and incubated at 30 °C (*S. cerevisiae*) or 37 °C (*C. albicans*) until individual colonies could be identified by eye (~ 24 h). Five individual colonies were transferred from the agar plate with an inoculating loop to the liquid YPD medium. The liquid culture was incubated overnight at 30 °C (*S. cerevisiae*) or 37 °C (*C. albicans)* in a shaker incubator (200 rpm). The saturated cell culture was diluted with YPD medium to an OD_{600} of 0.1 (~ 3 x 10^7 cells/mL) as measured on a Shimadzu PharmaSpec UV-1700 UV/Visible spectrophotometer. Aliquots (195 µL) of the resulting cell suspension were added to a 96-well plate. Compounds for testing were prepared as 400 µM solution in DMSO and this stock solution was serially diluted to concentrations of 320, 240, 200, 160, 120, 80, 40, 20, 10, and 5 µM. Aliquots (5 µL) of each DMSO solution were added to the 96-well plate, with each row of the plate containing a different concentration. This 40-fold dilution resulted in final compound concentrations of 10, 8, 6, 5, 4, 3, 2, 1, 0.5, 0.25, and 0.125 µM. DMSO (5 µL) was added as a control to each well of the final row. Each concentration was tested in triplicate. Plates were covered with Corning Thermowell aluminum sealing tape and incubated at 30 °C (*S. cerevisiae*) or 37 °C (*C. albicans*) for 18 hours. MIC values were determined as concentration corresponding to the row which showed no visible growth. The assay was repeated three times and the reported values represent the average of these three experiments.

REFERENCES

1) Sowinski, P.; Pawlak, J.; Borowski, E.; Gariboldi, P. *Magn. Res. Chem.* **1992**, *30*, 275-279.
2) Ganis, P.; Avitabile, G.; Mechlinski, W.; Schaffner, C.P. *J. Am. Chem. Soc.* **1971**, *93*, 4560-4564.
3) (a) In pioneering studies, Nicolaou and coworkers reported an alternative degradative synthesis of **3**: Nicolaou, K.C.; Chakraborty, T.K.; Ogawa, Y.; Daines, R.A.; Simpkins, N.S.; Furst, G.T. *J. Am. Chem. Soc.* **1988**, *110*, 4660-4672. (b) A degradative synthesis of **4** is described in the patent literature: Driver, M.J.; Greenless, A.R.; and MacPherson, D.T. U.S. Patent # 5,204,330, **1993**. (c) MacPherson, D.T.; Corbett, D.F.; Costello, B.C.; Driver, M.J.; Greenlees, A.R.; MacLachlan, W.S.; Shanks, C.T.; Taylor, A.W. In *Recent Advances in the Chemistry of Anti-infective Agents*; Bentley, P.H., Ponsford, R., Editors, Royal Society of Chemistry, Cambridge, **1993**; 205-222. (d) An impure sample of **4** was prepared via genetic engineering of the producer: Carmody, M.; Murphy, B.; Byrne, B.; Power, P.; Rai, D.; Rawlings, B.; Caffrey, P. *J. Biol. Chem.* 2005, *280*, 34420.
4) Kennedy, R.M.; Abiko, A.; Masamune, S. *Tetrahedron Lett.* **1988**, *29*, 447-450.
5) Palacios, D.S.; Anderson, T.M.; Burke, M.D. *J. Am. Chem. Soc.* **2007**, *129*, 13804-13805
6) (a) Delaglio, F.; Grzesiek, S.; Vuister, G. W.; Zhu, G.; Pfeifer, J.; Bax, A. *J. Biomol. NMR*, **1995**, *6*, 277-293. (b) Delaglio, F.; Wu, Z.; Bax, A. *J. Magn. Reson.* **2001**, *149*, 276-281.
7) In COSYPS spectra, crosspeaks near the diagonal are typically obscured by the broad, tailing shape of the diagonal. Diagonal suppression subtracts the diagonal from the spectrum, allowing a clear view of all crosspeaks.
8) Cavanagh, J.; Fairbrother, W. J.; Palmer, W. G. III; Rance, M.; Skelton, N. J. *Protein NMR Spectroscopy: Principles and Practices, 2nd Ed.* **2006**, *Academic Press*, San Diego.
9) Haasnoot, C. A. G.; de Leeuw, F. A. A. M.; Altona, C. *Tetrahedron*, **1980**, *36*, 2783-2792.
10) http://www.mestrec.com/producto.php?id=8
11) Auricchio, S.; Fronza, G.; Mele, A. *J. Org. Chem.* **1992**, *57* (2), 452-455.
12) Egan, R. S.; Martin, J. R.; Perun, T. J.; Mitscher, L. A. *J. Am. Chem. Soc.* **1975**, *97* (16), 4578- 4583.
13) *Molecular Operating Environment*, version 2006.08; Chemical Computing Group: Montreal, Quebec, Canada.
14) National Committee of Clinical Laboratory Standards. Performance Standards for Antimicrobial Disk Susceptibility Tests, M2-A8 Approved Standard-8th Ed. Vol. 23, Number 1, **2003**.
15) National Committee of Clinical Laboratory Standards. Reference Method for Broth Dilution Antifungal Susceptibility Testing, M27-A2, Approved standard-2nd Ed. Vol. 22, Number 15, **2002**.
16) Pangborn, A.B.; Giardello, M.A.; Grubbs, R.H.; Rosen, R.K.; Timmers, F.J. *Organometallics* **1996**, *15*, 1518-1520.
17) Still, W.C.; Kahn, M.; Mitra, A. *J. Org. Chem.* **1978**, *43*, 2923-2925.
18) Goddard, T. D.; Kneller, D. G. SPARKY 3, University of California, San Francisco, http://www.cgl.ucsf.edu/home/sparky/
19) *Molecular Operating Environment*, version 2006.08; Chemical Computing Group: Montreal, Quebec, Canada.
20) AccelRys Software, Inc. http://www.accelrys.com/products/cerius2/
21) Humphrey, W.; Dalke, A; and Schulten, K., *J. Molec. Graphics* **1996**, *14*, 33-38.

22) National Committee of Clinical Laboratory Standards. Performance Standards for Antimicrobial Disk Susceptibility Tests, M2-A8 Approved Standard-8th Ed. Vol. 23, Number 1, 2003.
23) National Committee of Clinical Laboratory Standards. Reference Method for Broth Dilution Antifungal Susceptibility Testing, M27-A2, Approved standard-2nd Ed. Vol. 22, Number 15, 2002.
24) Paquet, V.; Carreira, E. M. *Org. Lett.* **2006**, *8*, 1807.
25) Gray, K.C.; Palacios, D.S.; Dailey, I.; Endo, M.M.; Uno, B.E.; Wilcock, B.C.; Burke, M.D. *Proc. Natl. Acad. Sci. U.S.A.* **2012**, *109*, 2234-2239.
26) Palacios, D.S.; Dailey, I.; Seibert, D.M.; Wilcock, B.C.; Burke, M.D. *Proc. Natl. Acad. Sci. U.S.A.* **2011**, *108*, 6733-6738.

CHAPTER 3

Discovery of a lipid platform for SSNMR analysis of AmB in phospholipid bilayers

ABSTRACT

Having discovered that the channel and antifungal activity of MeAmB is not consistent with the leading model for the antifungal action of AmB, we sought to complement these experiments with structural characterization of AmB in phospholipid bilayers. SSNMR has recently emerged as a powerful tool for studying membrane-bound molecules, particularly membrane proteins. However, application of SSNMR to the study of membrane-bound small molecules has been limited. To enable relevant SSNMR studies of AmB in the presence of lipid bilayers, we recognized a need to achieve three goals: 1) gain access to highly ^{13}C-enriched AmB, 2) develop a physiologically relevant phospholipid bilayer system compatible with high resolution SSNMR studies with AmB, and 3) complete de novo assignments of the ^{13}C spectrum of AmB. This chapter describes the development of solutions to each of these problems. First, by growing the AmB producing organism, *Streptomyces nodosus*, in the presence of growth medium containing only uniformly ^{13}C-labeled glucose as a carbon source, we have developed a reproducible process for the biosynthesis of >80% uniformly ^{13}C-labeled AmB (the highest percent incorporation reported to date).. Second, as part of our efforts to develop a physiologically relevant lipid bilayer platform suitable for SSNMR studies of AmB, we extensively investigated the use of nanoscale discoidal lipid bilayers (nanodiscs), multilamellar vesicles comprised of saturated lipids, and multilamellar vesicles comprised of unstaturated lipids. Multilamellar vesicles comprised of POPC:ergosterol:AmB 10:1:1 were found to be both highly amenable to high resolution SSNMR analysis and physiologically relevant. Achieveing these two goals directly enabled the SSNMR studies discussed in Chapter 4.

Nashrah Maryum contributed to the development of our protocol for preparation of ^{13}C-enriched AmB and to the nanodisc studies. Prof. Rienstra, Mary Clay, Andy Nieuwkoop, Gemma Comellas, and Lindsey Sperling acquired the preliminary SSNMR data described in this chapter.

3-1 BACKGROUND

Our discovery that oxidation at the C41 position of AmB is not required for antifungal activity challenged the leading model for the AmB structural underpinnings of the AmB ion channel. This left us with two possible conclusions: 1) the presumed critical polar interaction between the C41 carboxylate and the C19 mycosamine is not required for channel self-assembly, and/or 2) ion channel formation is not required for the antifungal activity of AmB. To further probe these questions, we sought to structurally characterize the putative ion channel aggregate formed by AmB in the presence of lipid bilayers. To this end, we engaged in a collaboration with Prof. Chad Rienstra and several members of his group to employ SSNMR to study the structure of AmB in the presence of lipid bilayers.

Over the last 20 years, SSNMR has emerged[1,2] as a powerful technique for studying membrane proteins in phospholipid bilayers. Many research groups[3,4,5] have successfully characterized membrane-embedded proteins by SSNMR. The Rienstra group has pioneered new techniques that have helped drive these advances, and demonstrated the unique capabilities of SSNMR to structurally characterize various membrane proteins including alpha-synuclein,[6] bacteriorhodopsin,[7] and cytochrome P450 3A4.[8]

In contrast, there are relatively few examples of SSNMR studies of membrane-bound small molecules, although several recent examples have been reported for liposome-bound estradiol,[9] cholesterol,[10] anandamide,[11] and cisplatin.[12] Most pertinent to the work described in this chapter, a series of SSNMR studies of AmB in the presence of lipid bilayers has been reported by Murata and coworkers.[13,14,15] These studies were reviewed in Chapter 1; key results and limitations of these studies will be described in detail below.

The initial REDOR studies reported by Murata and coworkers were performed in DSPC,[13] DMPC,[13] and DLPC[14] MLVs devoid of cholesterol. The key results of these investigations are depicted in Figure 3-1, with dephased nuclei of AmB shown in red. When short lipids were used (DLPC, DMPC), the pattern of REDOR dephasing at C39, C40, and C41 was interpreted as evidence for a single pore channel. When the longer DSPC was used, only C41 was dephased by phosphorus, and this was interpreted as evidence for a double pore channel. In the case of the AmB/DLPC system (Figure 3-1A), U-^{13}C-AmB was used, and a lack of observed dephasing for the middle portion of the molecule was interpreted so as to rule out the possibility that AmB was surface-bound. However, as will be demonstrated in Section 3-4, the

chemical shifts for the middle portion of AmB have a high amount of overlap, and cleanly interpreting results for these regions of the spectrum can be complicated.

As described in chapter 1, three further limitations with these experiments are noteworthy. First, the lipid system was devoid of sterol, yet AmB is known to manifest its biological activity only in membranes containing sterols. Second, the lipids used in these studies were fully saturated, whereas biological membranes contain a substantial proportion of unsaturated lipids.[15] As described below, this distinction has important biophysical consequences that impact the activity of AmB. Finally, the use of C12 acyl chains (DLPC), which are rarely observed in natural systems, raises further questions regarding the physiological relevance of these findings.

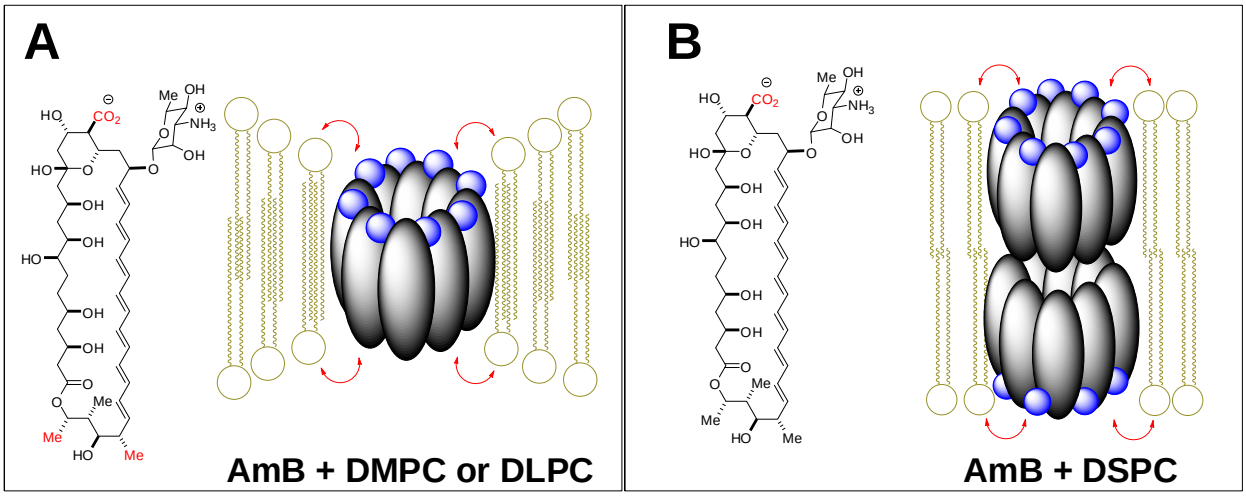

Figure 3-1. Visual depiction of REDOR dephasing and subsequent interpretation. A) In the presence of DMPC or DLPC (no sterol present), the nuclei shown in red are moderately dephased. This was interpreted as evidence for a single pore membrane-spanning channel, depicted schematically with red arrows indicating sites of REDOR dephasing. B) When longer DSPC lipids are used, only C41 (red) is moderately dephased. This was interpreted as evidence for a double pore channel, shown schematically as in A.

The Murata group also recently reported ^{13}C-^{19}F REDOR studies of 14-fluoro-AmB and a skipped ^{13}C-labeled ergosterol (**3.1,** Figure 3-2) in POPC MLVs.[16] These experiments revealed dephasing of ergosterol C21, C26, C27, and C19 in the presence of 14-fluoro-AmB (Figure 3-2). In addition, ^{13}C-^{31}P REDOR revealed dephasing of ergosterol C26 and C27 by ^{31}P of POPC. Viewed through the lens of the leading ion channel model for the mechanism of action of AmB and the previously described REDOR studies in saturated lipids, it was concluded based on these latest REDOR results that the AmB ion channel is comprised of both "head-to-head" and "head-to-tail" orientation of AmB and ergosterol. Importantly, however, the ^{13}C-^{31}P REDOR experiments that were previously performed in saturated lipids devoid of ergosterol.were not

repeated in this POPC based system. Also significantly, to the best of our knowledge, direct ^{13}C-^{31}P REDOR dephasing between AmB and POPC has not been reported.

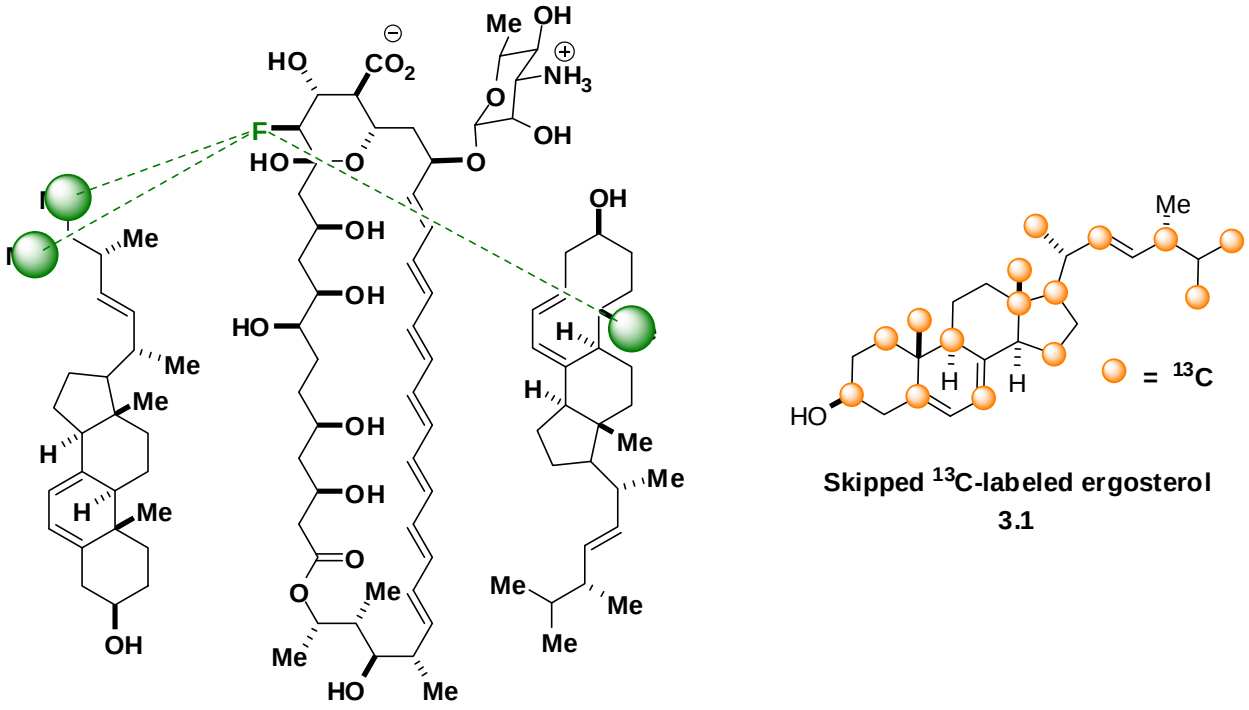

Figure 3-2. Shown at right is the skipped ^{13}C-labeled ergosterol used for ^{13}C-^{19}F REDOR experiments. At left, green spheres indicate nuclei dephased by ^{19}F. The authors proposed both head-to-tail and head-to-head interactions of AmB with ergosterol.

As described above, we recognized limitations with the aforementioned studies that complicated interpretation of the reported results. Most importantly, no functional validation of the liposome system was reported. In particular, the MLVs composed of saturated lipids (DMPC, DLPC, DSPC) contained no sterol. The functional relevance of studying AmB in this type of system remains controversial. As described below, POPC/AmB/Ergosterol MLVs have been found to be a physiologically relevant bilayer system. However, interpreting these data through the lens of the prior studies with saturated lipids complicates data interpretation.

Given all of the above, we decided to take a fresh look at this problem. We judged that to generate physiologically meaningful results via SSNMR, three goals needed to first be accomplished: 1) gain access to highly ^{13}C-enriched AmB, 2) develop a physiologically relevant phospholipid bilayer system compatible with high resolution SSNMR studies with AmB, and 3) complete de novo assignments of ^{13}C spectrum of AmB.

Research in our laboratories has extensively studied the biophysical properties of AmB in a variety of lipid environments. In parallel with the work discussed in this chapter, Palacios et al.[17] and Gray et al.[18] made several important discoveries which strongly impacted the course of the AmB SSNMR project.

Palacios et al. conducted extensive biophysical assays on AmB, MeAmB, AmdeB, and MeAmdeB. In the context of isothermal titration calorimetry studies of these 4 compounds, a direct binding interaction was discovered between AmB and ergosterol. MeAmB also binds directly to ergosterol, whereas AmdeB and MeAmdeB (lacking a mycosamine appendage) do not bind ergosterol. This binding interaction was found to be critical for AmB channel activity in K^+ efflux studies of AmB channel activity. Figure 3-3 depicts the K^+ efflux from *S. cerevisiae* cells and egg-yolk phosphocholine/Ergosterol liposomes upon addition of AmB, MeAmB, AmdeB, or MeAmdeB. Based on these results, we envisioned that ergosterol-dependent K^+ efflux from liposomes could serve as a measure of functional relevance of liposome systems under investigation for potential use in SSNMR of AmB (see below for details).

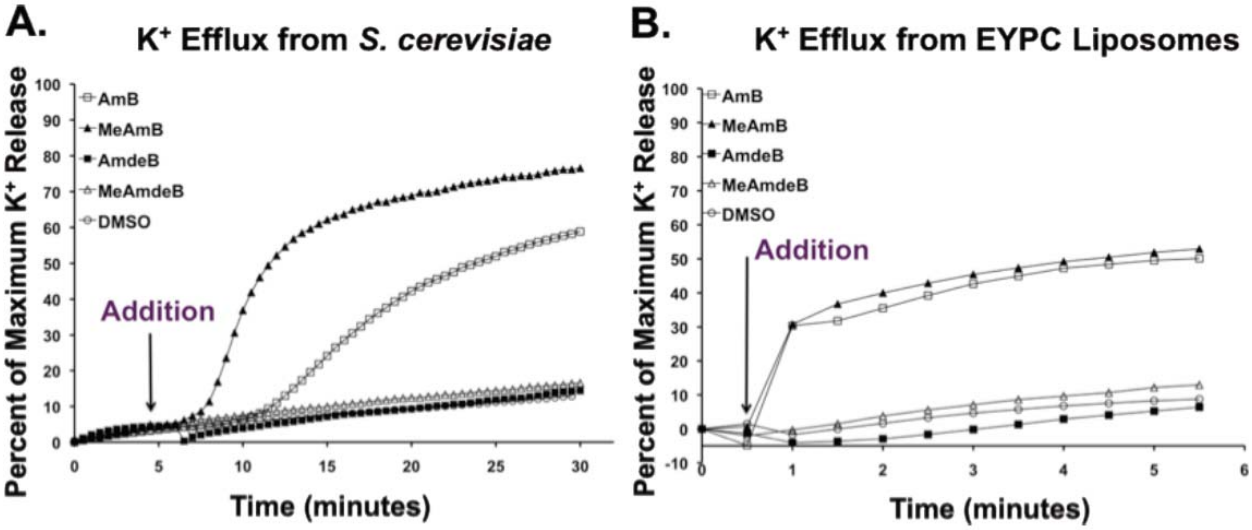

Figure 3-3. K^+ efflux from *S. cerevisiae* (A) and egg-yolk phosphochline liposomes (B) in the presence of AmB, MeAmB, AmdeB, and MeAmdeB. Each compound was added as a DMSO solution at the timepoints indicated, and efflux is reported as a percentage of maximum K^+ relase induced by the addition of Triton X-100 to the system. Adapted from Palacios, et al. *Proc. Natl. Acad. Sci. USA* **2011**, *108*, 6733-6738 Copyright 2011, National Academy of Sciences.

In the context of studying the biophysical properties of C35-deoxy-AmB, Gray et al. discovered that this molecule directly binds ergosterol, has no capability to form ion channels, and yet retains antifungal activity, albeit less potent, against both *S. cerevisiae* and *C. albicans*. Therefore, channel activity is not the primary mechanism of AmB antifungal activity, although it

does contribute to its potency. These discoveries allowed us to expand from a narrow focus of studying the AmB *ion channel* by SSNMR to a broader focus of studying the structural underpinnings of AmB binding to phospholipid bilayers and sequestering ergosterol.

In addition to these discoveries, Gray et al. found that the amount of AmB at its MIC is greater than the total amount of lipid present in fungal cells. This fact became very important in our investigations of liposomes for SSNMR analysis of AmB. Prior to this breakthrough, we had assumed that minimizing the amount of AmB in liposome systems was important for minimizing its potential to aggregate. In light of this discovery, however, we were confident that using greater amounts of AmB in our liposomes would be functionally relevant. The remainder of this chapter will detail our efforts in accomplishing the 3 goals articulated above: 1) developing a reproducible method for the preparation of highly 13C-enriched AmB, 2) discovery of a functionally relevant lipid milieu for SSNMR analysis of AmB, and 3) de novo chemical shift assignments of U-^{13}C AmB.

3-2 PREPARATION OF HIGHLY ENRICHED ^{13}C-LABELED AMPHOTERICIN B

To study AmB by SSNMR we first needed a robust and reproducible method for the production of uniformly ^{13}C-labeled AmB (U-^{13}C AmB). Murata prepared this molecule for his REDOR studies via biosynthesis[14] from the producing bacterium *Streptomyces nodosus*, using a modification of the medium originally reported by McNamara et al.[19] for biosynthesis of tri-^{13}C AmB. Murata's modification involved simply substituting ^{13}C-labeled glucose (U-^{13}C Glc) for natural abundance glucose in the culture medium. However, the medium also employs a large amount of natural abundance fructose. As a result, the ^{13}C incorporation into the AmB scaffold is only ~15% using this method. While our preliminary SSNMR experiments using 15% enriched U-^{13}C-AmB yielded spectra of satisfactory sensitivity, large amounts of instrument time were required to obtain these spectra. From these preliminary results it was clear we would need access to highly enriched U-^{13}C-AmB, the availability of which would enable 2 aspects of our SSNMR studies. First, highly enriched U-^{13}C AmB would maximize the number and types of potential SSNMR experiments we could perform. Second, highly enriched U-^{13}C-AmB would maximize sensitivity and thereby minimize instrument time required for our data acquisition.

The high cost of uniformly ^{13}C-labeled fructose prohibited a direct substitution for natural abundance fructose in the culture medium. A change in culture medium was not likely to be successful–McNamara et al. found that other media yielded no ^{13}C incorporation. We considered

the possibility that streptomycetes simply convert fructose to glucose and that these bacteria could thus grow in the absence of fructose. Indeed, Lapidot[20] has studied sugar metabolism in *S. parvalus*, and determined that fructose is directly converted to glucose by this bacterium. We experimented with growth conditions for *S. nodosus* in which U-^{13}C Glc is substituted for natural abundance fructose in the culture medium. Gratifyingly, this simple substitution yielded U-^{13}C-AmB with average isotope incorporation estimated at ~85% by ESI mass spectrometry, the highest incorporation reported to date for this natural product. With this highly enriched AmB in hand, we had accomplished the first of the three goals outlined above.

3-3 DISCOVERY OF A FUNCTIONALLY VALIDATED LIPID BILAYER PLATFORM FOR SSNMR ANALYSIS OF AMPHOTERICIN B

Our second goal was to discover a functionally validated lipid platform for our SSNMR studies. We identified 3 essential criteria for such a lipid platform: 1) AmB will stably incorporate into the phospholipid bilayer, 2) the lipid platform retains ergosterol-dependent channel formation as judged by K^+ efflux assays, and 3) the lipid platform will permit de novo assignment of AmB ^{13}C chemical shifts. We investigated the use of nanodiscs, fully saturated phospholipid liposomes, and POPC liposomes for fulfillment of these 3 criteria. These investigations are described in the following 3 sections.

3-3A INVESTIGATION OF NANOSCALE DISCOIDAL PHOSPHOLIPID BILAYERS AS A MILIEU FOR SSNMR STUDIES OF AMPHOTERICIN B

Nanoscale discoidal lipid bilayers, "nanodiscs," recently discovered by Sligar and coworkers[21] were an attractive option for our studies. Nanodiscs consist of a membrane scaffold protein (MSP), a recombinant derivative of human apolipoprotein A-I, which acts as a "belt" encircling a planar patch of phospholipid bilayer. The MSP controls the size of each disc, and nanodiscs thus have a very narrow and reproducible size distribution.

Sligar has demonstrated remarkable utility of nanodiscs for the study of membrane proteins, which are notorious for their poor solubility and propensity to aggregate. Use of nanodiscs has overcome both these limitations for many membrane proteins: the Sligar lab has successfully employed nanodiscs to study bacteriorhodopsin, cytochorome P450 3A4 (CYP3A4), β_2-adrenergice receptors, and others.[22] Notably, the Rienstra lab in collaboration with the Sligar lab has demonstrated that nanodisc-embedded membrane proteins are amenable to SSNMR analysis. They recently reported SSNMR studies of nanodisc-embedded CYP3A4.[8] Importantly, CYP3A4 retains its active, folded state within the nanodisc.

Despite the success of nanodiscs in the study of membrane proteins, the use of nanodiscs for the study of membrane-embedded small molecules has not been demonstrated. Interestingly, study of AmB has historically been challenging due to the same limitations described above for membrane proteins: poor solubility and propensity for aggregation. AmB has poor solubility in all solvents except DMSO and DMF, and it is notorious for its capacity to aggregate in solution and in lipid bilayers. We envisioned that nanodiscs could overcome these limitations and allow us to study membrane-bound AmB assembled into discrete ion channels within the nanodiscs.

Bolstered by the success of Sligar's nanodisc platform for studying membrane proteins, we began a search for conditions to incorporate AmB into nanodiscs for subsequent SSNMR analysis. Our investigations of nanodiscs focused on the DPPC nanodiscs reported by the Sligar lab.[21] These nanodiscs are reported to be 9-10 nm in diameter (depending on the method used to analyze their size). We anticipated these nanodiscs could comfortably accommodate the AmB ion channel with an estimated outer diameter of approx. 3 nm (measured using MOE with a channel structure similar to that reported by McCammon and coworkers). We investigated 3 strategies for preparation of nanodisc-embedded AmB:

1. *External addition*: Formation of empty nanodiscs followed by addition of AmB
2. *Pre-incorporation*: Pre-mixing of AmB with all nanodisc components, followed by dialysis to form nanodiscs
3. *Nanodiscs from liposomes*: Formation of AmB-impregnated liposomes followed by addition of MSP to form nanodiscs

In each case, size exclusion chromatography (SEC) was performed to measure the size and homogeneity of the resulting nanodiscs.

External addition. As reported by Sligar, nanodiscs are prepared by the "detergent dialysis method."[23] In this method, MSP and phospholipid are combined in the appropriate molar ratio and solubilized as mixed micelles with sodium cholate. As the cholate is removed by dialysis, the remaining MSP and phospholipid form nanodiscs. The size and homogeneity of the nanodiscs can then be analyzed by SEC. In addition, nanodiscs have been shown to contain a highly reproducible number of phospholipid molecules, thus allowing for addition of AmB at defined ratios of phospholipid to AmB.

For our studies, we first prepared DPPC nanodiscs and analyzed them by SEC. We successfully reproduced Sligar's results, with the size of our nanodiscs measured by SEC to be 9.5 nm in diameter based on a calibration against proteins of known size (see Figure 3-4).

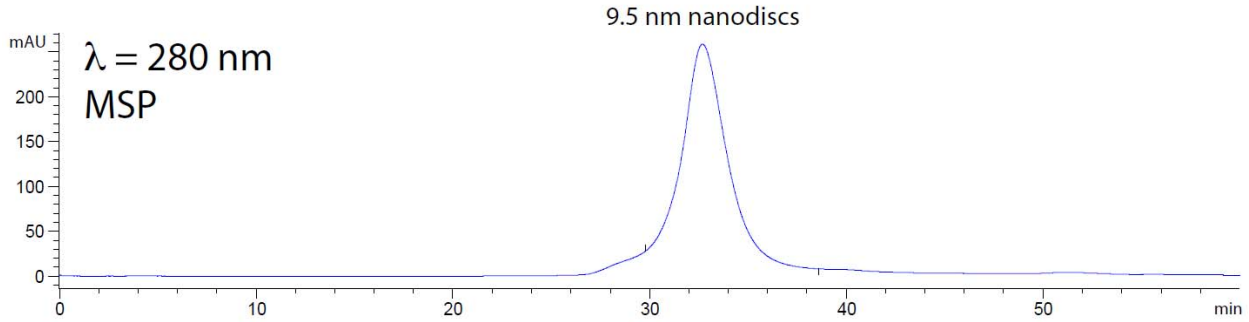

Figure 3-4. Size exclusion chromatogram of blank DPPC nanodiscs. The retention time of 32.7 min was calculated to correspond to a size of 9.5 nm, based on column calibration with proteins of known size.

We next formed nanodiscs containing DPPC and ergosterol, and AmB dissolved in DMSO was added to the nanodisc solution. SEC of the resulting solution revealed that the majority of AmB and MSP elute at a retention time corresponding to the void volume of the column (approx. 21.6 min, see Figure 3-5).

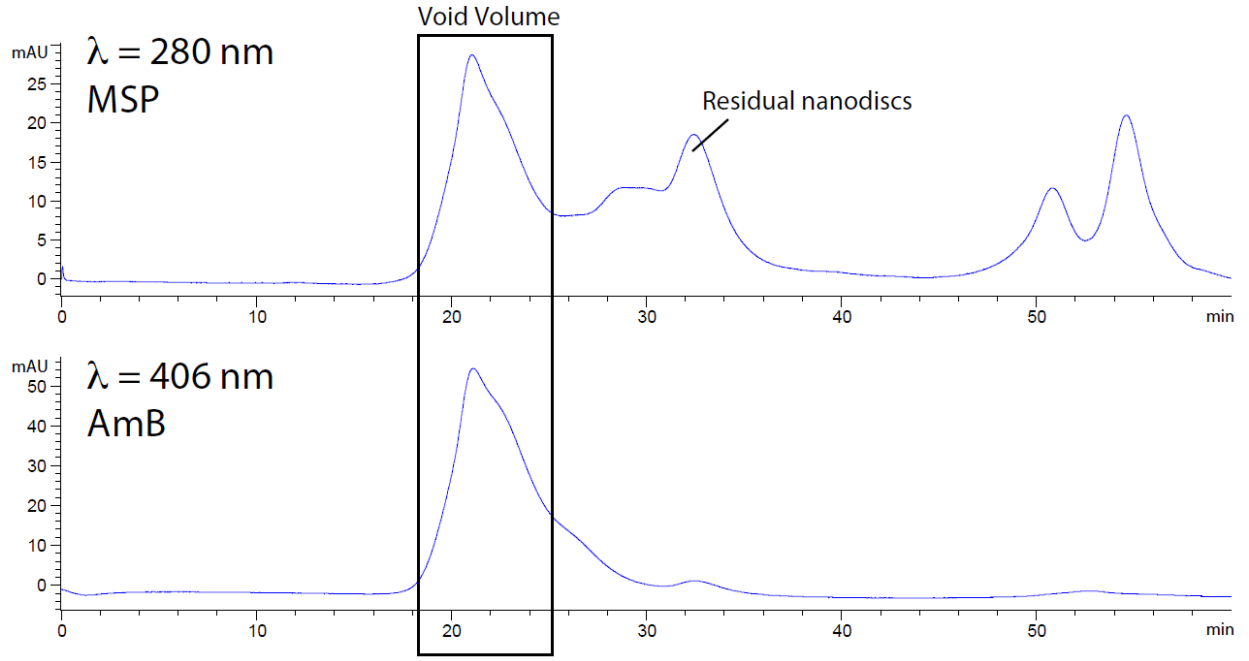

Figure 3-5. Size exclusion chromatogram of DPPC/AmB/Ergosterol nanodiscs prepared by external addition of AmB. AmB (λ = 406 nm) and the majority of MSP (λ = 280 nm) co-elute as a large aggregate at the retention time corresponding to the void volume for the column (approx. 21.6 min).

Pre-incorporation. Sligar and coworkers have reported a method[24] for preparation of nanodisc-embedded membrane proteins which involves solubilizing the protein with sodium cholate in the presence of all nanodisc components prior to nanodisc formation. Dialysis of cholate produces nanodisc-embedded membrane proteins. We investigated the possibility of forming AmB-impregnated nanodiscs via this pre-incorporation method. Solubilizing MSP,

DPPC, ergosterol, and AmB in this manner consistently yielded large aggregates of AmB that eluted at the void volume along with MSP (see Figure 3-6).

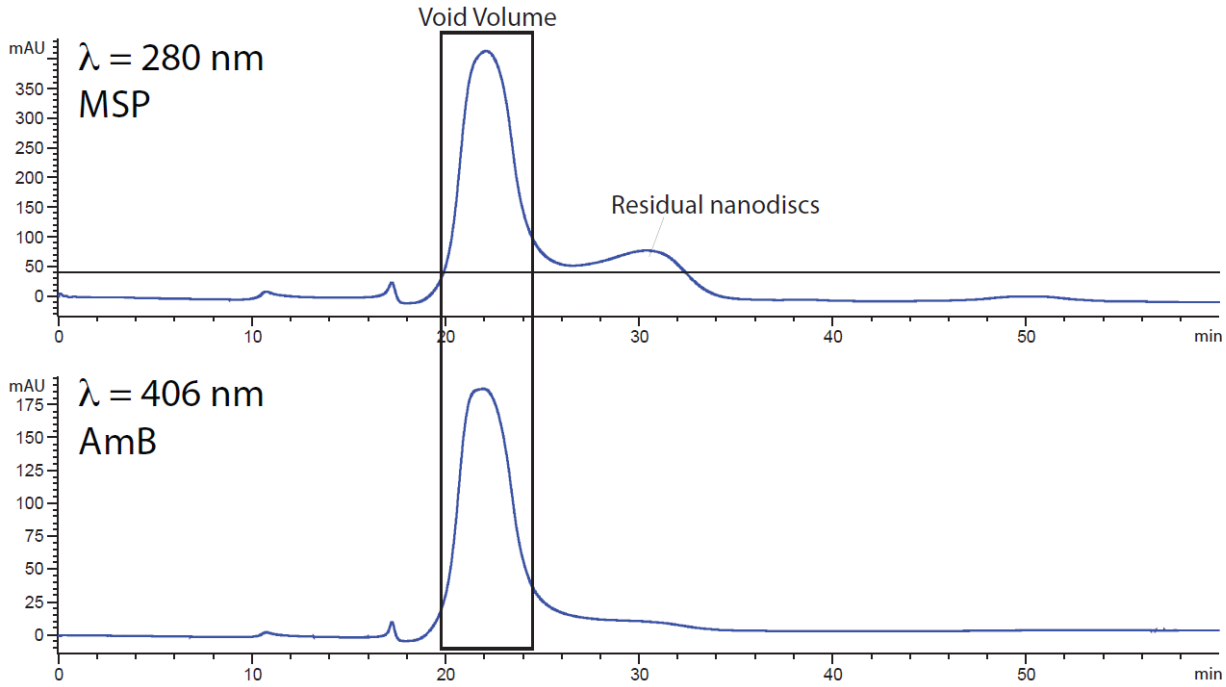

Figure 3-6. Size exclusion chromatogram of DPPC/AmB/Ergosterol nanodiscs prepared by the pre-incorporation. Note the large aggregate of AmB and MSP which elutes at the void volume.

Nanodiscs from liposomes. Given that AmB is known to bind stably to liposomes,[17] we attempted to form AmB-impregnated nanodiscs by the addition of MSP to AmB-impregnated MLVs (a similar method[23] has been reported for formation of discoidal HDL-like particles from liposomes using apoliporproteins). We envisioned that MSP would disrupt the AmB-impregnated liposomes and form nanodiscs containing embedded AmB. We were again disappointed to discover that AmB simply formed large aggregates eluting at the void volume (data not shown). This result is similar to that observed by Ryan and coworkers[25] who similarly observed a large aggregate after addition of recombinant apolipoprotein A-I to AmB-impregnated liposomes.

Summary of nanodisc studies. Based on the studies described above, nanodiscs did not meet our first criterion of stable binding/incorporation of AmB. While isolation of the AmB ion channel within nanodiscs remains an intriguing possibility, our results indicate that this will require extensive screening of conditions for AmB incorporation. We thus turned our attention to investigations of liposomes as a potential lipid milieu for SSNMR studies of AmB.

3-3B INVESTIGATIONS OF LIPOSOMES COMPOSED OF FULLY SATURATED LIPIDS FOR SSNMR STUDIES OF AMPHOTERICIN B

As noted above, Palacios et al.[17] discovered the direct binding interaction between AmB and ergosterol in liposomes and showed that binding ergosterol was critical for channel formation in liposome K^+ efflux studies. As a result of these discoveries, we were confident that liposomes could provide a suitable lipid milieu for SSNMR studies of AmB. Liposomes represent a diverse platform that has long been used for studies of membrane biophysics,[23] particularly for the study of membrane proteins. SSNMR has been applied to the study of various liposome-bound proteins by several research groups,[2,3,4,5] including the Rienstra group. In contrast, there are relatively few examples of SSNMR studies of liposome-bound small molecules, but several examples have been reported. As discussed above, SSNMR analysis of liposome-bound AmB has been reported by Murata, and SSNMR has also been applied to the study of liposome-bound estradiol,[9] cholesterol,[10] anandamide,[11] and cisplatin.[12]

The diversity of the liposome platform stems from the fact that virtually any phospholipid or combination of phospholipids has the capacity to form liposomes. The biophysical properties of liposomes are intimately tied to the physical properties of the lipids from which the liposomes are formed. Membrane properties can thus be fine-tuned for a variety of applications.. Ergosterol-dependent K^+ efflux provided a metric whereby we could functionally validate the relevance of our liposomes. Thus, the ideal liposome system for AmB would retain ergosterol-dependent channel formation and would also be amenable to SSNMR.

To measure AmB-induced K^+ efflux from lipoosomes, large unilamellar vesicles (LUVs) containing 150 mM KCl are prepared and dialyzed against 150 mM NaCl. A K^+-selective electrode is then used to measure K^+ efflux upon addition of AmB dissolved in DMSO. We screened liposomes of various compositions for AmB K^+ efflux activity both in the presence and absence of ergosterol. LUVs composed of DPPC exhibit robust K^+ efflux activity irrespective of the presence of ergosterol (Figure 3-7A). Similar results were observed for DLPC, DMPC, and DSPC (data not shown). Mixtures of DPPC/POPC yield only moderate differences in K^+ efflux for the plus-ergosterol and minus-ergosterol states (Figure 3-7B). Thus, we concluded that saturated lipids did not satisfy the criterion of ergosterol-dependent efflux activity.

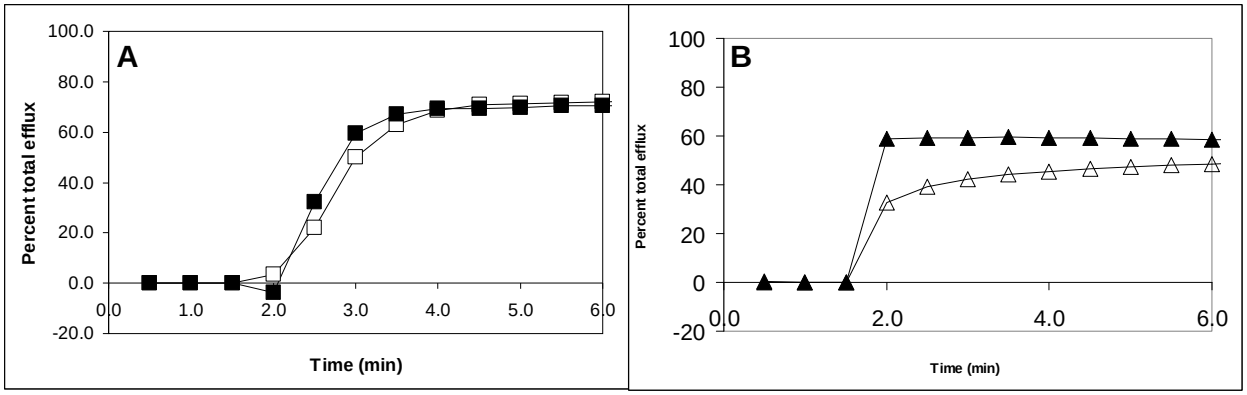

Figure 3-7. A) AmB initiates K^+ efflux from 200 μM LUVs composed of DPPC plus 10% ergosterol (black squares) and minus ergosterol (open squares). B) Similar activity is observed for 75:25 POPC:DPPC plus 1% ergosterol (black triangles) and minus ergosterol (open triangles). In both A and B, AmB was added as a DMSO solution at t = 1.5 min, and efflux is reported as a percentage of total efflux observed upon addition of Triton X-100 at t = 6.0 min.

3-3C INVESTIGATIONS OF LIPOSOMES COMPOSED OF POPC FOR SSNMR STUDIES OF AMPHOTERICIN B

We also investigated the use of POPC as the sole phospholipid in our liposomes. POPC is composed of a choline head group, one saturated palmitoyl chain, and one monounsaturated oleoyl chain. Thus, POPC forms bilayers composed of 50:50 saturated:unsaturated lipids, a ratio similar to that observed in physiologic membranes[15] (egg yolk phosphocholine, for example is primarily composed of POPC).[21] For these reasons, POPC has been very widely used as a phospholipid to form membranes in biophysical studies. When POPC liposomes were tested for K^+ efflux activity, strongly ergosterol-dependent K^+ efflux activity was observed (Figure 3-8).

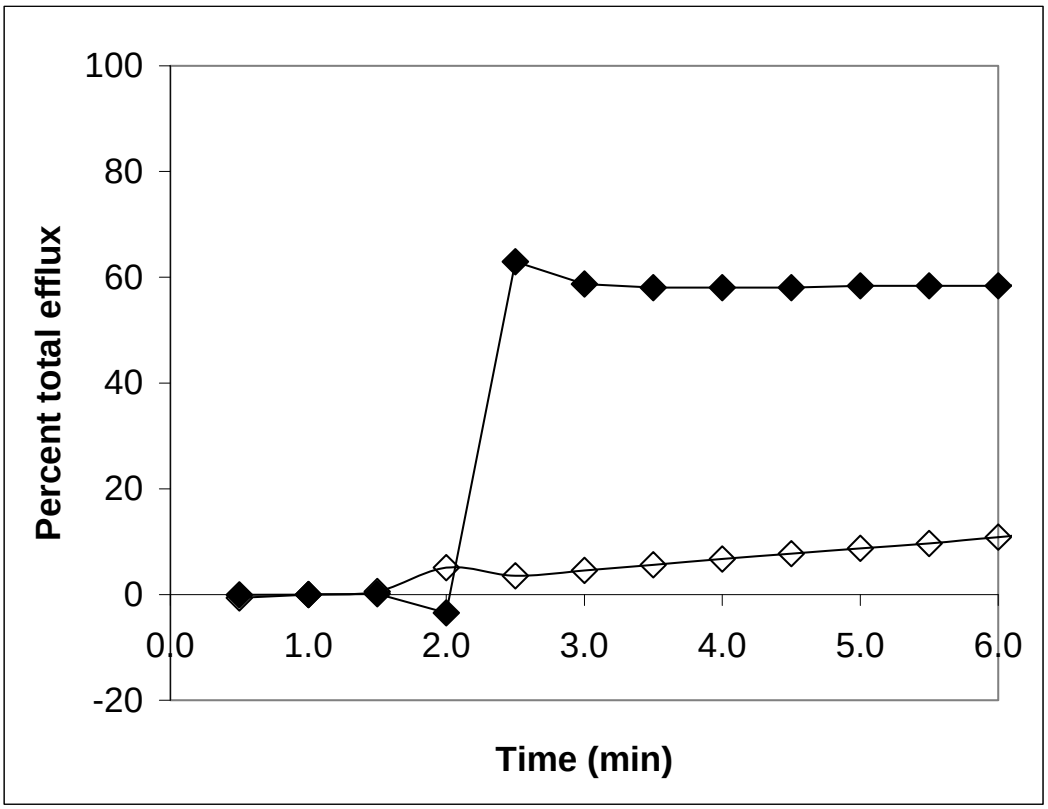

Figure 3-8. AmB initiates K^+ efflux from 200 μM LUVs composed of POPC plus 10% ergosterol (closed diamonds) and minus ergosterol (open diamonds). AmB was added as a DMSO solution at t = 1.5 min, and efflux is reported as a percentage of total efflux observed upon addition of Triton X-100 at t = 6.0 min.

The ergosterol-dependence of K^+ efflux activity in POPC LUVs was observed over a range of AmB concentrations, from 1000:1 lipid:AmB to 10:1 lipid:AmB (Figure 3-8 and Figure 3-9). To maximize sensitivity in our NMR experiments, we opted to use 10:1:1 POPC:U-^{13}C-AmB:Ergosterol. As noted above, 10 mol% AmB (relative to POPC) is significantly lower than the amount of AmB present at the MIC of AmB. Thus, this ratio achieved a balance between biolgocial relevance, maximizing sensitivity, and minimizing the amount of valuable U-^{13}C-AmB that would be required to make each sample. With this 10:1:1 POPC:AmB:Ergosterol liposome in hand, we proceeded to evaluate the potential of this system to provide SSNMR data of sufficient quality to allow for unambiguous de novo ^{13}C chemical shifts assignemtns for U-^{13}C-AmB.

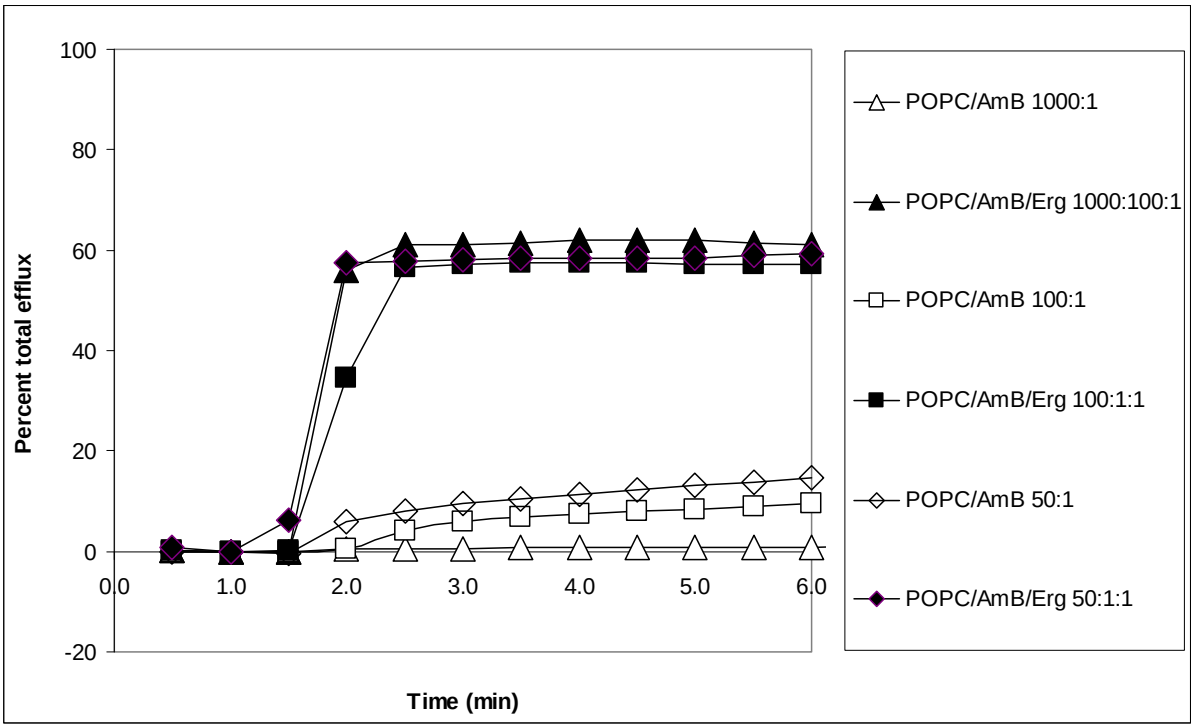

Figure 3-9. Ergosterol-dependent K^+ efflux from LUVs composed of POPC/AmB 1000:1 plus ergosterol (closed triangles) and minus ergosterol (open triangles); POPC/AmB 100:1 plus ergosterol (closed squares) and minus ergosterol (open squares), and POPC/AmB 50:1 plus ergosterol (closed diamonds) and minus ergosterol (open diamonds). AmB was added at t = 1.5 min, and efflux is reported as a percentage of total efflux observed upon addition of Triton X-100 at t = 6.0 min.

3-4 DE NOVO ^{13}C CHEMICAL SHIFT ASSIGNMENTS OF U-^{13}C-AMPHOTERICIN B

POPC liposomes met our first 2 requirements of a suitable lipid milieu for SSNMR of AmB. Our final requirement was the successful completion of de novo ^{13}C chemical shift assignments of U-^{13}C-AmB. For this purpose, an MLV sample comprised of 10:1:1 POPC:U-^{13}C-AmB:Ergosterol was prepared. We then acquired a series of two-dimensional ^{13}C-^{13}C dipolar-assisted rotational resonance (DARR)[26] and double quantum filtered (DQF)[27] spectra. Since only the AmB in our samples was ^{13}C-enriched, ^{13}C-^{13}C spectra allow for analysis of interactions between ^{13}C-^{13}C nuclei of AmB without interference from lipid and/or ergosterol signals (for natural abundance molecules, the probability that 2 adjacent carbon atoms are both 13C is 0.0001). The DARR experiment gives rise to crosspeaks between ^{13}C nuclei interacting through space via dipolar coupling. When mixing time is short, only correlations for those nuclei very close to one another are observed, i.e. one- and two-bond correlations. At longer mixing times, more crosspeaks are observed, and long range interactions are observed. Figure 3-10 depicts the DARR spectrum of U-^{13}C-AmB with 50 ms mixing.

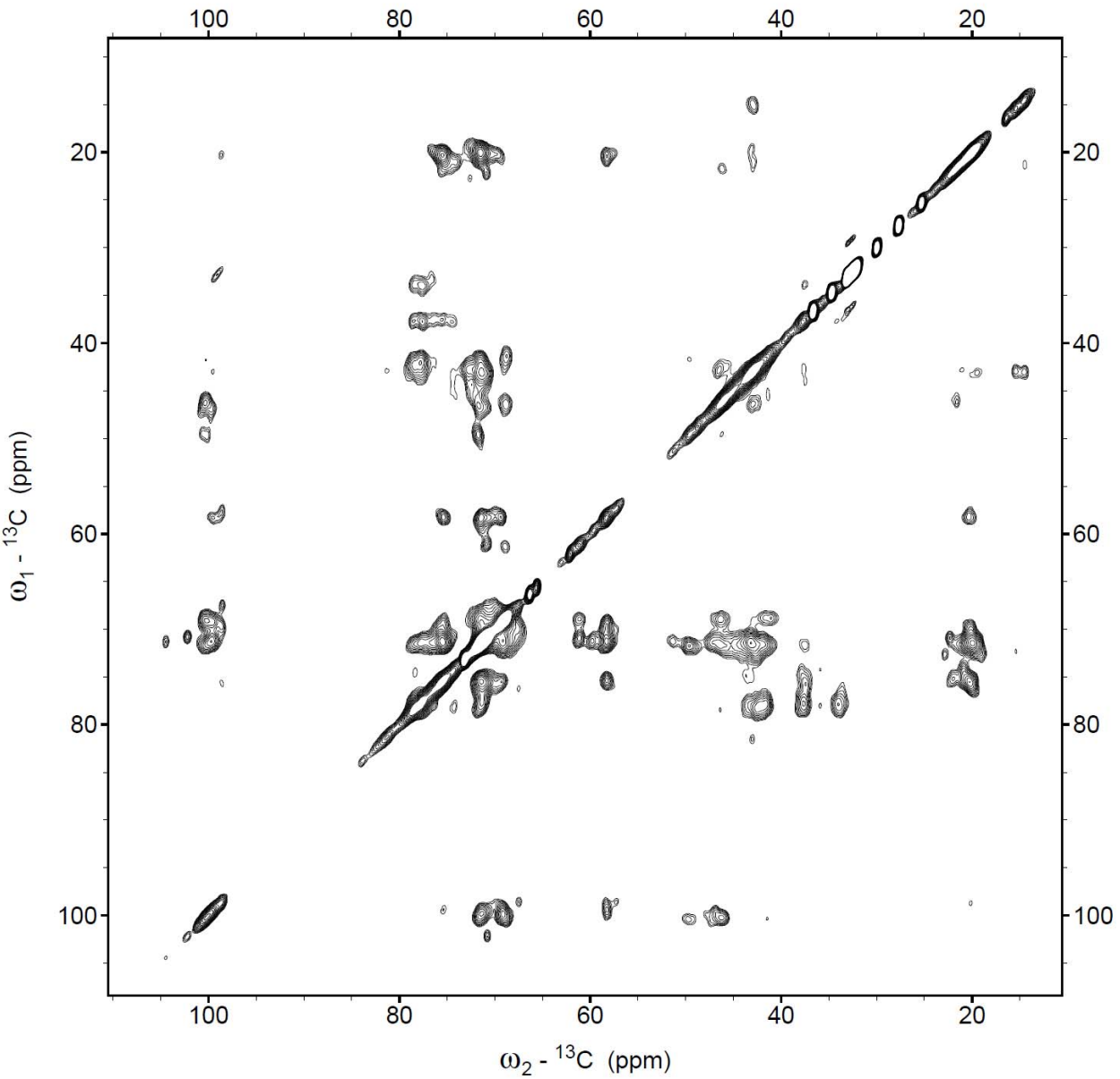

Figure 3-10. 13C-13C DARR spectrum of AmB with 50 ms mixing.

Examining the structure of AmB, several nuclei are predicted to fall in unique regions of the spectrum: C1 and C41 carbonyls (160-180 ppm), C38, C39, C40, and C6' methyls (10-25 ppm), C13 hemiketal and C1' acetal (95-105 ppm). These resonances were striaghtforward to assign, and by following the pattern of crosspeaks through the spectrum, approximately 50% of the resonances were assigned confidently (not counting the polyene, the chemical shifts of which are not sufficiently resolved to make any site-specific assignments). Further examination of the non-polyene portion of AmB reveals predominantly a repeating pattern of 1,3-diols, with methylenes intervening. The chemical shifts for the methane carbons bearing these hydroxyl

groups fall between 70 and 90 ppm, and those of the methylene carbons fall between 30 and 60 ppm. Hence, this region of the spectrum (~75 ppm x ~45 ppm) is very crowded. We also noted some 2 bond correlations even at this short mixing time, thus further crowding the spectrum.

To allow assignment of the remaining resonances with high confidence, we employed DQF spectra to reduce the number of crosspeaks in the spectrum. In this experiment, only one-bond correlations between adjacent ^{13}C nuclei are observed due to filtering of single-quantum transitions in the pulse sequence. The DQF spectrum of U-^{13}C-AmB is shown in Figure 3-11. We noted that this spectrum contained more peaks than would be predicted if every bonded pair gave rise to just one crosspeak. From DQF spectra, assignments of the non-polyene ^{13}C resonances of AmB were completed, and we noted that the extra crosspeaks form a second, and in some cases a third, series of assignments. One set of assignments was clearly dominant, and these primary assignments were used for subsequent studies. As an example of the multiple assignments for AmB from this spectrum, Figure 3-12 depicts the crosspeaks for the mycosamine sugar. Two sets of assignments (with colored labels for differentiation) are clearly found. While one set was assigned as the primary assignment, these multiple assignments provide direct evidence that AmB does not exist in a homogeneous chemical environment within liposomes. Furthermore, mycosamine has rotational degrees of freedom about its glycosidic attachment to the macrolactone, and these assignments potentially represent multiple configurations about this linkage. Further studies will be required to elucidate the significance of these secondary assignments. Figure 3-13 depicts the structure of AmB with all assignments that could be unambiguously determined from DQF spectra, with confirmation from 2- and 3-bond correlations from DARR spectra. These assignments are also found in Table 3-1.

With the completion of de novo 13C assignments for AmB, POPC MLVs now met our 3 criteria to qualify as a suitable lipid system for SSNMR: AmB readily binds to these MLVs, the vesicles retain ergosterol-dependent K^+ efflux activity, and we successfully completed de novo assignments of U-^{13}C-AmB in this lipid system. Moreover, we had accomplished the three goals defined in section 3-1: 1) developing a reproducible method for the preparation of highly ^{13}C-enriched AmB, 2) discovery of a functionally relevant lipid milieu for SSNMR analysis of AmB, and 3) de novo chemical shift assignments of U-^{13}C AmB. We were thus poised to proceed with the SSNMR studies described in Chapter 4.

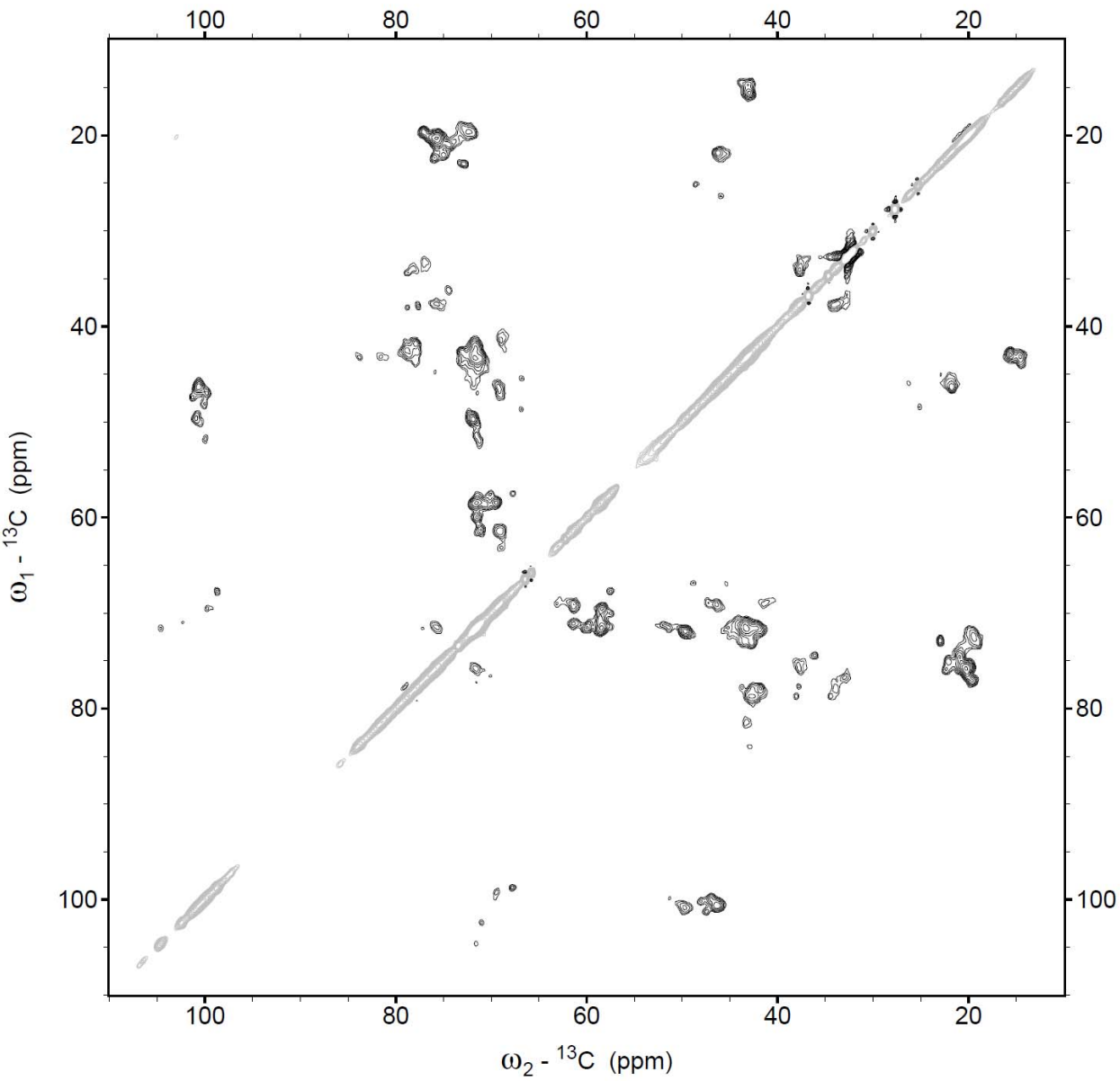

Figure 3-11. DQF spectrum of AmB.

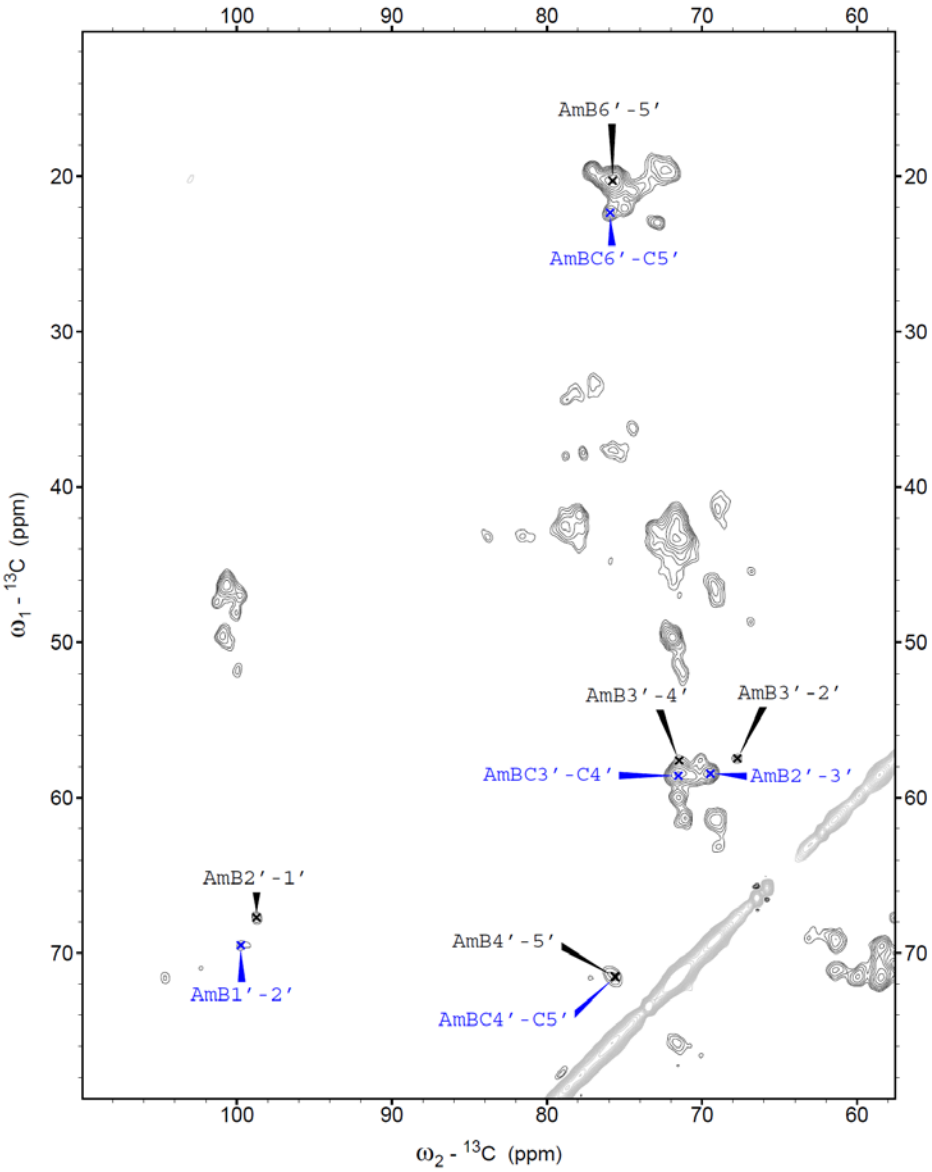

Figure 3-12. Two complete sets of assignments were identified for the mycosamine sugar, possibly indicating multiple configurations about the glycosidic linkage to the macrolactone.

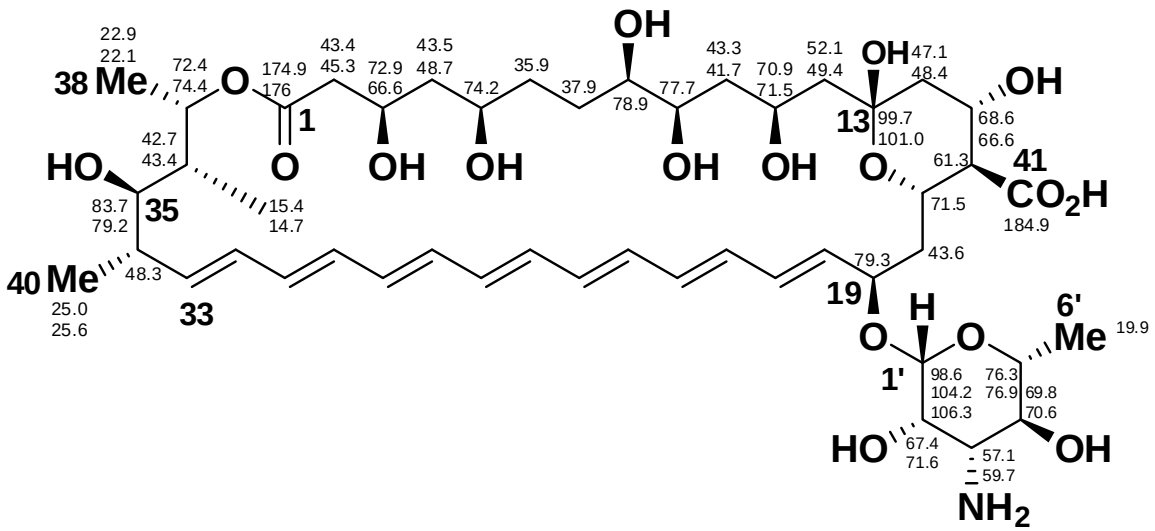

Figure 3-13. AmB 13C chemical shift assignments. When multiple assignments were made for a given site, all assignments are listed, with the value closest to the atom itself representing the primary assignment.

	δ (ppm)		
Carbon	Major	Minor	Minor
1	176	174.9	
2	45.3	43.4	
3	66.6	72.9	
4	48.7	43.5	
5	74.2		
6	35.9		
7	37.9		
8	78.9		
9	77.7		
10	41.7	43.3	
11	71.5	70.9	
12	49.4	52.1	
13	99.7	101	
14	48.4	47.1	
15	68.6	66.6	
16	61.3		
17	71.5		
18	43.6		
19	79.3		
34	48.3		
35	83.7	79.2	
36	43.4	42.7	
37	74.4	72.4	
38	22.1	22.9	
39	15.4	14.7	
40	25	25.6	
41	184.9		
1'	98.6	104.2	106.3
2'	67.4	71.6	
3'	57.1	59.7	
4'	69.8	70.6	
5'	76.3	76.9	
6'	19.9		

Table 3-1. AmB ^{13}C chemical shift assignments.

3-5 EXPERIMENTAL SECTION

I. Nanodisc preparation and SEC analysis. Membrane scaffold protein was expressed from *e. coli* and nanodisc samples prepared and analyzed according to the methods reported by Sligar and coworkers. [21,24]

II. Preparation of U-13C-AmB.

U-^{13}C-Glc (Cambridge Isotopes, Cambridge, MA) was substituted for fructose in the medium reported by McNamara and coworkers.[19] The procedure reported by Murata for preparing U-^{13}C-AmB[14] was followed. Due to the slow-growing nature of streptomycetes and the resulting ease with which cultures can be contaminated, all manipulations with cell cultures were carried out in a Labconco Clean Bench sterilized with 70% EtOH before and after manipulations. 20 mL cultures in 250 mL baffled flasks were used. For pulse feeding of glucose, 140 uL of 50% w/v U-^{13}C-Glc were added to each baffled flask.

After work-up of the U-^{13}C-AmB, if there remained any sign of Aliquat 336 (dark yellow solid, sticky solid, not free flowing), then this material was further purified via C18 reverse phase flash chromatography as follows: AmB was dissolved in DMF and Celite 545 was added to form a slurry. AmB was concentrated onto the Celite *in vacuo*, and the resulting Celite was loaded onto a C18 flash column equilibrated with 20% MeCN / 5 mM ammonium aceate. Purification with a gradient of 20% MeCN / 5 mM ammonium acetate to 100% MeCN followed by 100% Optima MeOH. This material could then be safely HPLC purified. If signs of Aliquat 336 still remained, the material was purified again by C18 flash column.

U-^{13}C-AmB was HPLC-purified using a Waters SunFire Prep C18 OBD 30x150 mm column with a gradient of 5% to 65% MeCN / 5 mM ammonium acetate over 12 minutes. Post-column, solvent was removed in vacuo and the solid was suspended via bath sonication in 1:1 acetonitrile:toluene and concentrated *in vacuo* to azeotrope residual acetic acid.

K^+ efflux assays.

General Information.

These experiments were carried out by the method reported by Gray et al.[17] and Palacios et al.,[18] with a small modification when saturated lipids (such as DPPC) were used (see below). Ion selective measurements were obtained using a Denver Instruments (Denver, CO) Model 225 pH meter equipped with a World Precision Instruments (Sarasota, FL) potassium selective electrode inside a Faraday cage. The electrode filled with 1000 ppm KCl standard solution and conditioned in a 1000 ppm KCl standard solution for 30 minutes prior to ion selective measurements. Measurements were made on 3 mL solutions that were magnetically stirred in 7 mL Wheaton vials incubated in a 30 °C aluminum block (S. cerevisiae) or at 23 °C (LUVs). The instrument was calibrated daily with KCl standard solutions to 10, 100, and 1000 ppm potassium. The potassium concentration was sampled every 30 seconds throughout the course of the efflux experiments.

Data Analysis.

The data from each run was normalized to the percent of total potassium release, from 0 to 100%. Thus for each experiment a scaling factor S was calculated using the following relationship:

$$\left[\frac{[K^+]_{final}}{[K^+]_{initial}} - 1\right] \cdot S = 100$$

Each concentration data point was then multiplied by S before plotting as a function of time. Efflux from 10% ergosterol LUVs.

LUV Preparation.

Phospholipids were obtained as a stock solution in $CHCl_3$ from Avanti Polar Lipids (Alabaster, AL) and was stored at -20 °C under an atmosphere of dry argon and used within 3 months. A 4 mg/mL solution of ergosterol in $CHCl_3$ was prepared monthly and stored at 4 °C under an atmosphere of dry argon. Prior to preparing a lipid film, the solutions were warmed to ambient temperature to prevent condensation from contaminating the solutions. A 13 x 100 mm test tube was charged with 640 µL POPC and 230 µL of the ergosterol solution. The solvent was removed with a gentle stream of nitrogen and the resulting lipid film was stored under high vacuum for a minimum of eight hours prior to use. The film was then hydrated with 1 mL of 150 mM KCl, 5

mM HEPES pH 7.4 (K buffer) and vortexed vigorously for approximately 3 minutes to form a suspension of multilamellar vesicles (MLVs). The resulting lipid suspension was pulled into a Hamilton (Reno, NV) 1 mL gastight syringe and the syringe was placed in an Avanti Polar Lipids Mini-Extruder. For saturated lipids with high temperature phase transitions, this was done on a heating block above the transition temperature of the lipid. The lipid solution was then passed through a 0.20 μM Millipore (Billerica, MA) polycarbonate filter 21 times, the newly formed large unilamellar vesicle (LUV) suspension

being collected in the syringe that did not contain the original suspension of MLVs to prevent the carryover of MLVs into the LUV solution. To obtain a sufficient quantity of LUVs, three independent 1 mL preparations were pooled together for the dialysis and subsequent potassium efflux experiments. The newly formed LUVs were dialyzed using Pierce (Rockford, IL) Slide-A-Lyzer MWCO 3,500 dialysis cassettes. The samples were dialyzed three times against 600 mL of Na buffer. The first two dialyses were two hours long, while the final dialysis was performed overnight.

Determination of Phosphorus Content.

Determination of total phosphorus was adapted from the report of Chen and coworkers.[9] The LUV solution was diluted tenfold with Na buffer and three 10 μL samples of the diluted LUV suspension were added to three separate 7 mL vials. Subsequently, the solvent was removed with a stream of N_2. To each dried LUV film, and a fourth vial containing no lipids that was used as a blank, was added 450 μL of 8.9 M H_2SO_4. The four samples were incubated open to ambient atmosphere in a 225 °C aluminum heating block for 25 min and then removed to 23 °C and cooled for 5 minutes. After cooling, 150 μL of 30% w/v aqueous hydrogen peroxide was added to each sample, and the vials were returned to the 225 °C heating block for 30 minutes. The samples were then removed to 23 °C and cooled for 5 minutes before the addition of 3.9 mL water. Then 500 μL of 2.5% w/v ammonium molybdate was added to each vial and the resulting mixtures were then vortexed briefly and vigorously five times. Subsequently, 500 μL of 10% w/v ascorbic acid was added to each vial and the resulting mixtures were then vortexed briefly and vigorously five times. The vials were enclosed with a PTFE lined cap and then placed in a 100 °C aluminum heating block for 7 minutes. The samples were removed to 23 °C and cooled for approximately 15 minutes prior to analysis by UV/Vis spectroscopy. Total phosphorus was

determined by observing the absorbance at 820 nm and comparing this value to a standard curve obtained through this method and a standard phosphorus solution of known concentration.

Determination of Ergosterol Content.

Ergosterol content was determined spectrophotometrically. The LUV solution was diluted tenfold with Na buffer, and 50 μL of the dilute LUV suspension was added to 450 μL 2:18:9 hexane:isopropanol:water (v/v/v). Three independent samples were prepared and then vortexed vigorously for approximately one minute. The solutions were then analyzed by UV/Vis spectroscopy and the concentration of ergosterol in solution was determined by the extinction coefficient of 10400 L mol^{-1} cm^{-1} at the UVmax of 282 nm and was compared to the concentration of phosphorus to determine the percent sterol content. The extinction coefficient was determined independently in the above ternary solvent system. LUVs prepared by this method contained between 7 and 14% ergosterol.

Efflux from LUVs.

The LUV solutions were adjusted to 1 mM in phosphorus using Na buffer. 3 mL of the 1 mM LUV suspension was added to a 7 mL vial and the solution was gently stirred. The potassium ISE probe was inserted and data were collected for one minute prior to the addition of the compound. Then, 30 μL of a 0.1 mM, 1.0 mM, or 3.0 mM DMSO solution of the compound in question was added and data were collected for five minutes. Then to effect complete potassium release, 30 μL of a 10% v/v solution of triton X-100 was added and data were collected for an additional five minutes. The experiment was duplicated with similar results.

SSNMR Experiments

SSNMR Sample preparation

HPLC purified U-^{13}C-AmB was suspended in a large volume of Optima methanol, typically ~75 mL for 10 mg. Using a Hamilton gastight syringe, 3 x 10 μL of this solution were diluted with Optima methanol to a final volume of 510 μL. The concentration of each resulting solution was calculated based on UV/Vis absorbance at 406 nm using ε = 146000 and the average concentration was used as the concentration of the original AmB stock solution. The appropriate volume of stock solution (typically 30-40 mL) was concentrated *in vacuo* to a small volume that

could then be transferred to a 7 mL Wheaton vial, with three methanol washes to ensure complete transfer. This resulting AmB suspension was concentrated *in vacuo*. Stock solutions of phospholipid and ergosterol in $CHCl_3$ were added to the vial via Hamilton syringe along with an equivalent volume of Optima MeOH. This suspension was briefly vortexed and sonicated until no AmB remained on the sides of the vial (2-3 cycles). Solvent was removed under a gentle stream of nitrogen gas. Residual solvent was removed under high vacuum overnight.

To the dried AmB/lipid film was added filter-sterilized 0.3 mM HEPES buffer, pH 7.0 to yield a final phospholipid concentration of 40 mM. This aqueous suspension was vortexed and sonicated 3 times or until a homogeneous suspension was observed. Samples were then submitted to 5 freeze/thaw cycles in liquid nitrogen followed by lukewarm tapwater. Samples were then frozen in liquid nitrogen a 6^{th} time and placed in a lyophilizer for a minimum of 8 hours. The lyophilization chamber was then back-filled with dry argon to prevent samples from absorbing ambient water. Samples were immediately capped and packed into rotors for SSNMR as soon as possible.

Dry samples were packed in 3.2 mm diameter SSNMR rotors and hydrated with 7-10 μL of MilliQ H_2O. Rubber discs were used in the rotors to maintain hydration levels by creating a seal against which the rotor cap and drive tip were placed. Samples were placed at 4 °C for at least 24 hours to allow water to equilibrate.

SSNMR Experiments.

MAS SSNMR experiments were performed at 600 MHz ^{1}H frequency on Varian InfinityPlus spectrometers, with a 3.2-mm Varian ^{1}H-^{13}C-^{15}N T3 probe at an MAS rate of 10 kHz. The temperature control point was set to 20 °C, and actual sample temperature of 19.5 °C for all experiments, as calibrated by ethylene glycol.[28] All experiments utilized tangent ramped cross-polarization (CP)[29] with an average of 75 kHz SPINAL[30,31] decoupling of protons applied during evolution and acquisition periods. A series of ^{13}C-^{13}C 2D spectra were acquired with 25 to 500ms DARR, and double quantum filtered spectra were acquired using the SPC5 pulse sequence, with q = 30.[27] Chemical shifts are referenced to adamantane.[32]

REFERENCES

1) McDermott, A.E. *Annu. Rev. Biophys.* **2009**, *38*, 385-403
2) Hong, M.; *Acc. Chem. Res.* **2006**, *39*, 176-183
3) Manasi, P.B.; Wylie, B.J.; Tian, L.; McDermott, A.E. *J. Mol. Biol.* **2010**, *401*, 155-166
4) Cady, S.D.; Schmidt-Rohr, K.; Wang, J.; Soto, C.S.; DeGrado, W.F.; Hong, M. *Nature* **2010,** *463*, 689-693.
5) Tang, M.; Sperling, L.J.; Berthold, D.A.; Schwieters, C.D.; Nesbitt, A.E.; Nieuwkoop A.J.; Rienstra, C.M. *J. Biomol. NMR*, **2011**, *51*, 227-233.
6) Comellas G.; Lemkau L.R.; Zhou, D.H.; George J.M.; Rienstra, C.M. *J. Am. Chem. Soc.*, **2012**, *134*, 5090-5099
7) Higman, V.A.; Varga, K.; Aslimovska, L.; Judge, P.J.; Sperling, L.J.; Rienstra, C.M.; Watts, A. *Angew. Chemie.*, **2011**, *50*, 8432-8435.
8) Kijac, A. Z.; Li, Y.; Sligar, S. G.; Rienstra, C. M. *Biochemistry* **2007**, *46*, 13696-13703
9) Cegelski, L.; Rice, C.V.; O'Connor, R.D.; Caruano, A.L.; Tochtrop, G.P.; Cai, Z.Y.; Covey, D.F.; Schaefer, J. *Drug Develop. Res.* **2006**, *66*, 93-102.
10) Sankaram, M.P.; Thompson, T.E. *Proc. Natl. Acad. Sci. USA* **1991**, *88*, 8686-8690.
11) Tian, X.; Guo, J.; Yao, F.; Yang, D.-P.; Makriyannis, A. *J. Biol. Chem.* **2005**, *280*, 29788-29795.
12) Jensen, M.; Bjerring, M.; Nielsen, N.C.; Nerdal, W. *J. Biol. Inorg. Chem.* **2009**, *15*, 213-223.
13) Matsuoka, S.; Ikeuchi, H.; Matsumori, N.; Murata, M. *Biochemistry* **2005**, *44*, 704-710.
14) Matsuoka, S.; Ikeuchi, H.; Umegawa, Y.; Matsumori, N.; Murata, M. *Bioorg. Med. Chem.* **2006**, *14*, 6608-6614
15) Champe, P.C.; Harvey, R.A.; Ferrier, D.A. *Lippincott's Illustrated Reviews: Biochemistry, 4th Ed.* **2008**, *Lippincott Williams & Wilkins,* Baltimore.
16) Umegawa, Y.; Nakagawa, Y.; Tahara, K.; Tsuchikawa, H.; Matsumori, N.; Oishi, T.; Murata, M.; *Biochemistry* **2012**, *51*, 83-89
17) Gray, K.C.; Palacios, D.S.; Dailey, I.; Endo, M.M.; Uno, B.E.; Wilcock, B.C.; Burke, M.D. *Proc. Natl. Acad. Sci. U.S.A.* **2012**, *109*, 2234-2239.
18) Palacios, D.S.; Dailey, I.; Seibert, D.M.; Wilcock, B.C.; Burke, M.D. *Proc. Natl. Acad. Sci. U.S.A.* **2011**, *108*, 6733-6738.
19) McNamara, C.M.; Box, S.; Crawforth, J.M.; Hickman, B.S.; Norwood, T.J.; Rawlings, B.J. *J. Chem. Soc. Perkin Trans. 1* **1998**, 83-87.
20) Inbar, L.; Lapidot, A. *J. Bacteriol.* **1991**, *173*, 7790-7801.
21) Bayburt, T.H.; Grinkova Y.V.; Sligar, S.G. *Nano Lett*, **2002**, *2*, 853-856
22) Nath, A.; Atkins, W.M.; Sligar, S.G. *Biochemistry* **2007**, *46*, 2059-2069
23) Jonas, A. *Methods Enzymol*. **1986**, *128*, 553-582.
24) Bayburt, T.H.; Sligar, S.G. *Prot. Sci.* **2003**, *12*, 2476-2481.
25) Nguyen, T.-S.; Weers, P.M.M.; Raussens, V.; Wang, Z.; Ren, G.; Sulchek, T.; Hoeprich, Jr., P.D., Ryan, R.O. *Biochim. Biophys. Acta* **2008**, *1778*, 303-312.
26) Takegoshi, K.; Nakamura, S.; Terao, T. *Chem. Phys. Lett.* **2001**, *344*, 631-637.
27) Hohwy, M.; Rienstra, C.M.; Jaroniec, C.P.; Griffin, R.G. *J. Chem. Phys.* **1999**, *110*, 7983=7992
28) Van Geet, A.L. *Analytical Chemistry* **1968**, *42*, 2227.
29) Hediger, S.; et al. *Chem. Phys. Lett.* **1994**, *223*, 283.
30) Brauniger, T.; Wormald, P.; Hodgkinson, P. *Monatsh. Chem*. **2002**, *133*, 1549-15

31) Comellas, G.C.; Lopez, J.J.; Nieuwkoop, A.J.; Lemkau, L.R.; Rienstra, C.M. *J. Magn. Reson.*, **2011**, *209*, 131-135.
32) Morcombe, C.R.; Zilm, K.W. *J. Magn. Reson.* **2003**, *162*, 479-486.

CHAPTER 4

SSNMR studies of amphotericin B in the presence of phospholipid bilayers reveal that large, extramembranous aggregates of amphotericin extract ergosterol from the membrane

ABSTRACT

Our laboratories recently discovered that the antifungal activity of AmB involves two complementary mechanisms: sterol sequestration and membrane permeabilization. Of these two mechanisms, sterol sequestration was shown to be the primary mechanism of antifungal activity. However, the structural underpinnings of how AmB binds to membrane phospholipids and ergosterol remain unclear. To probe the primary location of AmB within the phospholipid bilayer, we conducted paramagnetic relaxation enhancement (PRE) SSNMR studies of membrane-bound AmB in the presence of 1-palmitoyl-2-stearoyl-(16-doxyl)-*sn*-glycero-3-phosphocholine (16-DOXYL-PC) and 1-palmitoyl-2-stearoyl-(5-doxyl)-*sn*-glycero-3-phosphocholine (5-DOXYL-PC). Three sets of PRE experiments were performed: 1) measurement of POPC PREs, 2) measurement of U-^{13}C AmB PREs in the presence of these same lipids, and 3) measurement of ^{13}C-labeled ergosterol PREs at increasing ratios of AmB:ergosterol. The results of these experiments reveal that the majority of AmB is not embedded within the phospholipid bilayer but is instead bound to the bilayer as a large aggregate phase-separated from membrane phospholipids. In the presence of ergosterol, this large aggregate functions to bind and extract ergosterol from the phospholipid bilayer, thus acting as a "sponge" for ergosterol. These results indicate that AmB has greater proximity to water than to phospholipid. Based on all of these results, we propose a new model in which AmB exerts its antifungal activity primarily via self-assembly into large, extramembranous aggregates that function as sponges for ergosterol, thus depleting fungal membranes of this physiologically vital lipid.

Prof. Chad Rienstra, Mary Clay, and Gemma Commellas acquired the SSNMR data described in this chapter. Data were analyzed primarily by Mary Clay and the author. Brice Uno assisted with purification of AmB and preparation of SSNMR samples. Alex Cioffi, Matt Endo, and Shu Wang assisted in preparation of ^{13}C-labeled ergosterol. Alex Cioffi contributed to preparation of SSNMR samples containing ^{13}C-labeled ergosterol.

4-1 BACKGROUND

For nearly 40 years, the barrel stave ion channel model[1,2,3] discussed in Chapter 1 has dominated the structural model for AmB (**4.1**) in the presence of lipid bilayers. Three major postulates form the basis for this model: 1) In phospholipid bilayers, AmB primarily exists as discrete, nanometer-scale barrel stave pores, 2) These pores are embedded in the phsopholipid bilayer, and 3) Ergosterol (**4.2**) binds to these embedded pores. To date, most of the structural studies of AmB, including many SSNMR experiments, have been interpreted almost exclusively through the lens of this inserted ion channel model. As discussed in Chapter 3, we have taken a fresh approach to this problem by preparing highly ^{13}C-enriched AmB, identifying a functionally relevant lipid bilayer system for SSNMR analysis of membrane-bound AmB, and completing de novo AmB ^{13}C chemical shift assignments. We were thus in a position to plan a suite of high resolution SSNMR experiments to study AmB in a phospholipid environment.

Rather than focus our studies exclusively on the barrel stave ion channel model, we chose to focus our SSNMR experiments on simply elucidating interactions between AmB and membrane phospholipids As described in Chapter 3, work in our laboratories recently identified ergosterol sequestration as the primary mechanism of AmB antifungal activity.[4] However, the structural and biophysical underpinnings of this unique small molecule-small molecule interaction remain unknown. Ergosterol is known to form a variety of functions in yeast membranes including enabling the proper functioning of membrane proteins,[5] microdomain formation,[6] vacuole fusion,[7] endocytosis,[8] and pheromone signaling[9]

In light of our recent discovery that there is approximately 10 times more AmB than ergosterol at the MIC for AmB,[4] we hypothesized that the primary significance of AmB binding ergosterol is to preclude ergosterol from performing its critical physiological functions in fungal membranes. We identified three possible models for how AmB carries out the task of sequestering ergosterol (Figure 4-1):

1) The classic ion channel model (Figure 4-1A) in which ergosterol is bound between adjacent AmB molecules
2) Surface adsorption model (Figure 4-1B) in which AmB binds to the hydrophilic portion of the lipid bilayer and sequesters ergosterol
3) Sterol sponge model (Figure 4-1C) in which AmB binds to lipid bilayers as a large, extramembranous aggregate and extracts ergosterol from the lipid bilayer

We recognized that the key to differentiating these 3 models was determining the primary location of AmB within the lipid bilayer and the location of ergosterol in the absence and presence of AmB.

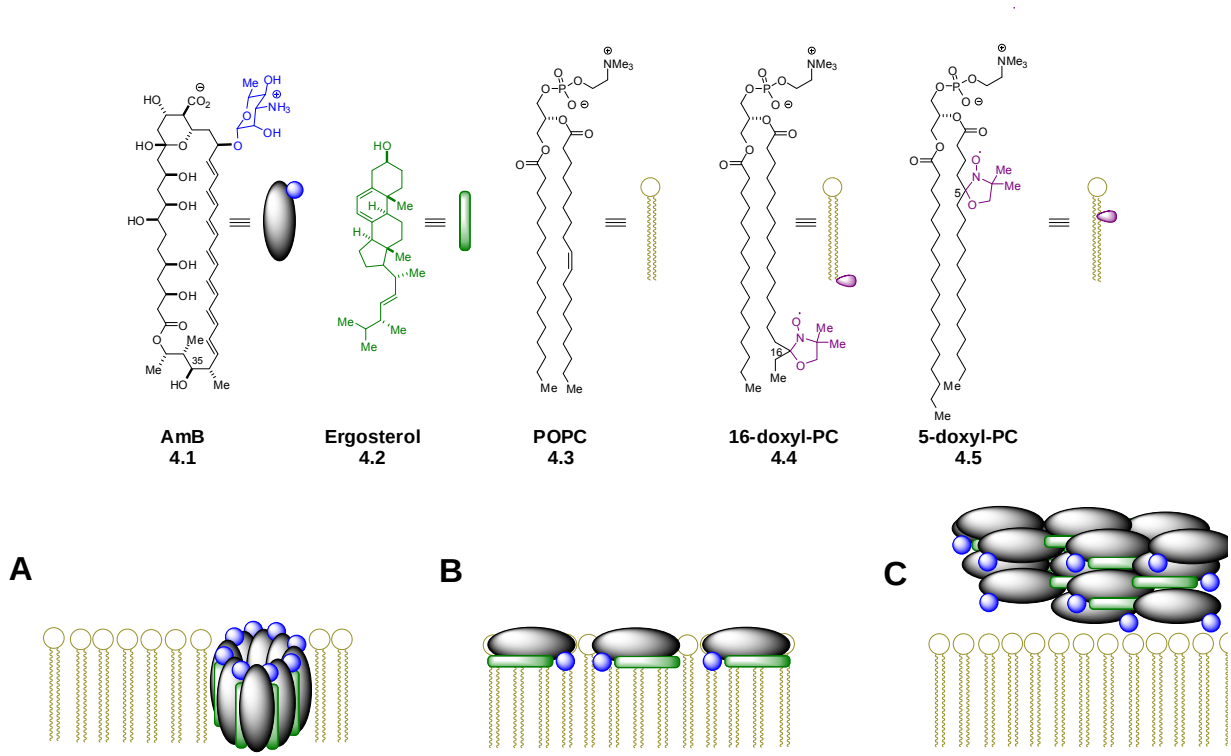

Figure 4-1. A) Structure of AmB and ergosterol. B) Classic barrel-stave model of the AmB ion channel. C) Surface adsorption model of AmB bound to ergosterol. D) Sterol sponge model wherein a large, phase-separated aggregate of AmB binds to the phospholipid bilayer and extracts ergosterol.

To do this, we performed a series of ^{13}C paramagnetic relaxation enhancement (PRE)[10,11] studies of AmB and ergosterol in the presence of phospholipid bilayers containing lipids with appended nitroxyl spin labels: 1-palmitoyl-2-stearoyl-(16-doxyl)-*sn*-glycero-3-phosphocholine (16-DOXYL-PC **4.4**) and 1-palmitoyl-2-stearoyl-(5-doxyl)-*sn*-glycero-3-phosphocholine (5-DOXYL-PC **4.5**). Unpaired electrons are known to dramatically decrease both the T_1 and T_2 relaxation properties of proximal nuclei in NMR experiments.[10,11] PRE studies in the presence of various paramagnetic probe reagents have been reported.[12]

Paramagnetic phospholipids such as **4.4** and **4.5** have been used for a variety of EPR studies[13] of membrane biophysics, but their use in SSNMR has been limited. Notably, Sankaram and Thompson[14] employed SSNMR to determine the position of ^{13}C-labeled cholesterol in DPPC MLVs containing 5% 5-DOXYL-PC. This method involves measuring DPPC PREs to determine

the effect of the nitroxyl spin-label at specific depths within the bilayer. Subsequently, ^{13}C PREs of ^{13}C-labeled cholesterol were measured and the position of cholesterol in the bilayer was determined.

We recognized three advantages to this method for determining the position of AmB and ergosterol in the lipid bilayer. First, paramagnetic spin-labels have the unique capacity to perturb nuclei up to 24 Å from the unpaired electron[12] (in contrast, REDOR experiments have an upper limit of approximately 8-12 Å,[15] depending on the nuclei involved). Second, unlike REDOR, use of U-^{13}C-AmB does not complicate analysis due to neighboring ^{13}C nuclei. Third, in comparison to many other more complicated SSNMR experiments (such as REDOR), the PRE experiment is relatively straightforward and data can be acquired fairly quickly. We have adapted the method of Sankaram and Thompson for our purposes in studying AmB. We opted to use both 16-DOXYL-PC **4.4** and 5-DOXYL PC **4.5** in parallel PRE studies to probe both the bilayer interior (16-DOXYL-PC) and the outer portion of the bilayer (5-DOXYL-PC) for AmB and ergosterol.

This chapter details the use of these spin-labeled lipids to measure ^{13}C PREs of AmB in POPC MLVs and the subsequent measurement of ^{13}C PREs of ergosterol in the presence of increasing amounts of AmB. In stark contrast to the leading ion channel model, our results indicate that AmB primarily exists as large, phase-separated aggregates that function to extract ergosterol from the membrane (Fig. 4-1C.)

4-2 PARAMAGNETIC RELAXATION ENHANCEMENT STUDIES OF POPC AND U-^{13}C AMPHOTERICIN B

To assess the position of AmB within the phospholipid bilayer, we first needed to assess the PRE effects of **4.4** and **4.6** on POPC. Due to the unique location of the nitroxyl moiety in each of these compounds, this set of lipids allowed us to probe the entire bilayer for PRE effects. We probed the hydrophobic core with 16-DOXYL-PC, bearing a nitroxyl spin label near the end of the lipid acyl chain. We probed the outer portion of the bilayer with 5-DOXYL-PC, bearing a nitroxyl spin label near the acyl C1 carbonyl.

To measure POPC PREs, we prepared three POPC MLV samples in parallel, each consisting of 10:1 POPC:ergosterol with 2 of the 3 samples each containing 5 mol% of either **4.4** or **4.5**. T_1 values were measured by the inversion recovery method:[16] a 180º pulse followed by a delay, τ, followed by a 90º pulse and acquisition. The τ delay is arrayed, and the magnetization following the 90º pulse varies with τ as

$$M(\tau) = M(0)[1 - 2\exp(-\tau/T_1)] \quad \text{Eq. 4.1}$$

For each array, a series of spectra with varying intensities is produced, and integrations for any given peak vary exponentially according to Eq. 4.1. The integrations for each peak in the spectrum were fit to exponential curves to determine the T_1. PREs were calculated by simply subtracting T_1 values for the samples containing DOXYL-PCs from the corresponding T_1 values in the control sample.

The results of these PRE experiments were consistent with the predicted location of each nitroxyl spin label (Figure 4-2). Specifically, 16-DOXYL-PC (Figure 4-2A) gave rise to very strong PREs for those POPC nuclei near the bilayer center, with decreasing PREs as the distance from the bilayer center increased. 5-DOXYL-PC (Figure 4-2B) gave rise to strong PREs for nuclei in the outer and middle portion of the bilayer, with PREs decreasing toward the bilayer center.

To probe the position of AmB within the bilayer, we next measured the PRE effect of **4.4** and **4.5** U-^{13}C AmB. Importantly, the 3 models presented in Figure 4-1 each lead to distinct predictions for these experiments. In the ion channel model (Fig. 4-1A), AmB is predicted to experience large PRE effects in the presence of both 16-DOXYL-PC and 5-DOXYL-PC, in the surface adsorption model (Fig. 4-1B) AmB is predicted to display large PRE effects only in the presence of 5-DOXYL-PC, and in the sterol sponge model, no PRE effects are expected for AmB in the presence of either membrane-embedded spin label.

To measure the AmB PREs, three POPC MLV samples were prepared in parallel, each consisting of 10:1:1 POPC:U-^{13}C AmB:ergosterol with two of the three samples containing 5 mol% of either **4.4** or **4.5**. Strikingly, in both cases, no significant PRE effects were observed for any ^{13}C nucleus of AmB (Figure 4-2, D and E). These results strongly indicate that the majority of AmB is phase-separated from membrane phospholipids, thus existing far from and unaffected by the nitroxyl spin labels.

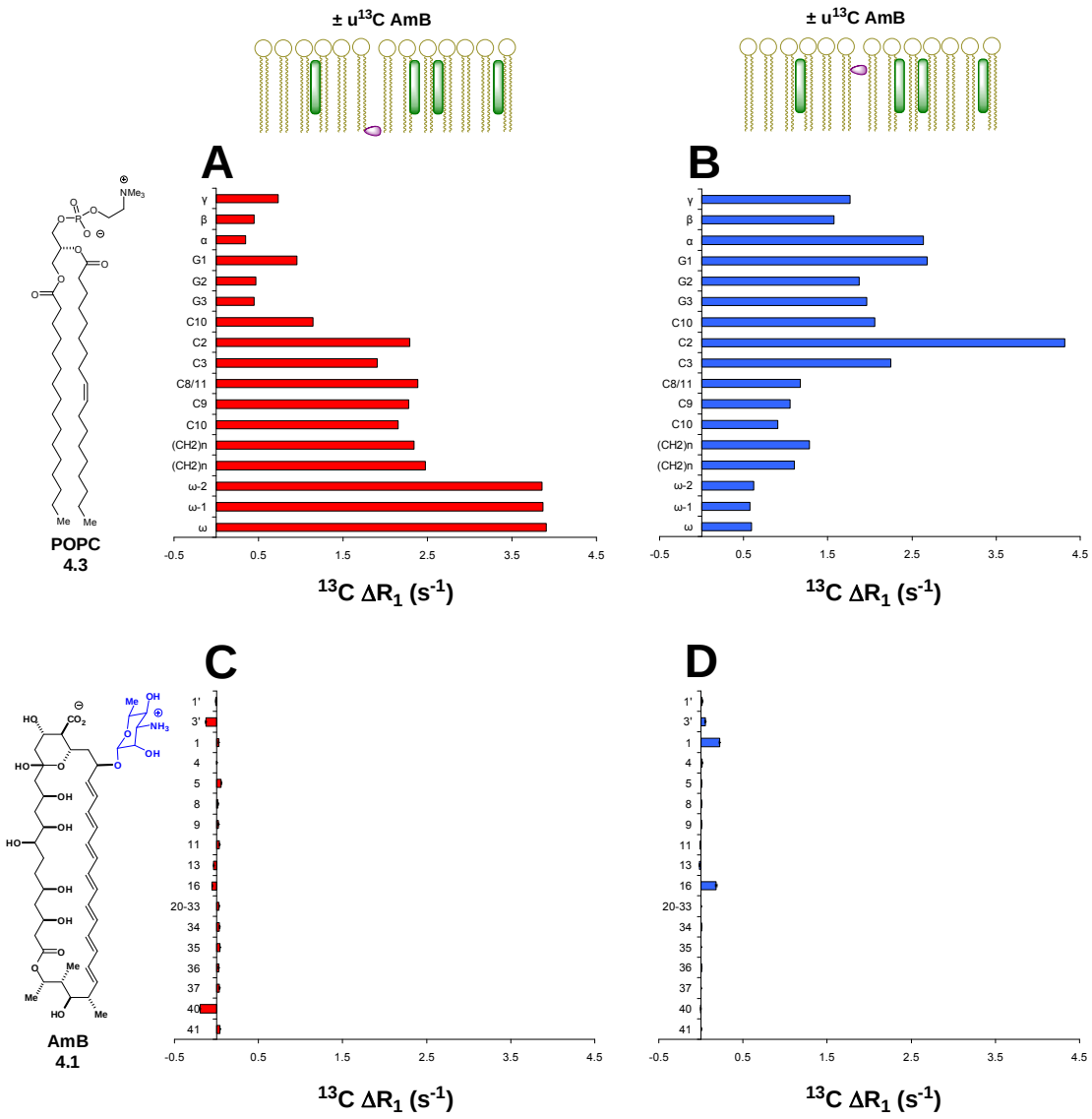

Figure 4-2. **^{13}C PRE effects in POPC/Ergosterol MLVs.** A, B, and C depict POPC PRE effects in the presence of 5% 16-DOXYL-PC (A), 5-DOXYL-PC (B), and TEMPO-PC (C). The y-axis labels are arranged in order of depth within the bilayer. As predicted, 16-DOXYL-PC has the strongest effect at the termini of the ljpid acyl chains. 5-DOXYL-PC has the greatest effect in the middle, and TEMPO-PC has the greatest effect in the headgroup. D, E, and F depict AmB ^{13}C PRE effects in the presence of 5% of each nitroxyl spin-labeled lipid. Only well resolved AmB resonances are reported.

A second striking observation from our PRE data was the magnitude of T_1 values of AmB ^{13}C nuclei (Figure 4-3A). Notably, the majority of T_1 values for the ^{13}C of POPC are between 0.3 and 0.5 s, while the T1s for AmB range from 3.0 to 4.5 s (Figure 4-3B). The much longer AmB T_1 values are suggestive of a large, immobile aggregate (see Section 4-5 for further discussion).

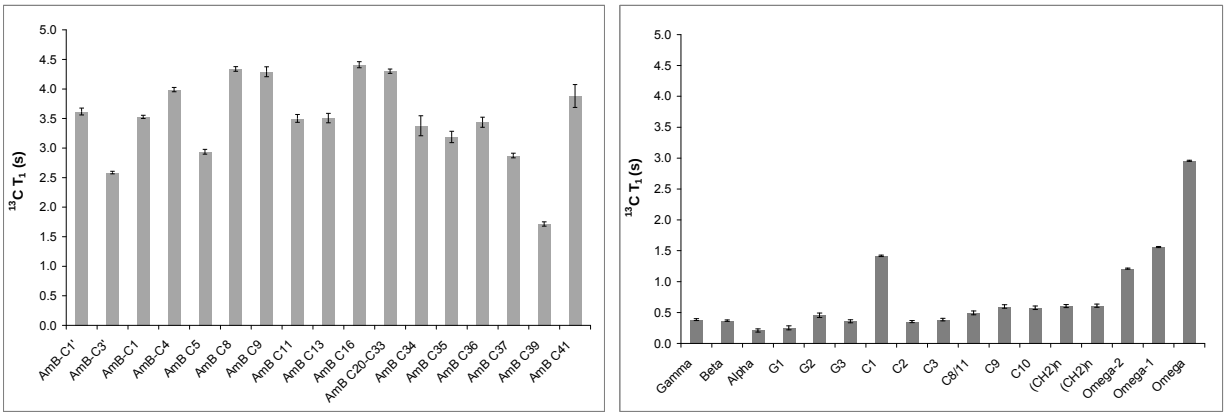

Figure 4-3. **T_1 relaxation values of AmB (left) and POPC (right).** In most cases, AmB T1 values are nearly an order of magnitude longer than those of POPC, indicative of different motional properties for these 2 molecules.

4-3 PARAMAGNETIC RELAXATION ENHANCEMENT OF ^{13}C-LABELED ERGOSTEROL IN THE PRESENCE OF INCREASING AMOUNTS OF AMPHOTERICIN B

To test the hypothesis that AmB extracts ergosterol from lipid bilayers, we designed a series of ^{13}C PRE experiments using skipped ^{13}C-labeled ergosterol **4.6** (hereafter ^{13}C-Erg). As a critical lipid component of fungal cell membranes, ergosterol is intimately mixed with membrane phospholipids and is thus predicted to have motional properties similar to those of phospholipids. We thus hypothesized that in POPC/Ergosterol MLVs, ^{13}C-Erg would have ^{13}C T_1 values similar to POPC and would exhibit large PREs in the presence of 16-DOXYL-PC. Moreover, upon extraction by AmB, we hypothesized that ergosterol would then become part of the large, extramembranous aggregate, resulting in an increase in the T_1 values for ^{13}C-Erg with a corresponding decrease in PRE effects.

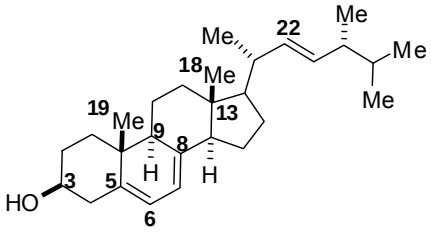

Ergosterol
4.2

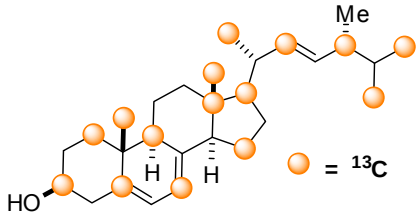

Skipped ^{13}C-labeled ergosterol
4.6

To perform this series of experiments we prepared the following samples for analysis: POPC:^{13}C-Erg 40:1 ± 16-DOXYL-PC, POPC:AmB:^{13}C-Erg 40:4:2 ± 16-DOXYL-PC, and POPC:AmB:^{13}C-Erg 40:4:1 ± 16-DOXYL-PC. The values for the POPC and ergosterol T_1

values are shown in Figure 4-4 for the POPC/^{13}C-Erg 40:1 sample (no DOXYL-PC). As predicted these two molecules have similar T_1's under these conditions.

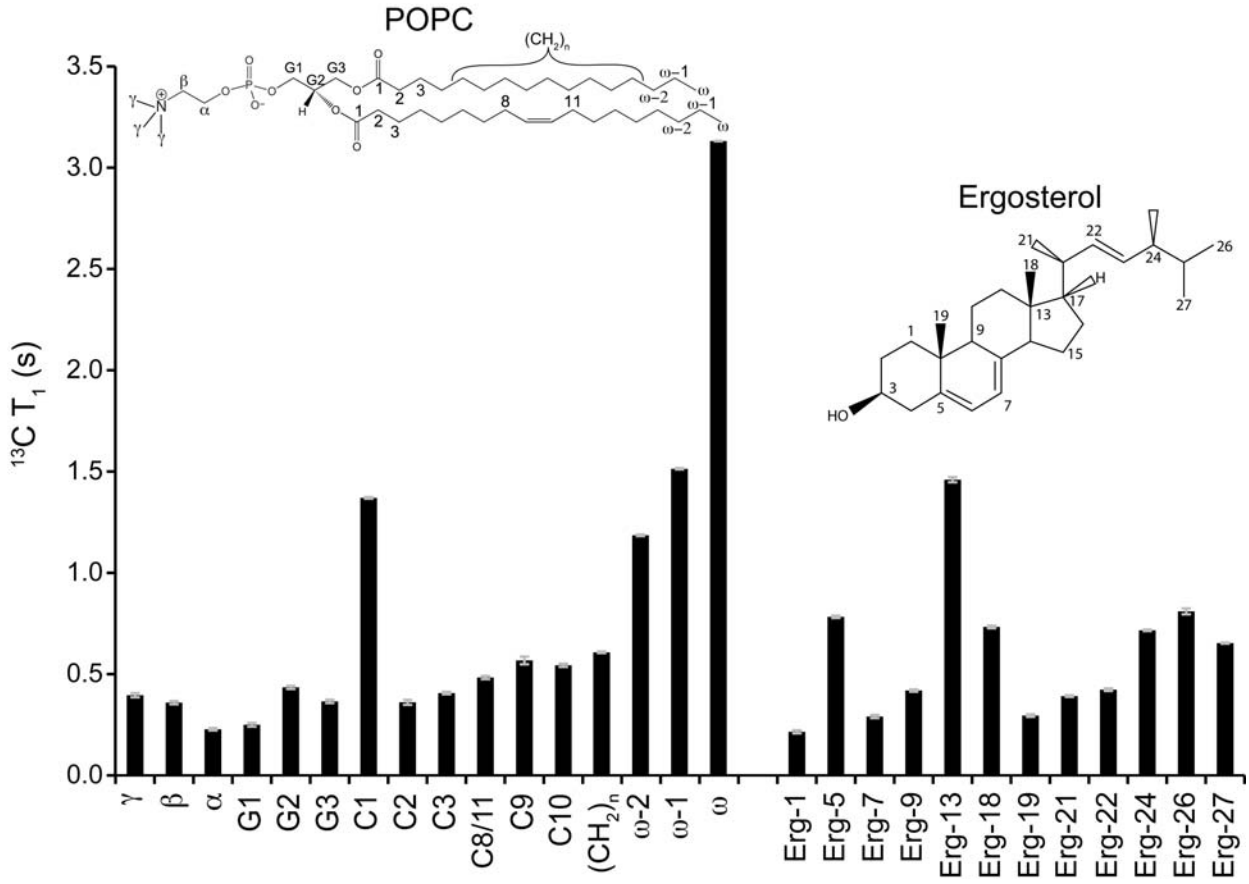

Figure 4-4. ^{13}C Longitudinal relaxation time (T_1) for POPC and ergosterol in MLVs composed of POPC/^{13}C-ergosterol 40:1.

As shown in Figure 4-5A, we observe a broadening, and in some cases a substantial (> 0.5 ppm) perturbation of the ergosterol resonances upon addition of AmB. Both of these observations are consistent with a change in environment of some portion of ergosterol upon addition of AmB (see Discussion section). To accurately asses the PREs for ^{13}C-Erg the integration boundaries were set according to the following criteria. (1) No overlap with neighboring resonances. (2) For chemical shift diefferences < 0.7 ppm, include the area for both the original and new, broad peak. (3) In cases where chemical shift differences > 1.0 ppm, include the area for only the original or new broad peak, with no overlap. In the cases where conditions 1 and 2 were satisfied, the average PRE is determined. As shown in Figure 4-5B, the T_1 values for the ^{13}C nuclei of ergosterol increase with increasing ratios of AmB:ergosterol. In addition, the average PRE for the same ^{13}C nuclei progressively decrease in the presence of

increasing AmB:ergosterol ratio (Figure 4-5C). Interestingly, the peak corresponding to ergosterol Erg-9 moves to a new position upon binding to AmB (Erg-9 and Erg-9', respectively, in Figure 4-5). The T_1 of Erg-9' is longer than that of Erg-9, and there is no significant PRE observed for Erg-9', consistent with a bound state of ergosterol remote from the 16-DOXYL PC.

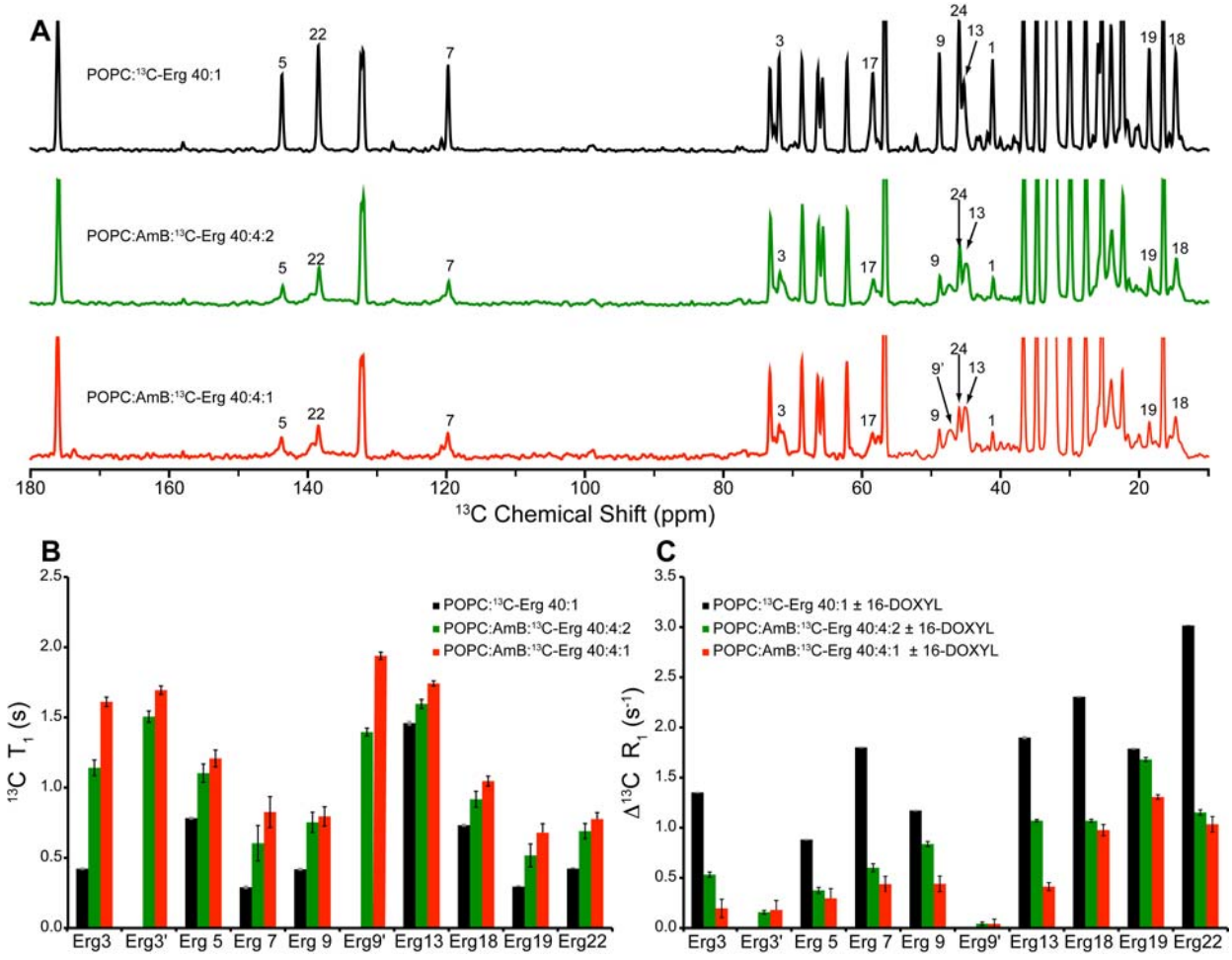

Figure 4-5. A) Direct polarization ^{13}C 1D spectra, processed with 50 Hz line broadening. B) Ergosterol T_1 values increase in the presence of increasing amounts of AmB, consistent with transfer of mobile ergosterol from the lipid bilayer into an immobile AmB aggregate. C) Ergosterol ^{13}C PREs decrease with increasing amounts of AmB, consistent with removal of ergosterol from proximity to the 16-DOXYL-PC spin label.

The identification of distinct resonances for the unbound and bound states of ergosterol further enabled us to determine the percentage of ergosterol extracted by AmB for each AmB:ergosterol ratio. The amount of ergosterol extracted was 51± 8% and 61±8% for the 40:4:1 and 40:4:2 POPC:AmB:^{13}C-Erg samples, respectively, based on a comparison of the relative integrated intensities of bound and unbound Erg 3, 9, 13, 17, 18, and 19 resonances in direct polarization ^{13}C 1D spectra. Thus, the results presented in this section are fully consistent with

the extraction of ergosterol from a highly mobile lipid environment into a more rigid extramembranous environment distant from the 16-DOXYL spin label.

4-4 ^{13}C-^{31}P REDOR SSNMR EXPERIMENTS

As discussed in Chapter 3, Murata and coworkers reported several different REDOR studies of AmB in liposomes. In these studies, small REDOR effects between AmB and phospholipid were observed, and these were interpreted as being consistent with the localization of AmB within the lipid bilayer membrane.

Using our functionally validated liposome system, we undertook ^{13}C-^{31}P REDOR experiments of MLVs consisting of POPC/U-^{13}C-AmB/ergosterol 10:1:1. Interestingly, these studies revealed measurable REDOR dephasing effects ranging from 10-25% for every sufficiently resolved peak in the AmB ^{13}C spectrum (Figure 4-6). These included the methyl groups C38, C39, C40, and C6' (Figure 4-6A), C1 and C41 carbonyls (Figure 4-6B), hemiketal carbons C1 and C13 (Figure 4-6C). Even the bulk signal of the polyol showed ~15% REDOR dephasing (Figure 4-6D). While these results indicate some degree of proximity of AmB ^{13}C nuclei to ^{31}P of POPC, there were three interesting features of these REDOR effects that strongly support an interpretation alternative to membrane localization of AmB.

First, these REDOR effects are small (generally 10-15%). Second, the REDOR curves display asymptotic behavior, and third, the curves never approach 100% REDOR dephasing ($S/S_0 = 0$), even after long REDOR periods. Small REDOR effects could be interpreted as a long distance between 2 nuclei, but the REDOR curves would be expected to approach 100% dephasing at longer REDOR times, and the curves would not have the asymptotic nature observed in our data. This effect has been clearly demonstrated by Hong and coworkers in their measurements of intramolecular POPC REDOR effects.[17]

Our results are thus inconsistent with a system in which each AmB carbon resides at a defined distance from the POPC headgroup. Alternatively, they are consistent with an average effect created by either 1) a small proportion of AmB residing in the bilayer with proximity to POPC headgroups and/or 2) a small proportion of POPC residing within the large AmB aggregate (see Discussion section).

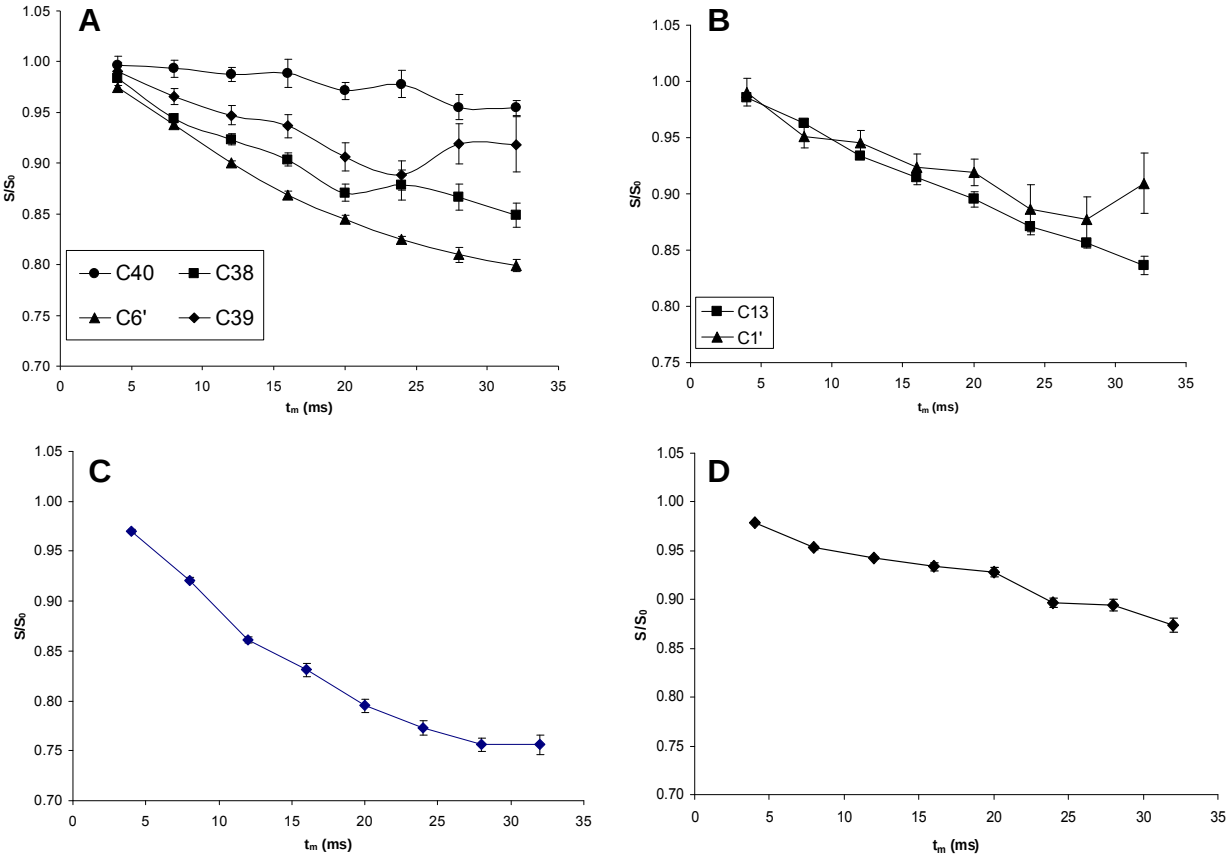

Figure 4-6. ^{13}C-^{31}P REDOR curves. A) AmB methyl groups. B) Hemiketal carbons C13 and C1'. C) C1 carbonyl. D) Bulk polyol. Each curve shows a small amount of dephasing. The asymptotic quality of these curves is consistent with the conclusion that only a small amount of AmB are interacting strongly.

4-5 DISCUSSION

In contrast to the leading model of AmB self-assembly in lipid bilayers, we have discovered that AmB binds to phospholipid bilayers as large, phase-separated aggregates which function to extract ergosterol from the membrane. These conclusions provide a structural rationale for the recent discovery that AmB primarily kills yeast cells by sequestering ergosterol. Just as channel activity is not the major mechanism of AmB antifungal activity, so the ion chanel is not the major structural component in the presence of lipid bilayers. We thus propose the sterol sponge model for the antifungal activity of AmB wherein large extramembranous aggregates of AmB bind to lipid bilayers and extract ergosterol from the yeast cell membrane (Figure 4-7).

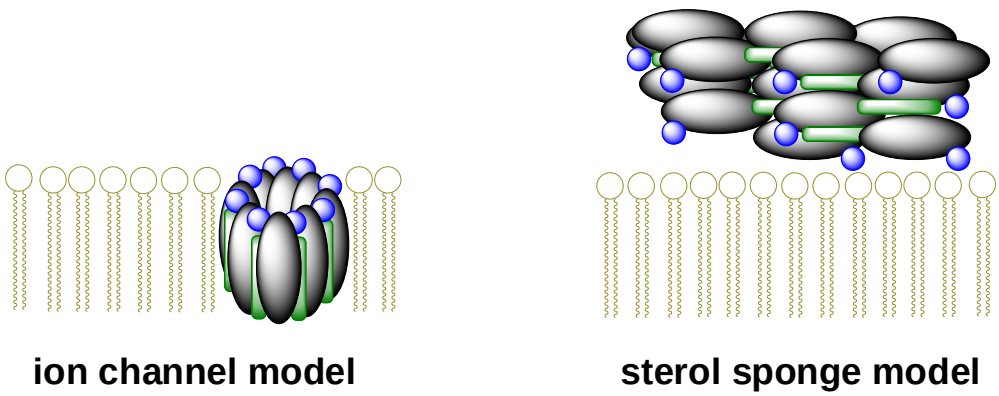

Figure 4-7. For nearly 50 years, the barrel stave ion channel has been the leading model for the interaction of AmB with phospholipid bilayers. Based on extensive SSNMR studies of liposome-bound AmB, we now propose the sterol sponge model in which large, phase-separated aggregates of AmB function to extract ergosterol from phospholipid bilayers.

The SSNMR studies presented in this chapter are inconsistent with the 3 key postulates of the ion channel model as a primary structural model for the antifungal activity of AmB: 1) In phospholipid bilayers, AmB primarily exists as discrete, nanometer-scale barrel stave pores, 2) These pores are embedded in the phsopholipid bilayer, and 3) Ergosterol binds to these embedded pores. This section will discuss our data relevant to each of these 3 postulates and the impact of our results on our understanding of the AmB ion channel.

1. T_1 measurements suggest AmB primarily exists as a large aggregate. The current prevailing model of AmB binding to phospholipid bilayers posits that membrane-bound AmB primarily exists as discrete, nanometer-scale pores. Moreover, these pores are predicted to have some translational mobility in the bilayer; in other words they have phase behavior similar to the lipids. AmB T_1 values much larger than those of POPC in our liposome system suggest instead a large AmB aggregate. However, T_1 relaxation alone does not allow for a definitive conclusion about size, since this parameter depends not simply on size, but also on both local and global motions.[10,11] In the solid-state, T_1 relaxation is minimized when the frequency of molecular motions are near the Larmor frequency. If the motions of POPC occur at a rate less than the Larmor frequency (150 MHz), then the larger AmB T1's would indicate a larger aggregate. As it stands, this T_1 result is suggestive, but not definitive, of a large aggregate of AmB.

2. PRE studies indicate AmB is not embedded. The ion channel model posits that AmB pores are embedded in lipid bilayers. In the presence of 5-DOXYL-PC or 16-DOXYL-PC, nuclei in an embedded pore would experience a significant PRE as a result of their position within the bilayer proximal to either one or both of the nitroxyl spin labels. We have demonstrated that

AmB has no significant PRE in the presence of either 5-DOXYL-PC or 16-DOXYL-PC. Thus, we concluded that the large AmB aggregate discussed above does not reside within the phospholipid bilayer but rather resides phase-separated from membrane phospholipids.

Of note in this experiment is the AmB polyene. While AmB polyene signals are not resolved to enable site-specific PRE analysis of this portion of the molecule, the broad polyene peak as a whole can be analyzed for PRE effects. As depicted in the bar graphs in Figure 4-2 C and D, no PRE is observed for the AmB polyene. Examination of 1D spectra further confirm this result – the polyene signal is not broadened or decreased in intensity by the presence of either DOXYL-PC.

3. Ergosterol PREs in the presence of increasing amounts of AmB indicates ergosterol is physically removed from the bilayer. In the ion channel model of AmB antifungal activity, ergosterol is sequestered by the embedded AmB pore. One- and two- dimensional ^{13}C spectra of liposome-bound ergosterol indicate that in the presence of AmB, several resonances experience a change in chemical shift and dramatic line broadening. Moreover, increased T_1 values are observed for ergosterol, consistent with loss of mobility upon binding to the large AmB aggregate. These observations alone are not sufficient to differentiate the ion channel model from the sterol sponge model. However, PRE studies of ergosterol indicate that ergosterol has a robust PRE in the presence of 16-DOXYL-PC. When AmB is present in the system, there is a decrease in this PRE effect for resolved peaks in the spectrum. Moreover, these ergosterol PREs decrease to a greater extent as the amount of AmB in the system increases, consistent with an equilibrium between bound and unbound ergosterol, with additional AmB driving the extraction forward.

The REDOR data presented above are further consistent with the sterol sponge model in which AmB and phospholipid are not intimately mixed. Further studies will be required to understand the significance of the small REDOR effects observed. However, as mentioned above, we conclude that either a small amount of AmB resides in the bilayer and/or a small amount of phospholipid is extracted into the AmB aggregate. Given that AmB forms ion channels, the first of these postulates is likely to be true; it is possible that a small amount of AmB embedded as an ion channel contributes to these small REDOR effects. Consideration of the second postulate is very interesting and perhaps implies a specific binding site within the AmB aggregate that binds ergosterol and is also a competent host for POPC when ergosterol does not fill all of these binding sites. This binding site theory could be tested by REDOR. We performed our REDOR

experiments at 10:1:1 POPC/AmB/Ergosterol and observed 10-25% REDOR dephasing for each resolved AmB resonance. If POPC indeed binds competitively with ergosterol to the AmB aggregate, then increasing the amount of ergosterol in the system should decrease the observed REDOR dephasing.

Reviewing Murata's REDOR results through the lens of the SSNMR data in this chapter reveals several key points. First, the magnitude of REDOR effects reported ranged from 10% to 50%. Consistent with our own observations, a 100% REDOR effect was never observed in either saturated or POPC liposomes. It is thus possible that these moderate REDOR effects represent binding of phospholipid to an AmB aggregate. Very interestingly, Murata observed greatest REDOR dephasing (~50%) in liposomes lacking ergosterol, consistent with the possibility that more phospholipid was able to occupy sites within the AmB aggregate.

In retrospect, other reports from Murata's lab are also consistent with the sterol sponge model. In the context of studying biophysical properties of AmB derivatives with intramolecular tethers between the C41 carboxylate and the C3' amine, Murata reports a large, relatively immobile AmB aggregate of >20 nm, fully consistent with our conclusion that the majority of AmB primarily exists within a large aggregate.

In addition, the deuterium mobility study is very interesting in light of our work. The observation that AmB and ergosterol have similar mobilities is expected, given that there is a direct binding interaction between these two small molecules in lipid bilayers. Our results provide further evidence that ergosterol is immobilized by AmB as a result of AmB extracting ergosterol from the lipid bilayer and binding it in t

A final observation by Murata's group is very though-provoking. Again in their paper on ^{13}C-Erg,[18] they report REDOR data consistent with both head-to-head and head-to-tail orientation of ergosterol relative to AmB, implying that AmB itself could aggregate in head-to-tail fashion. The capacity for AmB to form head-to-tail dimmers in solution has been reported,[19] and in our own ^{13}C-^{13}C DARR spectra, we observed through space interactions between C19 and C34 (among other anomalous crosspeaks). These atoms reside on opposite ends of the AmB scaffold, thus implying a head-to-tail orientation of AmB in our samples. Thus, as AmB extracts ergosterol from the membrane, it is possible that within the AmB aggregate some proportion of AmB participates in head-to-tail dimerization.

Our discoveries leading to development of the sterol sponge model represent a significant advancement of our understanding of the structural underpinnings of AmB antifungal activity. Yet, AmB retains the capacity to form channels in the presence of the sterol sponge. We are still intensely interested in the capacity of AmB to perform this protein-like function, and understanding the structural underpinnings of the AmB ion channel remains as a significant challenge for our research group. Insofar as we have observed in the studies presented herein, there is no definitive NMR evidence for the structure of this ion channel. The most likely reason for this observation is that only a small amount of AmB participates in forming the ion channel at any given time and thus is not observable by NMR. Indeed, AmB is known to form ion channels at ratios of AmB to PC as low as 1:1000.[20] The challenge in studying the ion channel is thus isolating the channel in a phospholipid membrane without the accompanying large AmB aggregate.

Reviewing the data presented in chapter 3 reveals that nanodiscs may still be useful for trapping the AmB ion channel. While the majority of AmB in our nanodisc studies typically eluted at the void volume with MSP, small amounts of AmB did elute at the same retention time as the nanodiscs, implying that a small proportion of AmB was bound within these nanodiscs. If conditions could be found to cleanly isolate and concentrate large quantities of nanodisc-embedded AmB, these discs could be prepared for SSNMR analysis. Thus, the nanodisc platform still has potential to enable direct study of the AmB ion channel by SSNMR.

4-6 DISSERTATION SUMMARY

The studies described in this dissertation have fundamentally altered our understanding of the mechanism of AmB and opened new avenues for studying its biological and biophysical properties The functional group deletion strategy has proved incredibly powerful in studying the salt bridge hypothesis for channel stabilization. We demonstrated through this approach that oxidation at C41 is not required for antifungal activity of AmB. High resolution solution NMR experiments directly enabled this study by providing the ability to determine the ground state conformation of AmB and our derivatives. Subsequently, this functional group deletion strategy has successfully been applied by Gray et al. in our laboratories to synthesize and study the activity of C-35-deoxy-AmB, and these studies led to the striking discovery that binding ergosterol is the primary mechanism of AmB antifungal activity. Efforts are currently underway in our laboratories toward synthesis and study of other functional group deficient derivatives.

In addition to demonstrating the power of the functional group deletion strategy, the studies described herein highlight the power of SSNMR for study of membrane-bound small molecules. In contrast to 50 years of research on the biophysical properties of AmB, we have demonstrated that the AmB ion channel is not the primary structural entity of membrane-bound AmB. This structural conclusion beautifully parallels the functional observation that ion channel activity is not the primary contributor to antifungal activity. In addition, our SSNMR studies have established a platform for future studies of AmB, and this technique promises to provide fruitful ground for discovery as this collaborative research program moves forward to new challenges in studying AmB. Ultimately, we envision SSNMR has the potential to fully elucidate the structural underpinnings of the functional properties of AmB, thus enabling us to harness the untapped potential of this fascinating small molecule.

4-7 EXPERIMENTAL SECTION

Biosynthesis of ^{13}C-Ergosterol. Biosynthesis of ^{13}C-Erg was performed using a modified version of the protocol reported by Seo et al.[21] *Saccharomyces cerevisiae* were incubated at 28 ºC and 140 r.p.m. for 48 h in a synthetic medium (2 x 1 L) containing sodium [1,2-$^{13}C_2$]acetate (450 mg/L), glucose (20.0 g/L), yeast nitrogen base (13.4 g/L), and L-asparagine monohydrate (3.0 mg/L). The cells were collected by centrifugation and refluxed with 15% potassium hydroxide in ethanol (200 ml) under nitrogen. The filtrate was diluted with water (300 mL) and extracted with ether (3 x 400 mL). The extracts were washed with water, dried, and evaporated to give a crude extract which was crystallized from methanol-chloroform to afford ergosterol

SSNMR Experiments. MAS SSNMR experiments were performed at 600 MHz ^{1}H frequency on Varian InfinityPlus spectrometer, with a 3.2-mm Varian T3 probe at an MAS rate of 10 kHz. The temperature control point was set to 20 °C, and actual sample temperature of 19.5 °C for all experiments, as calibrated by ethylene glycol.[22] All experiments utilized an average of 70-85 kHz SPINAL[23,24] decoupling of protons applied during evolution and acquisition periods, and Tangent ramped cross-polarization (CP)[25] where relevant. Chemical shift assignments were confirmed using a combination of ^{13}C 1D and ^{13}C-^{13}C 2D spectra acquired with 100, 250, and 500ms DARR mixing. Chemical shifts are references to adamantane.[26]

Measurements of longitudinal relaxation rates, R_1, were performed using a ^{13}C direct polarization (DP) T_1 inversion recovery sequence, with 75 kHz of SPINAL proton decoupling applied during acquisition. In addition, a short 1ms echo was applied prior to acquisition to remove background from probe, and rotor parts in final spectra. To insure uniformity in the determination of R_1 values for resolved ^{13}C resonances, integration boundaries were set based on the observed linewidth in the 1D and 2D ^{13}C spectra, with small adjustments (>0.3 ppm) maid to avoid overlap when possible.

De novo assignments for 13C-Erg were made from DARR spectra. The chemical shifts of both the bound and free ergosterol are shown in Table 4-1. The column at the right lists the number of spectra used to calculate the standard deviation for the chemical shift.

Assignment	δ (ppm)	Standard deviation	Assignments
Erg-1	41.18	0.04	29
Erg-3	72.02	0.04	37
Erg-5	143.74	0.05	40
Erg-7	119.75	0.03	30
Erg-9	48.87	0.06	35
Erg-13	45.39	0.07	39
Erg-15	25.95	0.03	22
Erg-17	58.53	0.04	35
Erg-18	14.74	0.04	40
Erg-19	18.59	0.02	18
Erg-21	24.04	0.02	21
Erg-22	138.51	0.04	36
Erg-24	45.93	0.13	30
Erg-26	20.89	0.55	6
Erg-27	22.21	0.33	15
Erg-1'	39.46	0.15	46
Erg-3'	71.44	0.12	59
Erg-5'	144.23	0.15	17
Erg-7'	120.14	0.08	12
Erg-9'	47.36	0.22	79
Erg-13'	44.92	0.10	107
Erg-15'	26.17	0.16	70
Erg-17'	57.39	0.15	77
Erg-18'	15.05	0.17	21
Erg-19'	17.65	0.15	27
Erg-21'	24.45	0.27	4
Erg-22'	139.24	0.14	37
Erg-24'	ND		
Erg-26'	ND		
Erg-27'	ND		

Table 4-1. Ergosterol chemical shift assignments.

REFERENCES

1) DeKruijff, B.; Demel R.A.; *Biochim. Biophys. Acta* **1974**, *339*, 57-70
2) Andreoli, T.E. *Ann. N.Y. Acad. Sci.* **1974**, *235*, 448-468.
3) Finkelstein, A.; Holz, R. in *Membranes* vol. 2. Lipid Bilayers and Antibiotics. Eisenman, G. Editor, Marcel Dekker, Inc., New York, **1973**, 377-408.
4) Gray, K.C.; Palacios, D.S.; Dailey, I.; Endo, M.M.; Uno, B.E.; Wilcock, B.C.; Burke, M.D. *Proc. Natl. Acad. Sci. U.S.A.* **2012**, *109*, 2234-2239.
5) Kato, M.; Wickner, W. *EMBO J*. **2001**, *20*, 4035-4040.
6) Heese-Peck, A.; Pichler, H.; Zanolari, B.; Watanabe, R.; Daum, G.; Riezman, H. *Mol. Biol. Cell* **2002**, *13*, 2664-2680.
7) Jin, H.; McCaffery, J.M.; Grote, E. *J. Cell Biol*. **2008**, *180*, 813-826.
8) Klose, C.; Ejsing, C.S.; Garcia-Sáez, A.J.; Kaiser, H.-J.; Sampaio, J.L.; Surma, M.A.; Schevchenko, A.; Schwille, P.; Simons, K. *J. Biol. Chem*. **2010**, *285*, 30224-30232.
9) Zhang, Y.Q. PLoS Pathog. 2010, 6, e1000939.
10) Solomon, I. *Phys. Rev.* **1955**, *99*, 559-565
11) Abragam, A.; Pound, R.V. *Phys. Rev.* **1953**, *92*, 943-962
12) Jaroniec, C.P. *Solid State Nucl. Magn. Reson.* **2012**, *43-44*, 1-12.
13) (a) Ellena, J.F.; Archer, S.J.; Dominey, R.N.; Hill, B.D.; Cafiso, D.S. Biochim. Biophys. Acta **1988**, *940*, 63-70. (b) Scheidt, H.A.; Müller, P.; Herrmann, A.; Huster, D. *J. Biol. Chem*. **2003**, *278*, 45563-45569. (c) Thomas, L.; Scheidt, H.A.; Bettio, A.; Beck-Sickenger, A.G.; Huster, D.; Zschörnig, O. *Eur. Biophys. J*. **2009**, *38*, 663-677. (d) Brûlet, P.; McConnell, H.M. *Proc. Natl. Acad. Sci. USA* **1975**, *72*, 1451-1455.
14) Sankaram, M.P.; Thompson, T.E. *Proc. Natl. Acad. Sci. USA* **1991**, *88*, 8686-8690.
15) Rienstra, C.M. *NMR Spectroscopy of Biological Solids*. A. Ramamoorthy, Ed. CRC Press, **2005**, 1-38.
16) Cavanagh, J.; Fairbrother, W. J.; Palmer, W. G. III; Rance, M.; Skelton, N. J. *Protein NMR Spectroscopy: Principles and Practices, 2nd Ed.* **2006**, *Academic Press*, San Diego.
17) Tang, M.; Waring, A.J.; Hong, M. *J. Magn. Reson.* **2007**, *184*, 222-227.
18) Umegawa, Y.; Nakagawa, Y.; Tahara, K.; Tsuchikawa, H.; Matsumori, N.; Oishi, T.; Murata, M.; *Biochemistry* **2012**, *51*, 83-89
19) Balkarishnan, A.R.; Easwaran, K.R.K. *Biochim. Biophys. Acta* **1993**, *1148*, 269-277.
20) Palacios, D.S.; Dailey, I.; Seibert, D.M.; Wilcock, B.C.; Burke, M.D. *Proc. Natl. Acad. Sci. U.S.A.* **2011**, *108*, 6733-6738.
21) Seo, S.; Uomori, A.; Yoshimura, Y.; Takeda, K.; Seto, H.; Ebizuka, Y.; Noguchi, H.; Sankawa, U. *J. Chem. Soc., Perkin Trans. 1*, **1988**, 2407−2414
22) Van Geet, A.L. *Analytical Chemistry* **1968**, *42*, 2227.
23) Brauniger, T.; Wormald, P.; Hodgkinson, P. *Monatsh. Chem*. **2002**, *133*, 1549-1554.
24) Comellas, G.C.; Lopez, J.J.; Nieuwkoop, A.J.; Lemkau, L.R.; Rienstra, C.M. *J. Magn. Reson.*, **2011**, *209*, 131-135.
25) Hediger, S.; et al. *Chem. Phys. Lett.* **1994**, *223*, 283.
26) Morcombe, C.R.; Zilm, K.W. *J. Magn. Reson.* **2003**, *162*, 479-486.